Precambrian Research 353 (2021) 106005

Contents lists available at ScienceDirect

Precambrian Research

journal homepage: www.elsevier.com/locate/precamres

Distribution of Ediacaran acanthomorphic acritarchs in the lower Doushantuo Formation of the Yangtze Gorges area, South China: Evolutionary and stratigraphic implications

Qing Ouyang [a,*], Chuanming Zhou [a,b], Shuhai Xiao [c], Chengguo Guan [a], Zhe Chen [a,b], Xunlai Yuan [a,b], Yunpeng Sun [a,d]

[a] State Key Laboratory of Palaeobiology and Stratigraphy, Nanjing Institute of Geology and Palaeontology, and Center for Excellence in Life and Palaeoenvironment, Chinese Academy of Sciences, Nanjing 210008, China
[b] University of Chinese Academy of Sciences, Beijing 100049, China
[c] Department of Geosciences, Virginia Tech, Blacksburg, VA 24061, USA
[d] University of Science and Technology of China, Hefei 230026, China

ARTICLE INFO

Keywords:
Ediacaran Period
Doushantuo Formation
Eukaryotic microfossil
Diversification
Biostratigraphy

ABSTRACT

As part of the most common eukaryotic fossils in early Ediacaran strata, acanthomorphic acritarchs are crucial for understanding the biostratigraphy and evolutionary dynamics of marine eukaryotes after the Marinoan global glaciation. Abundant and diverse acanthomorphic acritarchs have been reported from the Ediacaran Doushantuo Formation in the Yangtze Gorges area, South China, and different biozonation schemes have been proposed. However, these previously published biozones were based on biostratigraphic data compiled from different stratigraphic sections, with little effort to test whether these biozones can be consistently recognized at different sections, despite the fact that regional consistency is critical to a robust biostratigraphic framework. Also, the evolutionary pattern of the Doushantuo acritarchs has not been documented in detail, especially for acritarchs from the lowermost Doushantuo Formation, largely due to the perceived low taxonomic richness after the Marinoan global glaciation.

In this study, we report silicified acanthomorphic acritarchs and other eukaryotic microfossils from chert nodules in the lower part (Member II) of the Doushantuo Formation at the Jiulongwan, Jinguadun, and Wuzhishan sections in the Yangtze Gorges area. From a total of 1547 acanthomorphic acritarch specimens found, 24 genera and 69 species have been identified, including two new genera (*Annularidens* gen. nov. and *Crassimembrana* gen. nov.), six new species (*Annularidens inconditus* gen. et sp. nov., *Bispinosphaera vacua* sp. nov., *Crassimembrana crispans* gen. et sp. nov., *C. multitunica* gen. et sp. nov., *Distosphaera jinguadunensis* sp. nov., and *Mengeosphaera matryoshkaformis* sp. nov.), five unnamed species (*Annularidens* sp., *Mengeosphaera* sp. 1, *Mengeosphaera* sp. 2, *Sinosphaera* sp., and *Variomargosphaeridium* sp.), and three possible new forms tentatively placed in open nomenclatures (*Crassimembrana* cf. *C. crispans*, *Tanarium* cf. *T. conoideum*, and *Weissiella* cf. *W. grandistella*). The high-resolution fossil occurrence and abundance data from the three sections reveal both spatial variations in acritarch composition, and stratigraphic similarities in acanthomorph range and abundance, indicating that acanthomorph taxa can be applied to biostratigraphic subdivision and correlation only if their stratigraphic records are thoroughly investigated at least at the regional scale. The FADs (first appearance data) of acanthomorph species such as *Appendisphaera grandis*, *Appendisphaera heliaca* n. comb., *Ericiasphaera fibrilla*, and *Tianzhushania spinosa*, as well as the relative abundance variations of certain taxa, are recognized as promising biostratigraphic markers in lower Doushantuo Formation. The new data also reveal a rapid diversification of marine eukaryotes, with taxonomic richness of acanthomorphs increasing to notable levels within probably ten million years after the termination of the Marinoan glaciation, followed by continuing increase in both taxonomic richness and evenness afterwards.

* Corresponding author.
E-mail address: qouyang@nigpas.ac.cn (Q. Ouyang).

https://doi.org/10.1016/j.precamres.2020.106005
Received 2 April 2020; Received in revised form 15 October 2020; Accepted 6 November 2020
Available online 24 November 2020

1. Introduction

Acanthomorphic acritarchs—organic walled microfossils with spines or processes—are globally distributed in Ediacaran strata (e.g., Anderson et al., 2017; Golubkova et al., 2010; Grey, 2005; Knoll, 1992; Sergeev et al., 2011; Tiwari and Knoll, 1994; Vidal, 1990; Zhang et al., 1998). They have been considered as biostratigraphically important fossils for the subdivision and correlation of the Ediacaran System (Narbonne et al., 2012; Xiao et al., 2016), and provide key insights into the evolution and diversification of eukaryotic life in Ediacaran oceans after Cryogenian global glaciations.

Abundant and diverse acanthomorphic acritarchs have been discovered from the Ediacaran Doushantuo Formation in South China (e.g., Liu and Moczydłowska, 2019; Zhang et al., 1998; Zhou et al., 2007). Based on fossil data compiled from multiple stratigraphic sections in the Yangtze Gorges area, different biostratigraphic zonations have been proposed for the Doushantuo Formation (Liu and Moczydłowska, 2019; Liu et al., 2013; McFadden et al., 2009; Yin et al., 2011a). However, these studies also revealed that stratigraphic ranges of individual species vary markedly at different sections. Consequently, questions arise as to what taxon or taxa are most diagnostic of these biozones and whether these biozones are regionally consistent in the Yangtze Gorges area.

Ediacaran acanthomorphic acritarchs also record the evolutionary pattern of marine eukaryotic life in the aftermath of the Cryogenian global glaciation. Several researchers have scrutinized the lowermost Doushantuo Formation in South China for acanthomorphic acritarchs (e.g., Liu and Moczydłowska, 2019; McFadden et al., 2009; Zhou et al., 2007). At most sections examined by these researchers, fewer than ten species were reported from the lower 20 m of strata above the cap dolostone, except at the Sixi section (Fig. 1C, Section 4; McFadden et al.,

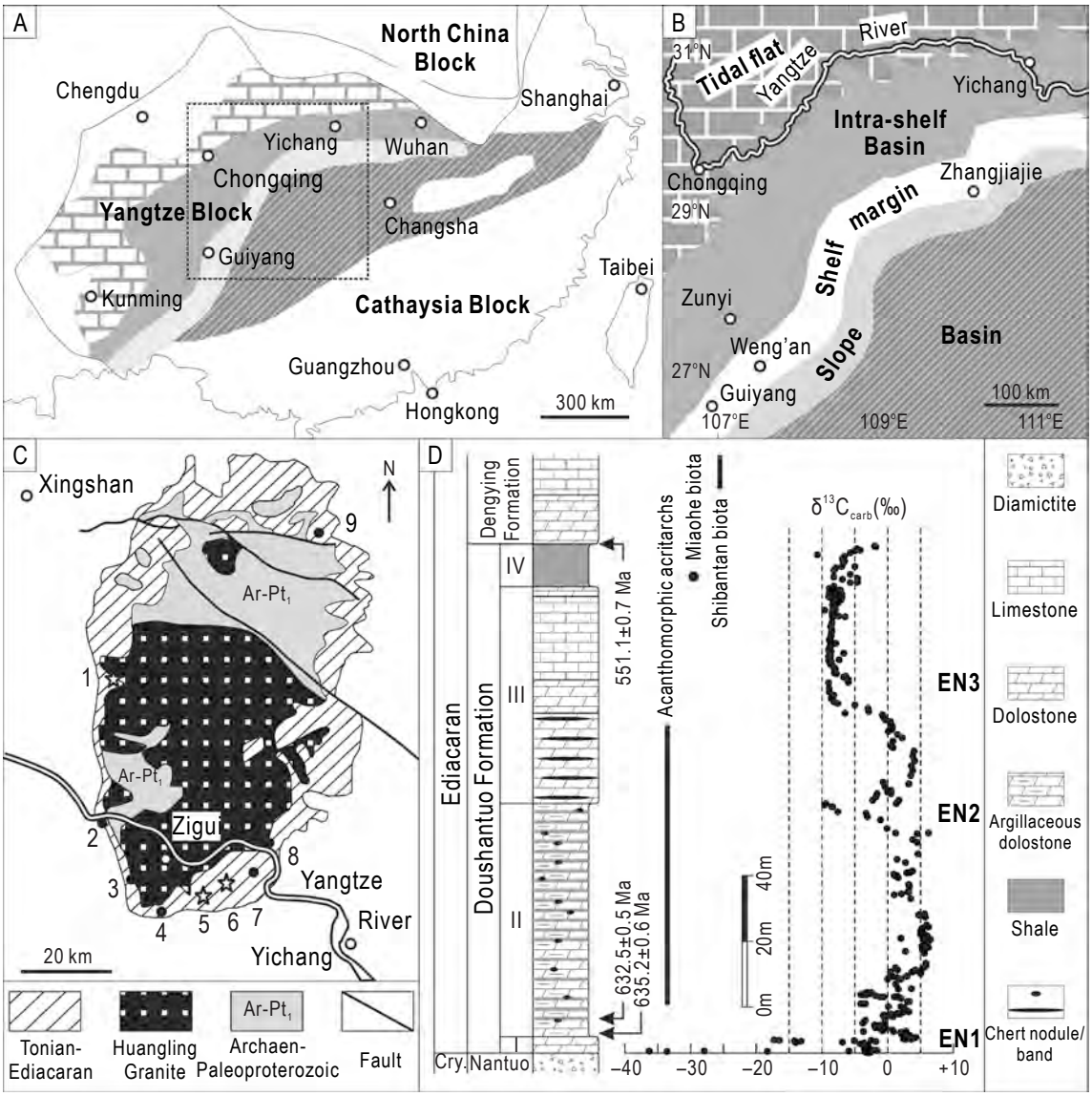

Fig. 1. Paleogeography, section locality, and simplified Ediacaran stratigraphy of the Yangtze Gorges area. (**A**) Paleogeographic map of the Yangtze Block (modified from Jiang et al., 2011). (**B**) Magnification of area marked by rectangle in (**A**) (modified from Jiang et al., 2011). (**C**) Simplified geological map showing the Precambrian strata around the Huangling anticline. Sections: 1, Wuzhishan; 2, Jiuqunao (Jijiawan); 3, Qinglinkou; 4, Sixi; 5, Jinguadun; 6, Jiulongwan; 7, Tianjiayuanzi and Chenjiayuanzi; 8, Wangfenggang (Liantuo); 9, Bailu section in the Zhangcunping area. (**D**) Generalized lithostratigraphy, biostratigraphy, and carbon isotopic chemostratigraphy of the Doushantuo Formation in the Yangtze Gorges area. Lithostratigraphic column and C isotopic curve are from the Jiulongwan section by McFadden et al. (2008).

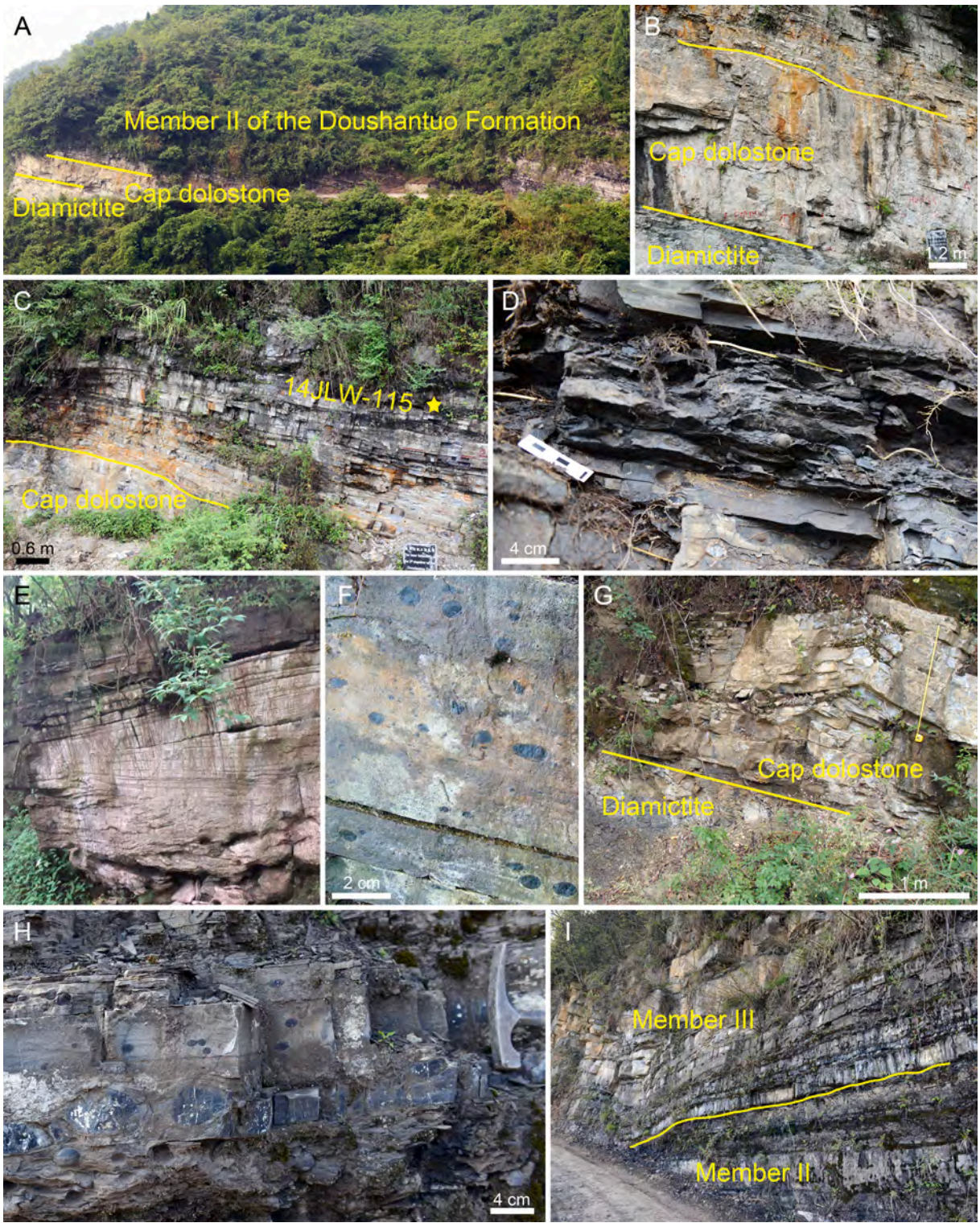

Fig. 2. Field photographs of the Doushantuo Formation at the Jiulongwan (**A**–**D**), Jinguadun (**E** and **F**), and Wuzhishan (**G**–**I**) sections. (**A**) Distant view of the Nantuo Formation diamictite, cap dolostone, and lower Member II of the Doushantuo Formation. (**B**) Closer view of the Nantuo Formation diamictite, cap dolostone, and basal Member II of the Doushantuo Formation. (**C**) Cap dolostone, lowermost Member II, and lowest occurrence of chert nodules (~2.8 m above the cap dolostone, sample 14JLW-115) of the Doushantuo Formation. (**D**) Chert nodules in argillaceous dolostone at ~8–8.2 m above cap dolostone (samples 05WH-5, 6/14JLW-47–49). (**E**) Cap dolostone. (**F**) Chert nodules in the argillaceous dolostone at ~62.5 m (sample 05MZX-5/16ZC32). (**G**) Nantuo diamictite and cap dolostone. (**H**) Chert nodules in argillaceous dolostone at ~28 m above the lowest chert nodule bed or ~22 m below the top of Member II (sample 15HFL-12). (**I**) Contact between Member II and Member III.

2009) and the Wangfenggang (Liantuo) section (Fig. 1C, Section 8; Liu and Moczydłowska, 2019). These results appear to indicate a relatively low diversity of acanthomorphic acritarchs at the beginning of the Ediacaran Period, but this needs to be tested with more data from additional sections of the lower Doushantuo Formation.

In this study, we report acanthomorphic acritarchs and multicellular algal fossils from the lower part (Member II) of the Doushantuo Formation at the Jiulongwan, Jinguadun, and Wuzhishan sections in the Yangtze Gorges area (marked by stars in Fig. 1C). Among them, the Jiulongwan section is one of the most intensively studied Ediacaran sections around the world. The diversity of acanthomorphic acritarchs recovered from these three sections is remarkably high, with taxonomical richness at each section higher than ever reported from the lower 20 m of Member II or even the entire Member II at any individual sections. Based on carefully recorded occurrence and abundance data, the taxonomic composition and stratigraphic range of acanthomorphic acritarchs are compared among the three sections. We use these new data combined with previously reported data to document the spatial and temporal distributions of different taxa in the lower Doushantuo Formation, their biostratigraphic significance, as well as the diversification pattern of eukaryotes in the early Ediacaran Period.

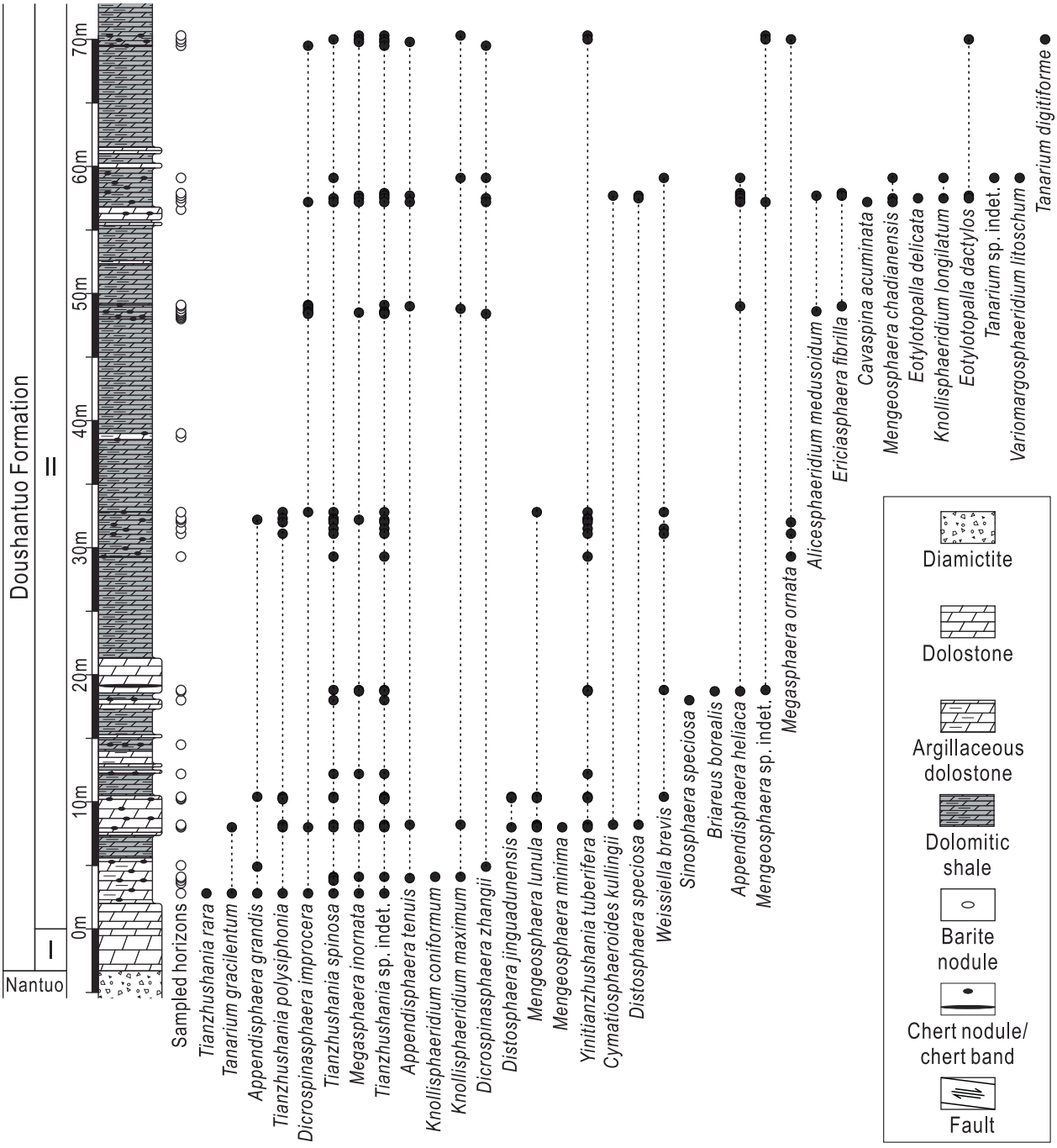

Fig. 3. Lithostratigraphy, sampling horizons and acanthomorphic acritarch distribution in Member II at Jiulongwan. Samples with prefixes "05WH" and "14JLW" were collected from this section. Legends also apply to Figs. 4, 5.

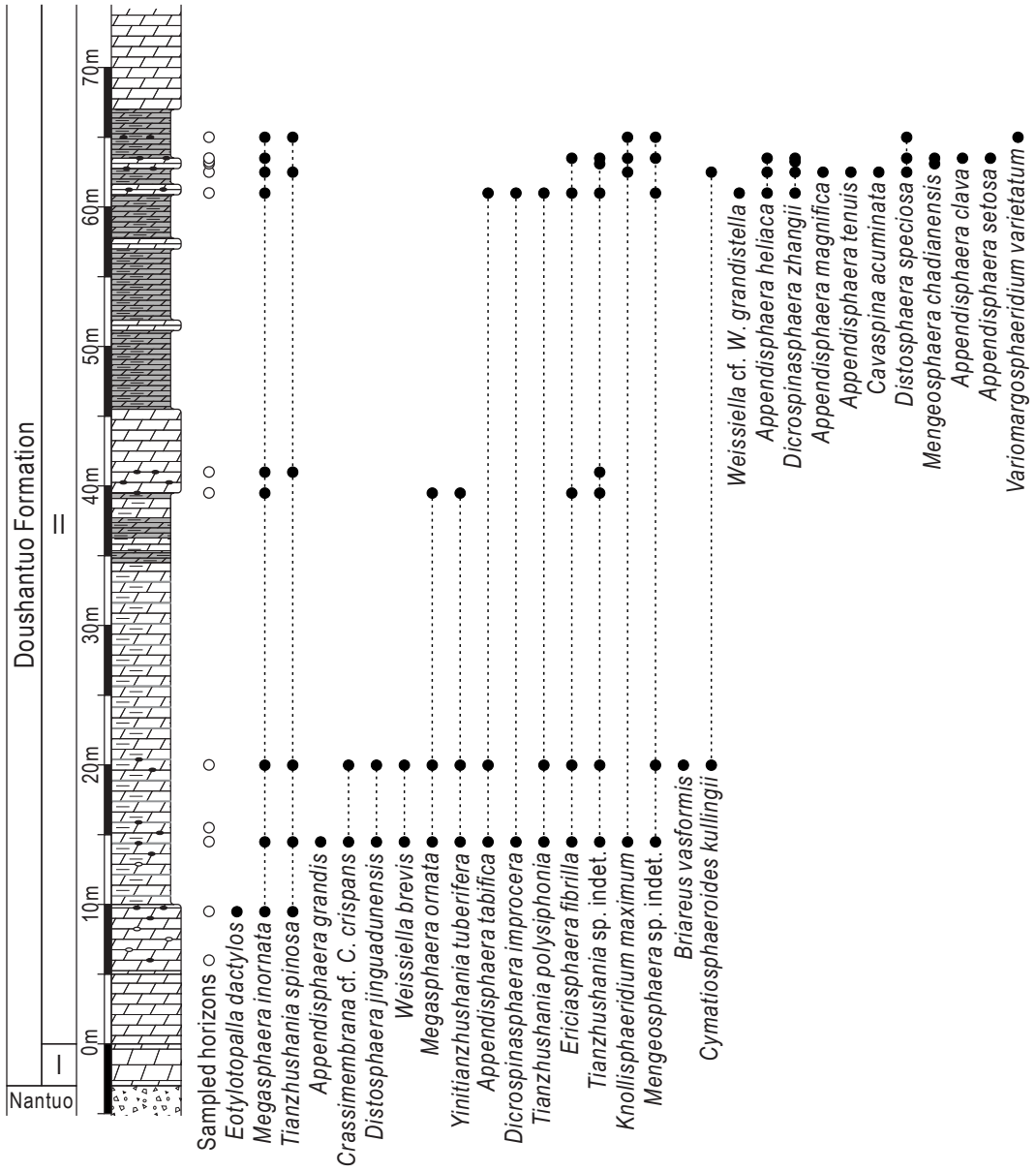

Fig. 4. Lithostratigraphy, sampling horizons and acanthomorphic acritarch distribution in Member II at Jinguadun. Samples with prefixes "05MZX" and "16ZC" were collected from this section. See Fig. 3 for legends.

2. Geological settings

The Ediacaran strata that crop out around the Huangling anticline in the Yangtze Gorges area (Fig. 1C) were deposited in an intra-shelf basin environment on the Yangtze Block of South China (Fig. 1A, B; Jiang et al., 2011). Stratigraphically bracketed by the Cryogenian Nantuo Formation diamictite and the Cambrian Yanjiahe Formation carbonate, Ediacaran strata in this area are composed of two formations: the Doushantuo Formation consisting of a mixture of siliciclastic and carbonate rocks, and the overlying Dengying Formation dominated by carbonate rocks. The Ediacaran strata in this area is richly fossiliferous, yielding acanthomorphic acritarchs and multicellular algae preserved in chert nodules (Liu et al., 2014b; Zhang et al., 1998), carbonaceous compressions preserved in black shales (Xiao et al., 2002; Ye et al., 2017), and Ediacara-type megafossils preserved in carbonates (Chen et al., 2014; Xiao et al., 2020).

At its type locality in the southeastern limb of Huangling anticline, the Doushantuo Formation has been lithostratigraphically subdivided into four members (Fig. 1D; Wang et al., 1998): Member I (cap dolostone, ca. 3 m thick), Member II (argillaceous dolostone and dolomitic shale, ca. 110 m thick), Member III (thin- to thick-bedded carbonates, ca. 80 m thick), and Member IV (black shales, ca. 8 m thick). Chert nodules and bands occur in both Member II and Member III, although they are more commonly seen in Member II. Three significant negative carbon isotopic excursions EN1, EN2, and EN3 (EN3 regarded as equivalent to the Shuram excursion) have been recognized in Member I, Member II–III transition, and upper Member III–IV, respectively (Zhou and Xiao, 2007). These lithostratigraphic units and C isotopic excursions have been widely applied in stratigraphic correlation of the Doushantuo Formation in South China (Jiang et al., 2007, 2011; Ouyang et al., 2019; Wang et al., 2017, 2016).

The Jiulongwan section (GPS: 30°48′0.32″ N, 111°3′15.39″ E) crops out along a roadcut near Jiulongwan in the southeastern limb of Huangling anticline (Fig. 1C, section 6, Fig. 2A). Since the type section of the Doushantuo Formation, the Tianjiayuanzi section (Fig. 1C, section 7), is now largely covered by vegetation, the Jiulongwan section has

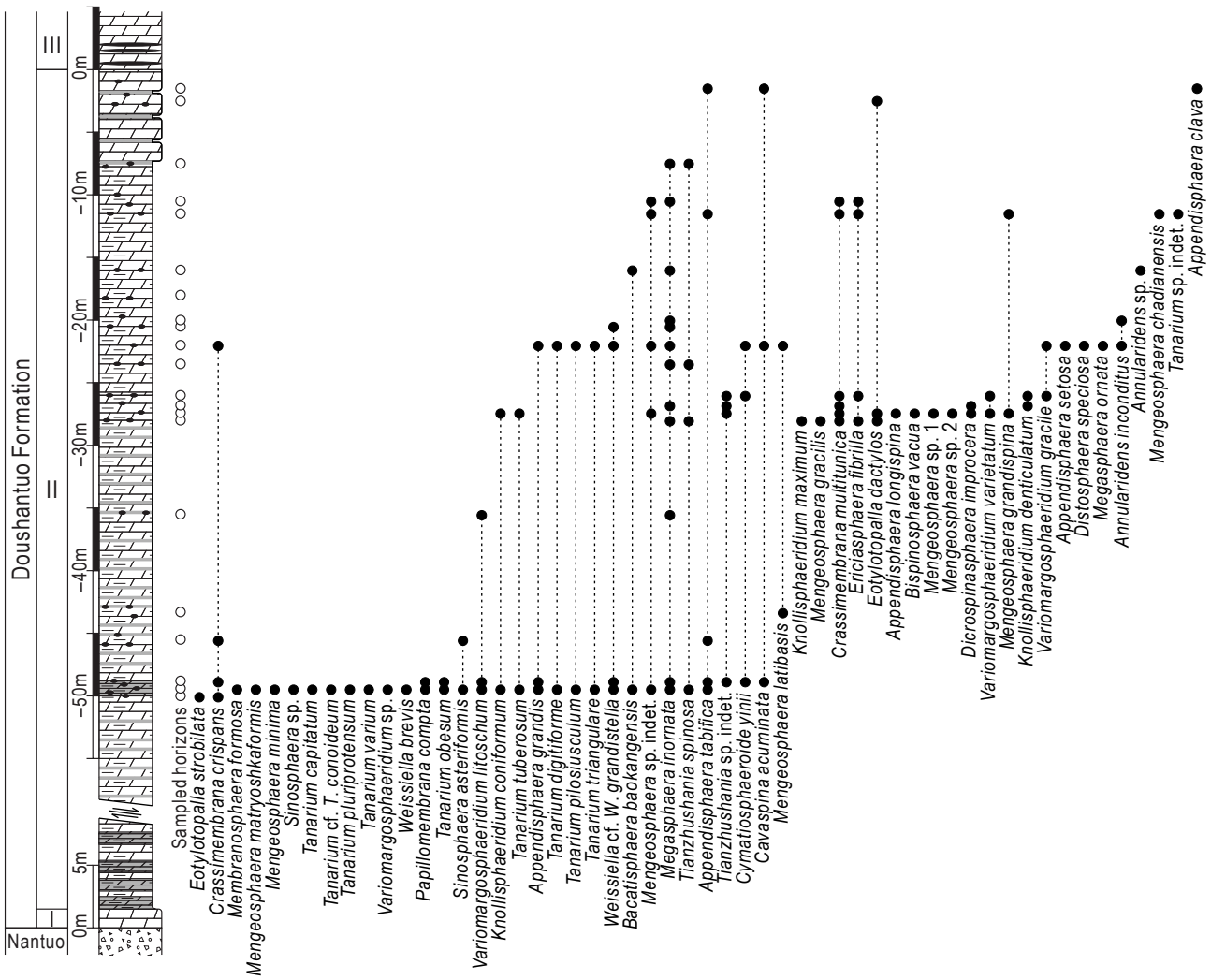

Fig. 5. Lithostratigraphy, sampling horizons and acanthomorphic acritarch distribution in Member II at Wuzhishan. Samples with prefix "15HFL" were collected from this section. See Fig. 3 for legends.

been widely used as a yardstick for the correlation of the Doushantuo Formation in South China. At the Jiulongwan section, Member II begins with 2 m of thinly bedded dolostone (Fig. 2B, C; equivalent to the C3 facies of cap dolostone in Jiang et al., 2003a, 2006), succeeded by ~3.6 m of thinly and lenticularly bedded argillaceous dolostone, with millimeter to centimeter sized chert and calcite nodules; the lowest chert nodule horizon is ~2.8 m above the cap dolostone (sample 14JLW-115, Fig. 2C). Further upsection, Member II consists primarily of dolomitic shale with dolostone interbeds, both of which contain chert nodules or bands (Fig. 2D). About 80 m of Member II strata is exposed along the roadcut, but a drill core adjacent to this section recovered about 110 m of Member II strata.

The Jinguadun section (GPS: 30°45′43.77″ N, 110°59′9.94″ E) is located in the southern limb of Huangling anticline (Fig. 1C, section 5), near the Jinguadun village. At this section, Member II is not well exposed, and it consists of argillaceous dolostone and dolomitic shale, with a few chert nodule horizons (Fig. 2F). At Jinguadun the upper part of Member II is mostly covered by vegetation with only a few dolostone outcrops, and it is overlain by Member III carbonates that form a steep cliff.

The Wuzhishan section (GPS: 31°5′9.48″ N, 110°53′55.56″ E) crops out along the Huofuling ridge in the western limb of Huangling anticline (Fig. 1C, section 1). Member II at this section consists of dolomitic shale interbedded with argillaceous dolostone, both of which contain a large number of chert nodules (Fig. 2H). The proportion of dolomitic shale decreases gradually upsection, succeeded in the uppermost Member II by argillaceous dolostone with thin black chert bands (Fig. 2I). Due to a fault that cuts through lower Member II, the total thickness of Member II is unknown at this section. The lowest chert nodule bed occurs above this fault, and is about 50 m below the Member II-III boundary, which is defined by the disappearance of dolomitic shale.

As the lithostratigraphic sequence and thickness of Member II are largely consistent in the Yangtze Gorges area, it is possible to roughly correlate chert nodule horizons in Member II at different sections, especially for sections in the southern to southeastern limb of Huangling anticline (e.g., Sixi, Jinguadun, Jiulongwan, Chenjiayuanzi, Wangfenggang), of which Member II is around 100–120 m thick. However, due to the fault in lower Member II at Wuzhishan in the western limb, the lithostratigraphic correlations of Member II at Wuzhishan with that at Jiulongwan and Jinguadun are not straightforward. If we accept that the Member II strata at these three sections are similar in thickness, then only the lowermost 10–20 m of sampled strata at Wuzhishan overlap with the sampled strata at Jiulongwan and Jinguadun. Alternatively, if Member II in the western limb is much thinner than that in the southern limb as reported at the Jiuqunao section (Liu and Moczydłowska, 2019) and Qinglinkou section (An et al., 2014; Ouyang et al., 2015), the sampled strata at Wuzhishan would overlap with more but still the upper part of sampled strata at Jiulongwan and Jinguadun.

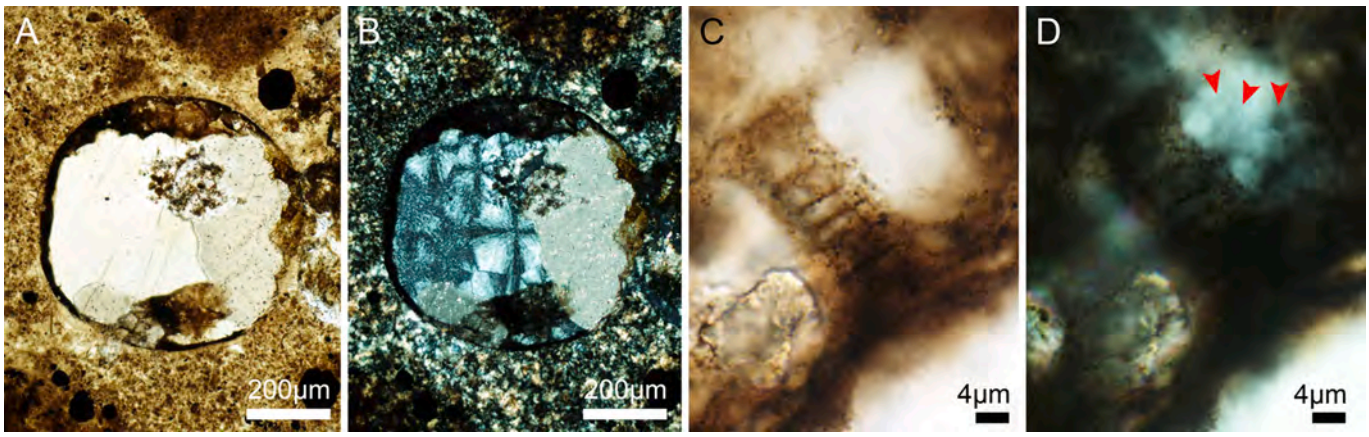

Fig. 6. Silicified acanthomorphs in thin sections under non-polarized light (N), plane-polarized light (PPL), and cross-polarized light (XPL). (**A** and **B**) *Yinitianzhushania tuberifera* (Yin et al., 2001) Xiao et al., 2014b, PB23439, thin section14JLW-80-13, M27/1 (ef). (**A**) N. (**B**) XPL. (**C** and **D**) *Weissiella brevis* Xiao et al., 2014b emend., showing a short cylindrical process with internal cross-walls and magnified views of a process marked by red arrowhead in Fig. 23E. Full specimen illustrated in Fig. 23E. (**C**) PPL. (**D**) XPL. Red arrowheads in (**D**) denote recrystallized micro-quartz crystals, which are about or less than one micron in size. For each specimen illustrated in this and all following figures, England Finder (ef) coordinates are given whenever possible and, when specimens are beyond the range of an England finder, stage coordinates (st) as determined on an Olympus BX51 microscope are given. (For interpretation of the references to colour in this figure legend, the reader is referred to the web version of this article.)

Two zircon U-Pb radiometric ages, 635.23 ± 0.57 Ma and 550.07 ± 0.61 Ma, from ash beds in the lowest Member II and the uppermost Doushantuo Formation, respectively, constrain the ~200 m thick Doushantuo Formation in the Yangtze Gorges area to ~86 million years in duration (Condon et al., 2005), suggesting either an exceedingly low depositional rate or the occurrences of long-lasting hiatuses. Previous studies have recognized two sequence boundaries in the lower and upper Doushantuo Formation, respectively. The lower one is marked by a karstic surface in shallow-water inner shelf facies (e.g., the Zhangcunping area), and has been correlated with a horizon in upper Member II (Zhu et al., 2013) or the Member II-III boundary (Jiang et al., 2011; Zhou and Xiao, 2007) in the Yangtze Gorges area although no karstic surface is present here. Two U-Pb radiometric ages, 614.0 ± 7.6 Ma and 609 ± 5 Ma, were obtained respectively from below and above the above-mentioned karstic surface at Zhangcunping (Fig. 1C, section 9; Liu et al., 2009; Zhou et al., 2017a). These two ages are indistinguishable within uncertainty, indicating that this karstic surface represents a relatively short time interval. It is possible that a major depositional break exists in the upper Doushantuo Formation in the Yangtze Gorges area, but this sedimentary break lies above Member III carbonates (An et al., 2015; Zhou et al., 2017b). Thus, in the Yangtze Gorges area Members II and III that contain acanthomorphic acritarchs represent more or less continuous but condensed sedimentation.

3. Materials and methods

In total, 40, 11, and 21 chert nodule or band horizons were sampled from Member II of the Doushantuo Formation at the Jiulongwan, Jinguadun, and Wuzhishan sections, respectively (Figs. 3–5). Thin sections were made for all chert nodule and band samples, with 1931, 334, and 556 thin sections from the Jiulongwan, Jinguadun, and Wuzhishan sections, respectively. Only one thin section was made from each chert nodule, except for those larger than two centimeters in diameter that can afford multiple thin sections. At least ten, generally 15–30 thin sections were made from each sampled horizon (or each sample) except for the sample 16ZC30 from the Jinguadun section, for which only seven thin sections were made. More than a hundred thin sections were made for three chert nodule samples from the lowermost 5 m of Member II at Jiulongwan (samples 14JLW-115, 33, 37), all of which contain many recrystallized calcite or dolomite crystals that compromised the preservation of microfossils. Thin sections were examined for microfossils under transmitted light microscopes (Olympus BX51 and ZEISS Scope A1). All acanthomorphic acritarchs encountered in thin sections were recorded with stage coordinates, positioned using an England Finder, photographed with an Olympus DP72 camera, and analyzed using the Image Pro software. Specimens were counted and relative abundance of each taxon was calculated for each fossiliferous horizon. All samples and thin sections are reposited in the Nanjing Institute of Geology and Palaeontology, Chinese Academy of Sciences.

4. Results

Member II of the Doushantuo Formation at the Jiulongwan, Jinguadun, and Wuzhishan sections yielded abundant silicified microfossils. The relative abundance of microfossils varied among horizons and even among chert nodules from the same horizon. Even at the most fossiliferous horizons, there were many chert nodules that yielded no microfossils at all. Organic-walled structures such as vesicles and ornamentations of acritarchs are typically preserved as dark organic matter surrounded by SiO_2 microcrystals. In most chert nodules or bands, quartz microcrystals are < 1 μm in size (Fig. 6B, D), allowing the preservation of micrometer-scale structures. The microfossils discovered in the present study include coccoidal and filamentous prokaryotes (Fig. 7A–N), multicellular algae (Fig. 8A–L, 9A–I), and acanthomorphic acritarchs (Figs. 6, 10–24). Prokaryote fossils are not the primary focus of this study due to their limited morphological variation and thus limited biostratigraphic significance in the Ediacaran Period.

Multicellular algae occur in almost all fossiliferous horizons at all three studied sections (Tables 2–4). These fossils show considerable morphological complexity and diversity even at their lowest occurrence horizon at ~2.8 m above the cap dolostone at the Jiulongwan section (Fig. 8A, B, F, K, L). At all three sections, *Wengania* is the dominant multicellular algal form, with most specimens identified as *W. minuta* (Fig. 8A–C) and *W. exquisita* (Fig. 8E, F), and very few as *W. globosa* (Fig. 8D). Larger forms also occur commonly, including *Sarcinophycus* (Fig. 8G–L), *Thallophycoides* (Fig. 9A–C), *Paramecia* (Fig. 9D), *Gremiphyca*-like thalli (Fig. 9E, F), and many taxonomically unidentifiable thallus fragments (Fig. 9G–I).

A total of 24 genera and 69 species of acanthomorphic acritarchs were recovered from the three sections (Table 1; taxonomically indeterminate acanthomorphic specimens were not included in the calculation of diversity or abundance statistics). At each section, acanthomorphic acritarchs occur from the lowest to the highest chert nodule horizons (Tables 2–4). Two new genera, six new species, five

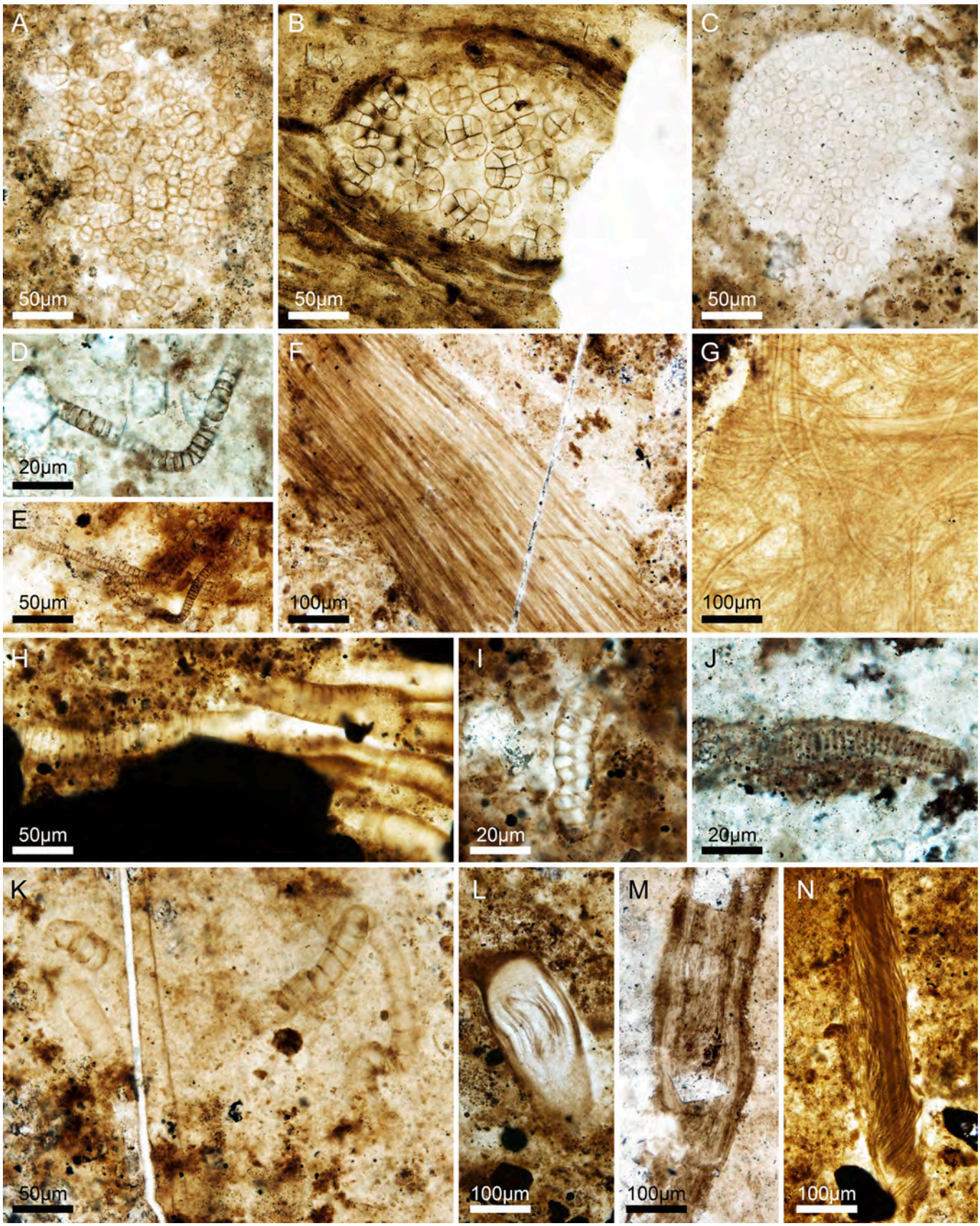

(caption on next page)

Fig. 7. Prokaryotes from Member II in the Yangtze Gorges area. (**A** and **B**) *Archaeophycus yunnanensis* (Song in Luo et al., 1982) Dong et al., 2009, a putative cyanobacterium. (**A**) Thin section # 16ZC28-23, N41/1 (ef). (**B**) Thin section # 15HFL-8-2, H36/1 (ef). (**C**) *Myxococcoides minor*? Schopf, 1968, thin section # 16ZC32-8, H37/3 (ef). (**D** and **E**) *Oscillatoriopsis obtusa* Schopf, 1968. (**D**) Thin section # 05MZX-2a-10, X43/4 (ef). (**E**) Thin section # 05MZX-3b-5, P34/3 (ef). (**F**) ? *Polytrichoides lineatus* Hermann, 1974, emend. Hermann in Timofeev et al., 1976, thin section # 05MZX-9, O29/3 (ef). (**G**) *Siphonophycus* spp., thin section # 14JLW-99-6, D35/3 (ef). (**H**) Unnamed trichome with flat and regular septa, thin section # 14JLW-108-4, N47/3 (ef). (**I**) *Obruchevella minor* Zhang, 1984, thin section # 14JLW-74-1, X39 (ef). (**J**) *Obruchevella blandita* Schenfil, 1980, thin section # 15HFL-15a-7, Q34 (ef). (**K**) *Salome svalbardensis* Knoll, 1982, thin section # 14JLW-101-5, A37/4 (ef). (**L** and **M**) *Salome hubeiensis* Zhang, 1986. (**L**) Thin section # 05MZX-9, G29 (ef). (**M**) Thin section # 14JLW-115-202, Q31 (ef). (**N**) Unnamed taxon with filament surrounded by coiled fibrils, thin section # 15HFL-19-1, O41 (ef).

unnamed species, and three possible new forms are described in the Systematic Paleontology section. Although *Megasphaera inornata* bears no ornamentation on the vesicle, it is also counted as an acanthomorphic acritarch species considering that other *Megasphaera* species are all ornamented.

To account for the impact of sampling intensity (i.e., number of thin sections prepared from each stratigraphic section) on the abundance of acanthomorph fossils, we calculated the average number of specimens per species per fertile thin section for each stratigraphic section. At each stratigraphic section, the total specimen number of each acanthomorph species was divided by the total number of thin sections yielding that species, resulting in the average abundance of that species per fertile thin section (AA/FTS). Excluding those species represented by only one specimen at a stratigraphic section, 72 measurements of AA/FTS were obtained. Among them, 45 AA/FTS measurements (62.5%) are 1.0 (e.g., *Dicrospinasphaera zhangii* at Jiulongwan, with eight specimens found from eight thin sections), nine measurements (12.5%) are between 1.0 and 1.5 (e.g., *Weissiella brevis* at Jiulongwan, with 28 specimens found from 19 thin sections), seven measurements (9.7%) are between 1.5 and 2.5 (e.g., *Tianzhushania spinosa* at Jiulongwan and Jinguadun, with 170 specimens found from 96 thin sections and 161 specimens found from 66 thin sections, respectively), and one measurement is higher than 2.5 (i.e., *Weissiella brevis* at Jinguadun, with 106 specimens found from 25 thin sections). The results show that AA/FTS varies by a factor of less than three.

At the Jiulongwan section, 18 genera and 31 species of acanthomorphic acritarchs were recognized from 37 fossiliferous horizons ranging from 2.8 m to 70.3 m above the cap dolostone (Table 2, Fig. 3). Twenty-nine acanthomorphic acritarch specimens have been found from the lowest chert nodule horizon (sample 14JLW-115, ~2.8 m above the cap dolostone), representing *Appendisphaera grandis* (Fig. 10M, N), *Dicrospinasphaera improcera* (Fig. 14C), *Megasphaera inornata*, *Tanarium gracilentum* (Fig. 19J), *Tianzhushania polysiphonia* (Fig. 20E, F), *Tianzhushania rara* (Fig. 20L, M), *Tianzhushania spinosa* (Fig. 21A, B), and *Tianzhushania* sp. indet. (Fig. 21M). Above the lowest chert nodule horizon, *Appendisphaera tenuis* (Fig. 11Q, R), *Dicrospinasphaera zhangii* (Fig. 14E), *Knollisphaeridium coniformum* (Fig. 15A–E) and *K. maximum* (Fig. 15K, L) occur within 5 m above the cap dolostone. Among all 31 taxa from the Jiulongwan section, 21 species (67.7%) occur within the basal 20 m of Member II. Species richness of acanthomorphic acritarchs from each horizon varies, with peaks (nine species) at three horizons: 8 m, 8.2 m, and 57.5 m above the cap dolostone. Abundance of acanthomorph taxa also varies stratigraphically, and *Tianzhushania spinosa* is by far the most abundant species, making up 26.1% of all acanthomorph specimens in the sampled interval of Member II.

At the Jinguadun section, 16 genera and 27 species of acanthomorphic acritarchs were recovered from chert nodules at ~9.5 m to ~65 m above the cap dolostone (Table 3, Fig. 4). Here, *Eotylotopalla dactylos*, *Megasphaera inornata*, and *Tianzhushania spinosa* occur at the lowest chert nodule horizon, and the latter two species are also the most long-ranging taxa. At this section, 16 species (59.3%) appeared within the lower 20 m of Member II. Acanthomorphic species richness peaks at 14.5 m above the cap dolostone, with a total of 13 species at this horizon. *T. spinosa* is also the most abundant species in the sampled interval of Member II at Jinguadun, making up 29.1% of all acanthomorph specimens.

At the Wuzhishan section, 21 genera and 51 species of acanthomorphic acritarchs were recovered from chert nodules at ~50 m to ~1.5 m below the Member II-III boundary (Table 4, Fig. 5). The chert horizon at ~49.4 m below the Member II-III boundary (sample 15HFL-2) yielded 26 acanthomorph species and records the highest species richness among all sampled horizons at this section. Acanthomorph abundance varies stratigraphically, and the overall abundance of each taxon at Wuzhishan is relatively low, with 45 species each represented by five or fewer specimens.

5. Discussion

5.1. Distribution of acanthomorph species and their stratigraphic significance

To understand the biostratigraphic significance of acanthomorph taxa, it is important to document the spatial consistency of their stratigraphic occurrence. For example, the *Tianzhushania spinosa* assemblage biozone was recognized in Member II in the Yangtze Gorges area on the basis of the consistent presence of *Tianzhushania spinosa* in Member II at multiple sections (Liu et al., 2013; Xiao et al., 2014b). Below we compare the range and relative abundance of Member II acanthomorphs across the Yangtze Gorges area, to explore their spatial variation and to assess their stratigraphic significance.

The taxonomic compositions of acanthomorphic acritarchs at the three studied stratigraphic sections show noticeable difference. Forty-one out of the 69 species (59.4%) found in this study occurred at only one section (Table 1; Fig. 25). Among these 41 species, 30 are from Wuzhishan (58.8% of all acanthomorph species at this section), showing a prominent difference in taxonomic composition of acanthomorphs between Wuzhishan and the other two sections. Although the sampled strata at Wuzhishan may not be exactly equivalent to the two other sections, 19 out of these 30 species at Wuzhishan (63.3%) occur in the lowermost 10 m of sampled strata (likely overlap with the upper part of sampled strata at Jiulongwan and Jinguadun). Therefore, the taxonomic difference between Wuzhishan and the two other studied sections may reflect true spatial variations, suggesting possible environmental, ecological, and/or taphonomic controls.

Despite the taxonomic differences, a number of species consistently occur in Member II at multiple stratigraphic sections in the Yangtze Gorges area, supporting their potential biostratigraphic significance. Among the 69 species found in this study, 12 (17.4%) occur in all three sampled sections (Table 1, Fig. 25). At least nine out of these 12 species have been reported from other sections of Member II in the Yangtze Gorges area (i.e., Liu and Moczydłowska, 2019; McFadden et al., 2009;

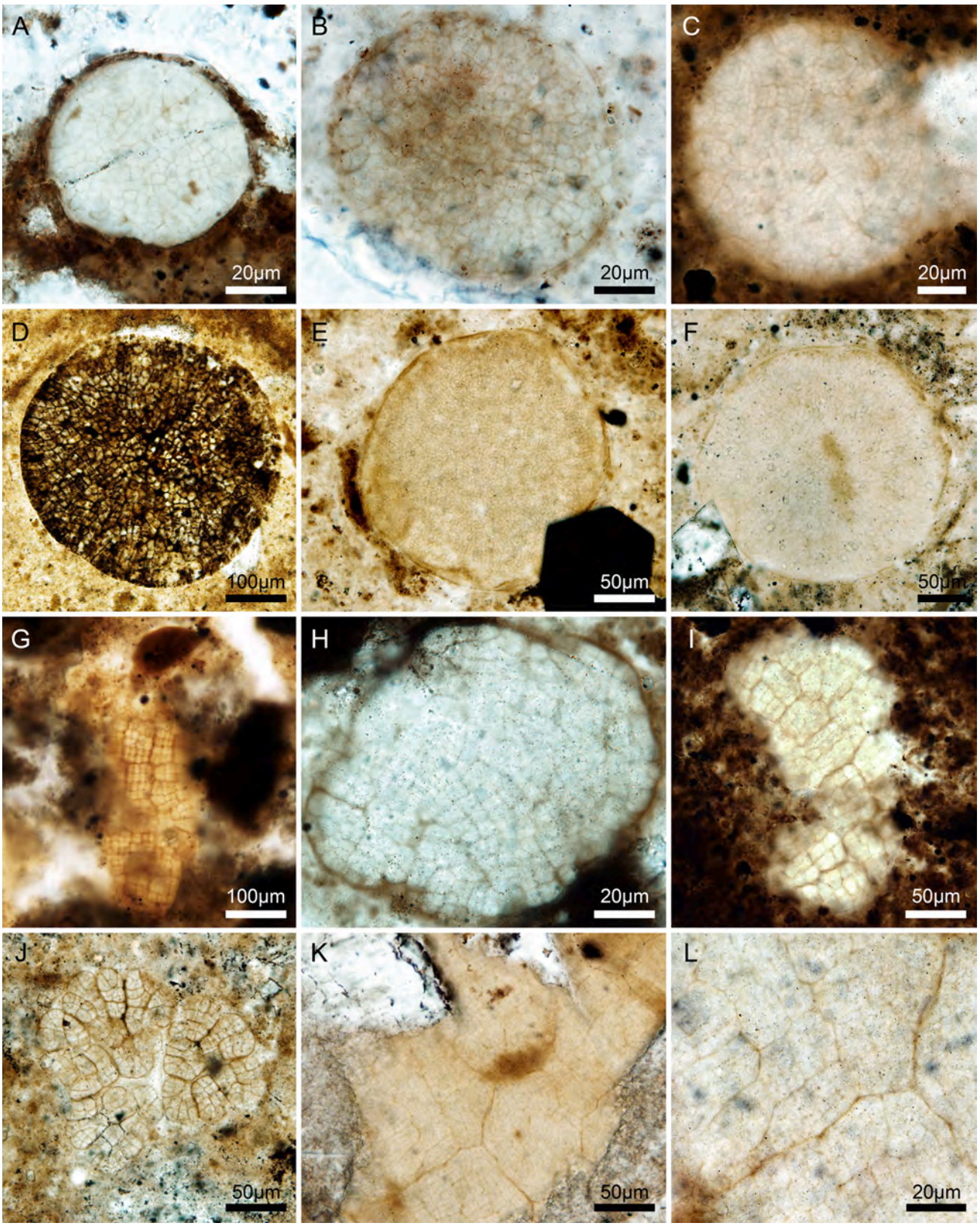

Fig. 8. Multicellular algae from Member II in the Yangtze Gorges area. (**A**–**C**) *Wengania minuta* Xiao, 2004. (**A**) Thin section # 14JLW-115-56, O31/1 (ef). (**B**) Thin section # 14JLW-115-106, L32/3 (ef). (**C**) Thin section # 14JLW-108-11, N36/2 (ef). (**D**) *W. globosa* Zhang, 1989, emend. Zhang et al., 1998, thin section # 05MZX-2a-6, H42/3 (ef). (**E** and **F**) *W. exquisita* Zhang et al., 1998. (**E**) Thin section # 16ZC32-31, J39/1 (ef). (**F**) Thin section # 14JLW-115-196, J34/3 (ef). (**G**–**L**) *Sarcinophycus radiatus* Xiao and Knoll, 1999. (**G**) Thin section # 14JLW-34a-9, L34/2 (ef). (**H**) Thin section # 15HFL-16a-3, H34 (ef). (**I**) Thin section # 14JLW-74-9, R37/4 (ef). (**J**) Thin section # 05MZX-3a-1, 23.8 × 150.4 (st). (**K** and **L**) thin section # 14JLW-115-50, L36/2 (ef). (**L**) Magnified view of (**K**), lower middle.

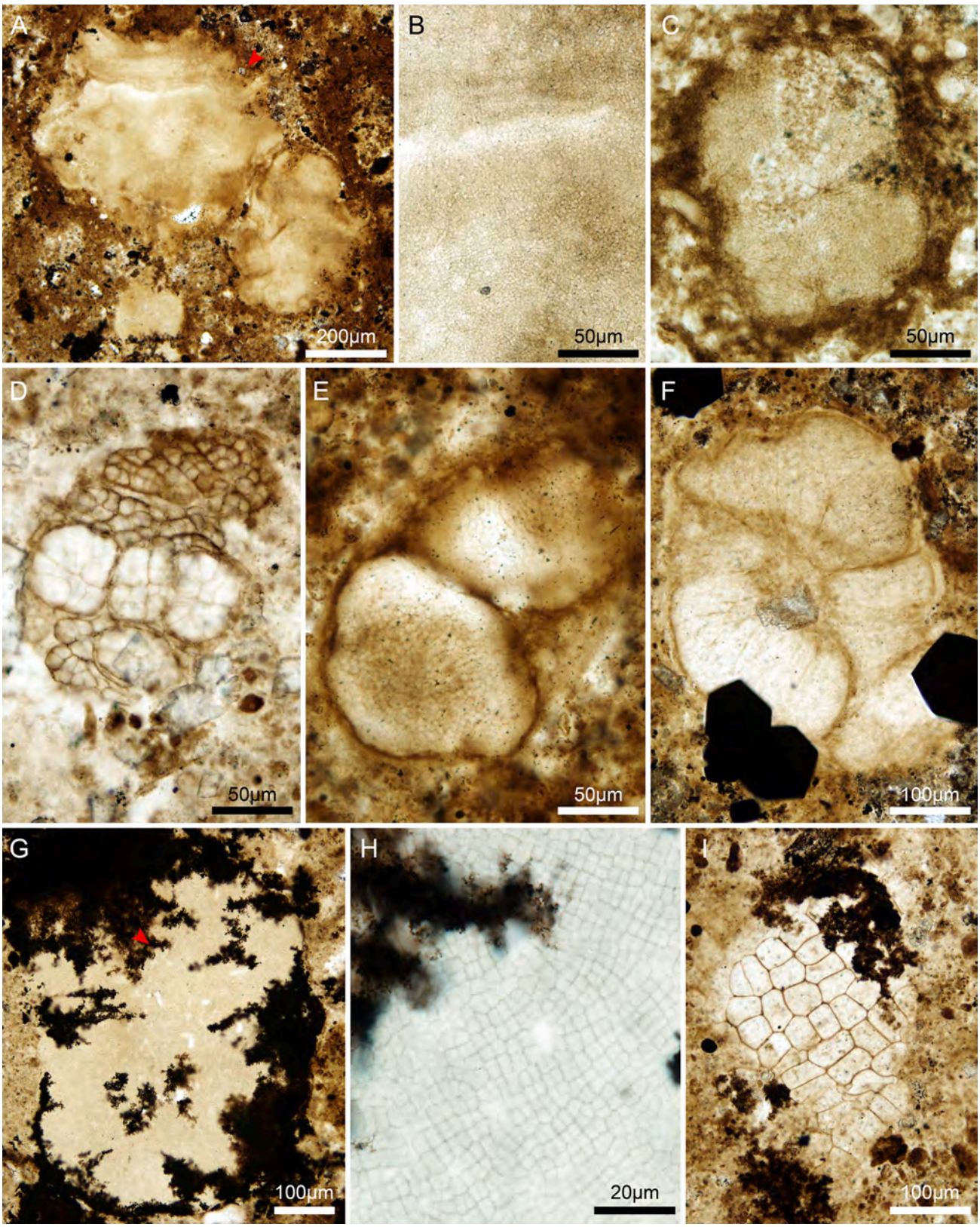

Fig. 9. Multicellular algae from Member II in the Yangtze Gorges area. (**A**–**C**) *Thallophycoides phloeatus* Zhang and Yuan, 1992 emend. Zhang et al., 1998. (**A** and **B**) Thin section # 15HFL-3-4, O42/2 (ef). (**B**) Magnified view of (**A**) (red arrowhead). (**C**) Thin section 15HFL-12a-d-1, 15.3 × 137.5 (st). (**D**) *Paramecia incognata* Zhang and Yuan, 1992, emend. Zhang et al., 1998, thin section 16ZC28-39, N42/1 (ef). (**E** and **F**) Thalli resemble *Gremiphyca corymbiata* Zhang et al., 1998. (**E**) Thin section 14JLW-93-16, S29/3 (ef). (**F**) Thin section # 16ZC33-41, O43/4 (ef). (**G** and **H**) Unnamed multicellular thallus without cell differentiation, thin section # 15HFL-2ad-3, 26.1 × 132.3 (st). (**H**) Magnified view of (**G**) (red arrowhead). (**I**) Unnamed multicellular form with relatively large cells, thin section # 16ZC33-39, R38 (ef). (For interpretation of the references to colour in this figure legend, the reader is referred to the web version of this article.)

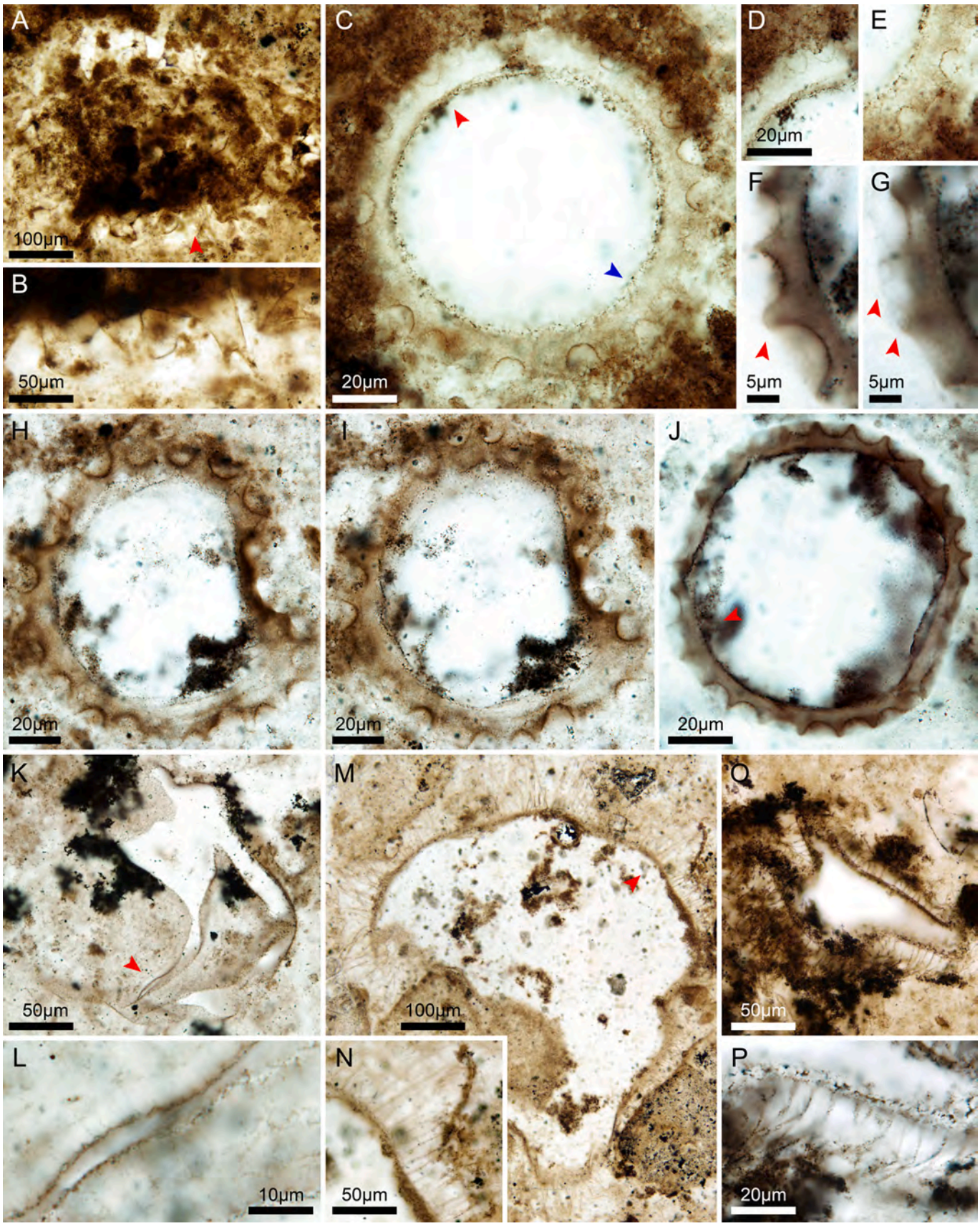

(caption on next page)

Fig. 10. Acanthomorphic acritarchs from Member II in the Yangtze Gorges area. (**A** and **B**) *Alicesphaeridium medusoidum* Zang in Zang and Walter, 1992 emend. Grey, 2005, PB23306, thin section # 14JLW-101-5, G36 (ef). (**B**) Magnified view of (**A**) (red arrowhead) at a different focal level. (**C**–**E**, **H**, **I**) *Annularidens inconditus* gen. et sp. nov. (**C**–**E**) Holotype, PB23307, thin section # 15HFL-12a-d-1, 26.8 × 145.3 (st). (**D** and **E**) Magnified views of (**C**) (red and blue arrowhead, respectively), showing the truncated terminations and deflated bases (with a concave profile) of the processes. Scale bar in (**D**) also applies to (**E**). (**H** and **I**) PB23309, thin section # 15HFL-14a-9, Q43/1 (ef), at different focal levels. (**F**, **G**, **J**) *Annularidens* sp., PB23308, thin section # 15HFL-16a-9, H37/3 (ef). (**F** and **G**) Magnified views of (**J**) (red arrowhead, at different focal levels), showing circular cross section of hollow processes (arrowheads). (**K** and **L**) *Appendisphaera clava* Liu et al., 2014b, PB23310, thin section # 15HFL-21a-9, J43/3 (ef). (**L**) Magnified view of (**J**) (red arrowhead). (**M-P**) *Appendisphaera grandis* Moczydłowska et al., 1993 emend. Moczydłowska, 2005. (**M** and **N**) PB23311, thin section # 14JLW-115–150, Q45 (ef). (**N**) Magnified view of (**M**) (red arrowhead). (**O** and **P**) PB23312, thin section # 15HFL-2a-2, K37/1 (ef). (**P**) Magnified view of (**O**) (lower right). (For interpretation of the references to colour in this figure legend, the reader is referred to the web version of this article.)

Zhou et al., 2007): *Appendisphaera grandis*, *Cavaspina acuminata*, *Dicrospinasphaera improcera*, *Distosphaera speciosa*, *Eotylotopalla dactylos*, *Ericiasphaera fibrilla*, *Knollisphaeridium maximum*, *Mengeosphaera chadianensis*, and *Tianzhushania spinosa*. Additionally, although only present at two of the three stratigraphic sections investigated in this study, seven species—*A. heliaca*, *A. tenuis*, *Cymatiosphaeroides kullingii*, *Dicrospinasphaera zhangii*, *K. coniformum*, *T. polysiphonia*, and *Yinitianzhushania tuberifera*—have also been reported from at least three other sections of Member II in the Yangtze Gorges area (Liu and Moczydłowska, 2019; McFadden et al., 2009; Ouyang et al., 2015; Zhou et al., 2007). The relatively common occurrence of the 16 species listed above highlights their potential significance in early Ediacaran biostratigraphy.

The first appearance datum (FAD) of the 16 species listed above appear to come in two waves or two groups, although more data are needed to confirm this pattern at other sections. The first group, including *Appendisphaera grandis*, *Dicrospinasphaera improcera*, *Knollisphaeridium coniformum*, *Tianzhushania polysiphonia*, *T. spinosa*, and *Yinitianzhushania tuberifera*, may have the lowest FADs among all Member II acanthomorphs in the Yangtze Gorges area. This group is recognized on the basis of fossil occurrence data from the lowest chert nodule horizons at Jiulongwan (this study) and Chenjiayuanzi (Liu and Moczydłowska, 2019), which are within 5 m above the cap dolostone at both sections (Fig. 26). At sections where the lowest chert nodule horizon is stratigraphically higher (e.g., Jinguadun, Wangfenggang, Niuping, northern Xiaofenghe), these species are also commonly found in the lowermost one or two fossiliferous chert nodule horizons, indicating their regionally consistent FADs. The second group includes *Appendisphaera heliaca*, *Cavaspina acuminata*, and *Ericiasphaera fibrilla*. Their FADs are all higher than species in the first group at Jiulongwan and Jinguadun, and generally higher than 20 m above the cap dolostone at other sections in previous reports (Fig. 26). The FADs of remaining taxa in the above-listed 16 species, such as *Dicrospinasphaera improcera* and *D. zhangii*, are variable among sections, suggesting that they are not particularly useful in biostratigraphic correlation. The last appearance data (LADs) of the above listed 16 species are also variable among sections, thus the LADs have limited value in stratigraphic subdivision. Previous studies reveal that some of these species, such as *Appendisphaera grandis* and *Cavaspina acuminata*, range upsection into the uppermost chert nodule horizons in Member III, so they may only serve as maximum age constraints.

Current data reveal no robust index fossils in the upper Member II, most likely due to the scarcity of fossiliferous chert nodule horizons in this interval. The FADs of four species (*Appendisphaera setosa*, *A. clava*, *Variomargosphaeridium varietatum*, *Weissiella* cf. *W. grandistella*) are stratigraphically higher than 50 m above the cap dolostone at Jinguadun, and they also occur at Wuzhishan where the sampled strata are assumed to represent middle–upper Member II. However, they have not been reported from upper Member II at other sections, and their stratigraphic significance remains to be demonstrated.

The variation in relative abundance of acanthomorphs at the three studied sections also reveals some consistent patterns, especially between the Jiulongwan and Jinguadun sections (Fig. 27). In lower Member II (i.e., the lower 50 m) at Jiulongwan and Jinguadun, *Tianzhushania* and *Yinitianzhushania* together account for more than 50% of acanthomorph relative abundance in all but one chert horizons, the exception being 39.5 m at Jinguadun. Also, *Weissiella brevis* becomes increasingly abundant in mid-lower Member II at both sections (18–32 m at Jiulongwan and 10–20 m at Jinguadun). In the upper part of Member II (i.e., higher than 50 m), the combined relative abundance of *Tianzhushania* and *Yinitianzhushania* decreases sharply at Jiulongwan and Jinguadun, to relative abundance levels broadly comparable with that of *Tianzhushania* at Wuzhishan (i.e., <20%). In the 57.2–57.7 m interval at Jiulongwan and the 61–65 m interval at Jinguadun, *Appendisphaera heliaca* is the most abundant acanthomorph species (with *Megasphaera inornata* excluded at Jinguadun). In upper Member II, the relative abundance of certain small acanthomorphs (≤100 μm in vesicle diameter, including *A. heliaca*, *Cymatiosphaeroides kullingii*, *Ericiasphaera fibrilla*, and all species of *Dicrospinasphaera*, *Distosphaera*, and *Eotylotopalla*) increases sharply at Jiulongwan and Jinguadun. The combined relative abundance of these small acanthomorphs also increases slightly from the basal to the middle part of sampled strata at Wuzhishan (Fig. 27).

Data from the three studied sections show that both the ranges and relative abundances of certain acanthomorph taxa from Doushantuo Member II may be stratigraphically useful. To establish the FAD/LAD sequence of these taxa in the Yangtze Gorges area requires a fuller documentation of the stratigraphic ranges at as many sections as possible. Also, additional abundance data from the Yangtze Gorges area are needed to test the stratigraphic pattern of acanthomorph relative abundance as revealed at the Jiulongwan and Jinguadun sections.

Most acanthomorph taxa that are predominant in the Doushantuo Formation in this study are only known from South China, aiding little to global biostratigraphic correlation. There are species in Member II of the Doushantuo Formation that occur globally and can be applied to the Ediacaran biostratigraphy on other continents, such as *Appendisphaera grandis* and *Variomargosphaeridium litoschum*, the latter of which is a nominal species of a biozone established in Australia (Grey, 2005). However, *A. grandis* is one of the most long-ranging species in the Doushantuo Formation (Liu and Moczydłowska, 2019), whereas the true stratigraphic range of *V. litoschum* is poorly constrained due to its low abundance. To resolve such problems, a consistent taxonomic scheme to minimize the influence of taphonomic bias, and more thorough investigation to fully document the stratigraphic ranges of these widely distributed species, are both required. However, it is also possible that the lower Doushantuo Formation may be stratigraphically older than

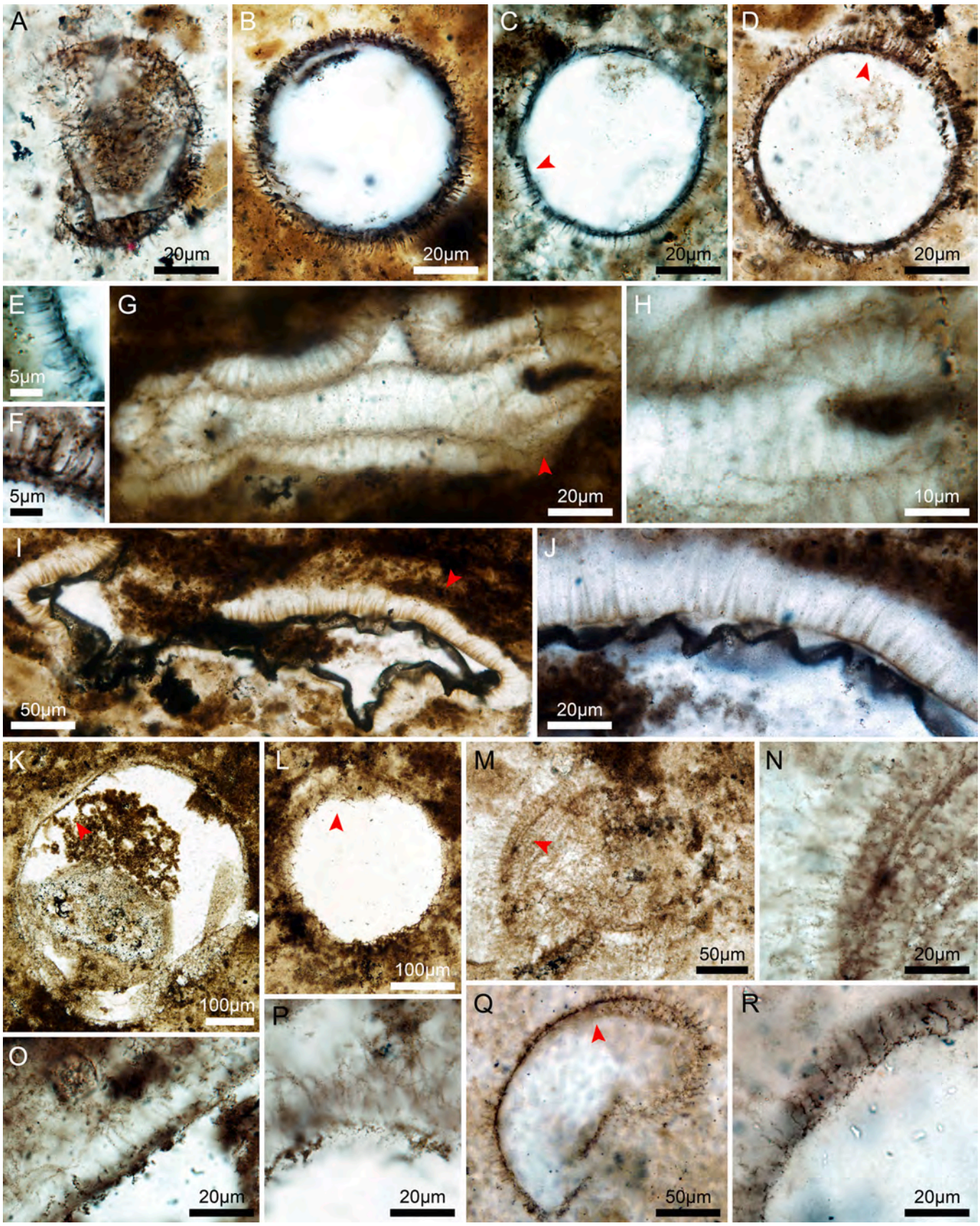

(caption on next page)

Fig. 11. Acanthomorphic acritarchs from Member II in the Yangtze Gorges area. (**A**–**F**) *Appendisphaera heliaca* (Liu and Moczydłowska, 2019) n. comb. (**A**) PB23313, thin section # 14JLW-99a-4, G44/3 (ef). (**B**) PB23314, thin section # 16ZC31-15, G40/3 (ef). (**C and E**) PB23315, thin section # 16ZC33-18, N28/2 (ef). (**D and F**) PB23316, thin section # 05MZX-8-5, S51/4 (ef). (**E** and **F**) Magnified views of (**C**) and (**D**) (red arrowheads), respectively. (**G** and **H**) *A. longispina* Liu et al., 2014b, PB23317, thin section # 15HFL-8-2, O39/1 (ef). (**H**) Magnified view of (**G**) (red arrowhead). (**I** and **J**) *A. magnifica* (Zhang et al., 1998) Liu et al., 2014b, PB23318, thin section # 05MZX-5-5, K48/1 (ef). (**J**) Magnified view of (**I**) (red arrowhead). (**K** and **O**) *A. setosa* Liu et al., 2014b, PB23319, thin section # 15HFL-12a-d, 27.9 × 148 (st). (**O**) Magnified view of (**K**) (red arrowhead). (**L**–**N**, **P**) *A. tabifica* Moczydłowska et al., 1993. (**L** and **P**) PB23320, thin section # 15HFL-2a-7, K32/4 (ef). (**P**) Magnified view of (**L**) (red arrowhead). (**M** and **N**) PB23321, thin section # 05MZX-2a-10, K34/3 (ef). (**N**) Magnified view of (**M**) (red arrowhead). (**Q** and **R**) *A. tenuis* Moczydłowska et al., 1993 emend. Moczydłowska, 2005, PB23322, thin section # 14JLW-33a-28, Q34/3 (ef). (**R**) Magnified view of (**Q**) (red arrowhead). (For interpretation of the references to colour in this figure legend, the reader is referred to the web version of this article.)

those well-studied acanthomorph-bearing strata outside South China (e.g., Australia and Siberia, see discussions in 5.2), making global biostratigraphic correlation of the lower Ediacaran strata a challenging task.

5.2. Rise of eukaryotes after the Marinoan glaciation

Terminal Tonian fossil records show a major crisis of eukaryotes before or at the onset of Cryogenian glaciations (Nagy et al., 2009; Riedman and Sadler, 2018). To date very few confirmed eukaryotic fossils have been reported from Cryogenian glacial deposits (Riedman et al., 2014; Ye et al., 2015), with more but still limited eukaryotic records from interglacial strata (e.g., Bosak et al., 2011; Cohen et al., 2020; Dalton et al., 2013; Moore et al., 2017; Riedman et al., 2014). It has been proposed that during Cryogenian time, eukaryotes may have managed to survive in restricted refugia such as the "cryoconite pans" (Hoffman, 2016). Geochemical studies revealed that primary productivity had recovered to some extent during the melting down of the Marinoan glaciation (Lang et al., 2016, 2018), which implies a rapid recovery of the marine ecosystem. However, the identity of these primary producers has not been identified, although biomarkers reveal stepwise increases in the sterane-hopane ratio after the Sturtian and Marinoan glaciations, suggesting a significant contribution of eukaryotes to the recovery of primary productivity (Bobrovskiy et al., 2020; Brocks et al., 2017).

The fossiliferous horizon 2.8 m above the cap dolostone at Jiulongwan provides some insights into the post-glacial recovery of eukaryotes. Astrostratigraphic tuning suggests that the 2.8 m horizon was deposited ~1.5 Ma after the termination of the Marinoan glaciation (Sui et al., 2018), which is consistent with the geochronological data from the lower Member II of the Doushantuo Formation in the Yangtze Gorges area (Condon et al., 2005). With eight acanthomorph species from this horizon, its species richness is comparable with or greater than that of pre-Cryogenian acritarch assemblages (Xiao and Tang, 2018). Furthermore, the occurrence of three species of multicellular algae at this horizon also indicates a rapid post-glacial diversification of eukaryotes. The occurrence of such a diverse fossil assemblage in the lowest chert nodule bed implies a still earlier appearance of these eukaryotic organisms, which has not been captured in the fossil record due to preservational bias related to the lack of chert nodules below this horizon (Muscente et al., 2015; Xiao et al., 2010).

The first appearance of eukaryotes represented by the FAD of specific acanthomorph species is considered as a potential criterion for the establishment of the Second Ediacaran Stage (SES) (Xiao et al., 2016). However, biostratigraphic data from this study suggest that the lowest occurrences of silicified acritarchs are strongly controlled by presence of chert nodules. Thus, caution is warranted when using the FAD of any acritarch species from this lowest chert horizon (e.g., *Tianzhushania spinosa*) to define the SES. Considering that the FAD of microscopic eukaryotes is only 2.8 m above the cap dolostone, one option is to define the SES at the top of the cap dolostone, although this would make the First Ediacaran Stage (FES) one of the shortest stages (e.g., <1 Ma, Zhou et al., 2019) in Earth history.

Following their first appearance at the 2.8 m horizon, acanthomorphic acritarchs continue to increase in taxonomic richness. In the basal 20 m of Member II, which is estimated to represent ~10 Myrs according to astronomical tuning of depositional cycles (Sui et al., 2018), acanthomorphic acritarchs have been found from seven sections in the Yangtze Gorges area (Fig. 26). At five of these seven sections, species with FADs in the basal 20 m make up more than half of all Member II species: the Wangfenggang section (15 of 20 species, 75.0%, Liu and Moczydłowska, 2019), the Chenjiayuanzi section (7 of 10 species, 70.0%, Liu and Moczydłowska, 2019), the Jiulongwan section (21 of 31 species, 67.7%, this study), the Jinguadun section (16 of 27 species, 59.3%, this study), and the Sixi section (14 of 16 species, 87.5%, McFadden et al., 2009). Since these data were collated from different studies rather than a composite succession, the conclusion is robust even if slightly different taxonomic treatments were used by different paleontologists. If data from different sections are combined to establish FADs of different taxa at a regional scale, the proportion of acritarch taxa that appear within the basal 20 m would be even greater [e.g., if data from the Jiulongwan and Jinguadun sections in this study are combined, the percentage of Member II species with FADs in the basal 20 m is 69.2% (27 of 39 species), higher than the percentage for any one of the two sections].

Whether there is a post-glacial environmental event that triggered the sudden rise of eukaryotes after the Marinoan glaciation is still unclear. Based on an investigation of the pyrite nodules preserved in the uppermost Nantuo Formation, Lang et al. (2018) proposed that enhanced continental weathering during the Marinoan deglaciation might have delivered abundant nutrients and sulfate into the ocean, resulting in sustained high primary productivity, ocean euxinia, and pyrite precipitation. Large amounts of pyrite and organic matter burial within a relatively short deglaciation period could lead to an increase of oxygen level in atmosphere and ocean water during the Cryogenian-Ediacaran transition, which may have triggered the eukaryote radiation shortly after the termination of the Marinoan glaciation. Nevertheless, the precise relationship between any rise in oxygen and the emergence of complex eukaryotes remains a matter of debate (Cole et al., 2020).

There may be a second diversification event in Member II, as revealed by the first appearance of species in strata higher than 50 m above cap dolostone at Jinguadun (Fig. 4) and the entire sampled strata at Wuzhishan (Fig. 5). The taxonomic evenness of the upper Member II (higher than 50 m above the cap dolostone) is higher than the lower Member II: the Pielou's evenness index (bootstrap resampling, 1000 simulations) is 0.63 ± 0.02 at Jiulongwan and 0.55 ± 0.02 at Jinguadun for the lower Member II, 0.86 ± 0.03 at Jiulongwan and 0.67 ± 0.04 at Jinguadun for the upper Member II, and 0.66 ± 0.03 at Wuzhishan for the sampled strata of Member II. The increase in evenness means that more taxa thrived and shared the ecological niche, and this may have led to ecologically more complex and stable communities. Strata that preserve the Weng'an biota in South China, which can be correlated with the upper Member II in the Yangtze Gorges area (Liu and Moczydłowska, 2019; Ouyang et al., 2019; Xiao et al., 2014b), also contain abundant and diverse acritarchs and other eukaryotes (Xiao et al., 2014a, 2014b), lending further support to a second episode of eukaryote diversification

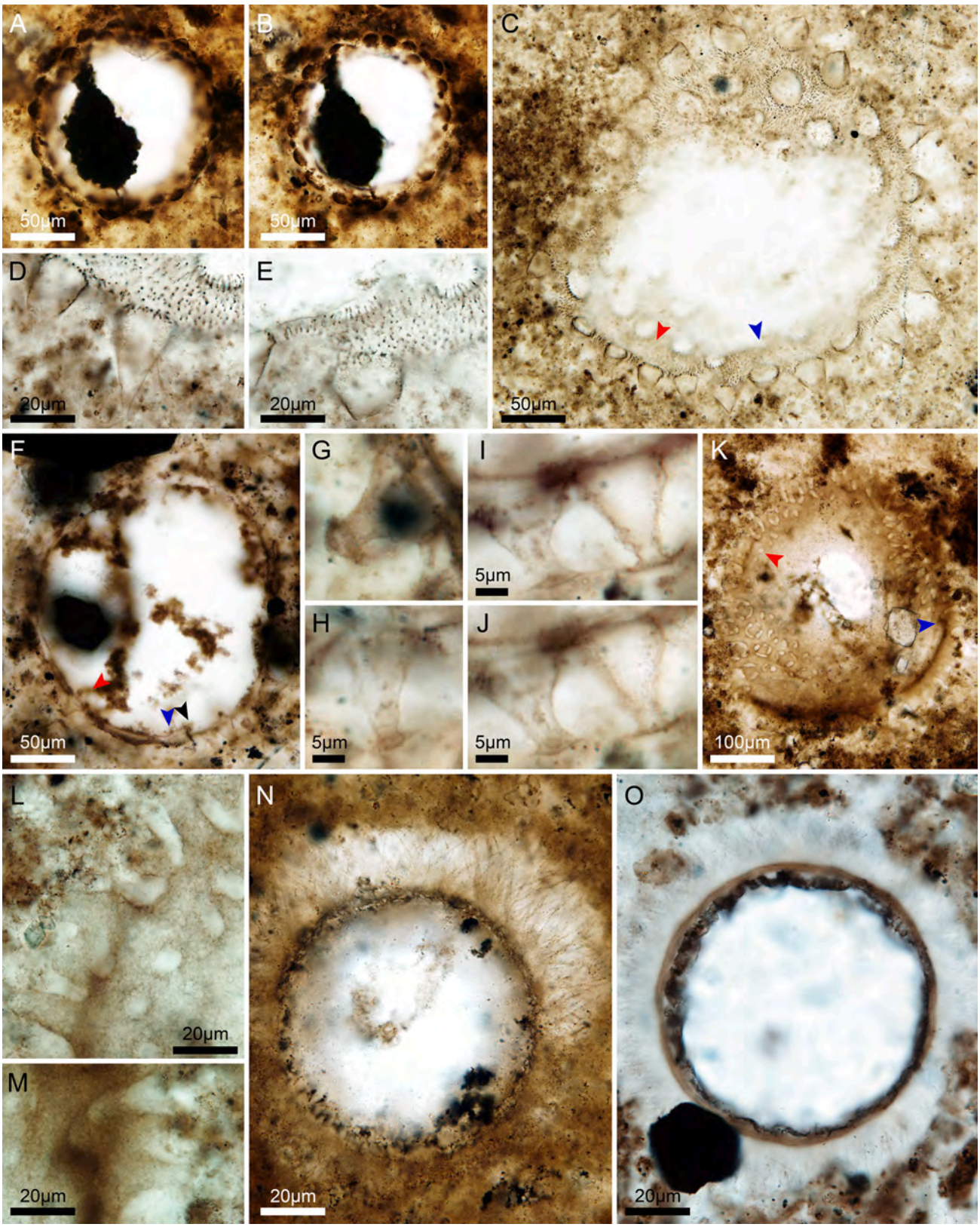

Fig. 12. Acanthomorphic acritarchs from Member II in the Yangtze Gorges area. (**A** and **B**) *Bacatisphaera baokangensis* Zhou et al., 2001 emend. Xiao et al., 2014b, PB23323, thin section # 15HFL-16-6, O41/4 (ef), at different focal levels. (**C**–**E**) *Bispinosphaera vacua* sp. nov., holotype, PB23324, thin section # 15HFL-8-1, O33/3 (ef). (**D** and **E**) Magnified views of (**C**) (red and blue arrowhead, respectively). (**F**–**J**) *Briareus borealis* Knoll, 1992, PB23325, thin section # 14JLW-113-8, P42/3 (ef). (**G** and **H**) Magnified views of (**F**) (red and blue arrowhead, respectively). Scale bar in (**H**) also applies to (**G**). (**I** and **J**) Magnified views of (**F**) (black arrowhead), at different focal levels. (**K**–**M**) *Briareus vasformis* Liu and Moczydłowska, 2019, PB23326, thin section # 05MZX-3a-14, G50 (ef). (**L** and **M**) Magnified views of (**K**) (red and blue arrowhead, respectively). (**N** and **O**) *Ericiasphaera fibrilla* Liu and Moczydłowska, 2019. (**N**) PB23327, thin section # 05MZX-8-1, C44/2 (ef). (**O**) PB23328, thin section # 14JLW-101a-1, H39/3 (ef). (For interpretation of the references to colour in this figure legend, the reader is referred to the web version of this article.)

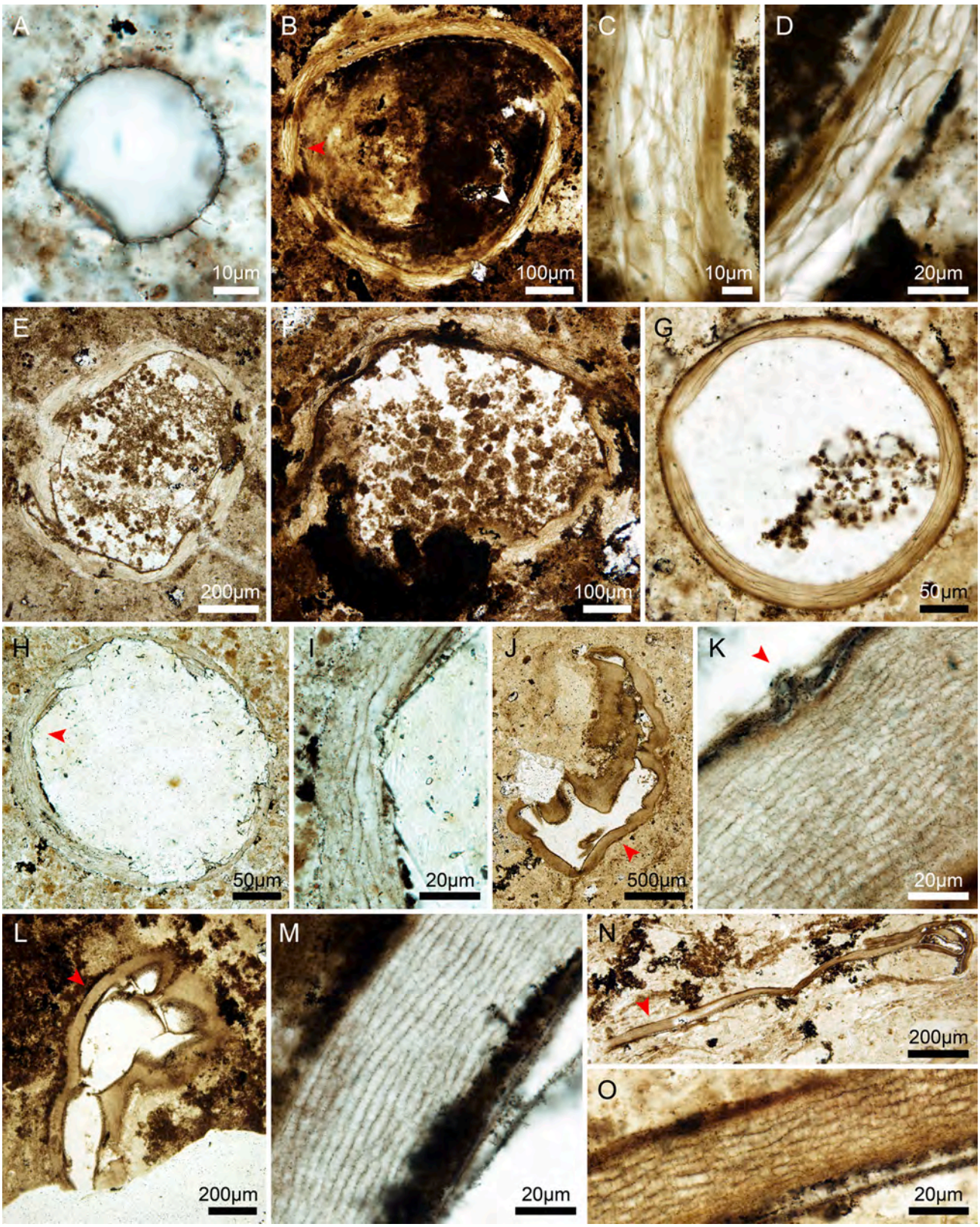

Fig. 13. Acanthomorphic acritarchs from Member II in the Yangtze Gorges area. (**A**) *Cavaspina acuminata* (Kolosova, 1991) Moczydłowska et al., 1993, PB23329, section # 14JLW-99a-8, N17/4 (ef). (**B**–**F**) *Crassimembrana crispans* gen. et sp. nov. (**B**–**D**) Holotype, PB23330, section # 15HFL-1-2, L36/2 (ef). (**C** and **D**) Magnified views of (**B**) (red and white arrowhead, respectively). (**E**) PB23331, thin section # 15HFL-12a-6, R33 (ef). (**F**) PB23332, thin section # 15HFL-3b-21, G34/4 (ef). (**G**–**I**) *Crassimembrana* cf. *C. crispans*. (**G**) PB23333, thin section # 16ZC28-37, O49/1 (ef). (**H** and **I**) PB23334, thin section # 05MZX-2a-3, J30 (ef). (**I**) Magnified view of (**H**) (red arrowhead). (**J**–**O**) *Crassimembrana multitunica* gen. et sp. nov. (**J** and **K**) PB23335, thin section # 15HFL-9a-4, R39/2 (ef). (**L** and **M**) Holotype, PB23336, thin section # 15HFL-9-4, H40/1 (ef). (**N** and **O**) PB23337, thin section # 15HFL-8b-15, K31/4 (ef). (**K**, **M**, **O**) Magnified views of (**J**, **L**, **N**) (red arrowheads), respectively. (For interpretation of the references to colour in this figure legend, the reader is referred to the web version of this article.)

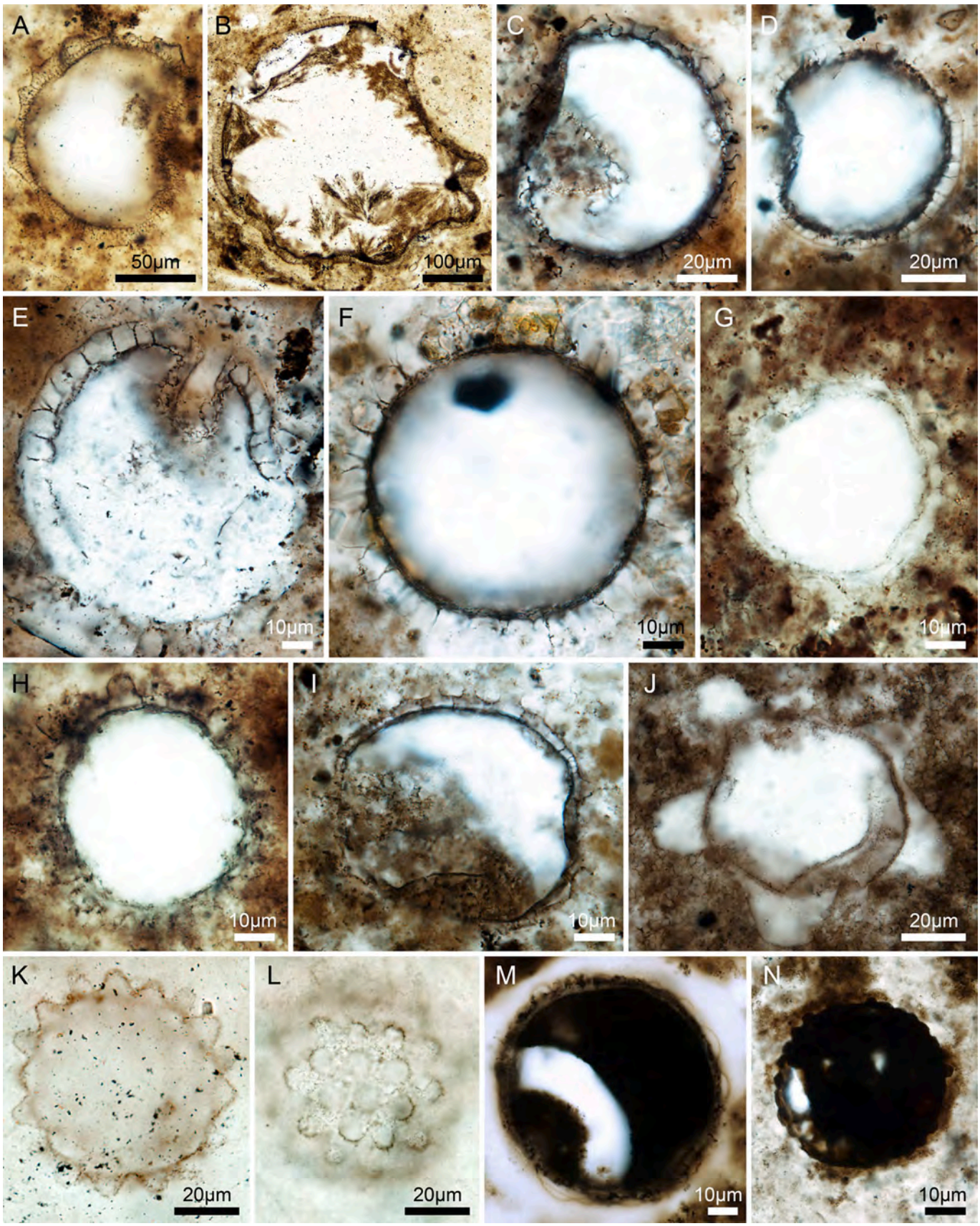

(caption on next page)

Fig. 14. Acanthomorphic acritarchs from Member II in the Yangtze Gorges area. (**A**) *Cymatiosphaeroides kullingii* Knoll, 1984 emend. Shang et al., 2019, PB23338, thin section # 14JLW-101-11, N49 (ef). (**B**) *Cymatiosphaeroides yinii* Yuan and Hofmann, 1998, PB23339, thin section # 15HFL-10a-1, N33/3 (ef). (**C** and **D**) *Dicrospinasphaera improcera* Liu and Moczydłowska, 2019. (**C**) PB23340, thin section # 14JLW-115-161, O41 (ef). (**D**) PB23341, thin section # 14JLW-93a-4, L18 (ef). (**E** and **F**) *Dicrospinasphaera zhangii* Yuan and Hofmann, 1998 emend. Liu and Moczydłowska, 2019. (**E**) PB23342, thin section # 14JLW-37-53, M33/3 (ef). (**F**) PB23343, thin section # 14JLW-99a-8, P25/1 (ef). (**G**) *Distosphaera speciosa* Zhang et al., 1998 emend. Liu and Moczydłowska, 2019, PB23344, thin section # 05MZX-9a-2, N36 (ef). (**H** and **I**) *Distosphaera jinguadunensis* sp. nov. (**H**) Holotype, PB23345, thin section # 05MZX-3a-5, 18.3 × 132.5 (st). (**I**) PB23346, thin section # 14JLW-57-2a-3, P35/4 (ef). (**J**–**L**) *Eotylotopalla dactylos* Zhang et al., 1998. (**J**) PB23347, thin section # 15HFL-7b-4, L32/2. (**K** and **L**) PB23348, thin section # 15HFL-8-8, L37/2 (ef), at different focal levels. (**M**) *E. delicata* Yin, 1987, PB23349, thin section # 05WH-24a, N49/3 (ef). (**N**) *E. strobilata* (Faizullin, 1998) Sergeev et al., 2011, PB23350, thin section # 15HFL-1-9, P29/3 (ef).

during the deposition of the upper Member II. This second wave of eukaryote diversification is also supported by the radiation of macroscopic, morphologically differentiated, and benthic eukaryotes in the Lantian biota, which is approximately equivalent in age to the upper Member II (Yuan et al., 2011).

An integration with Ediacaran acanthomorphs from outside South China can provide a global perspective on the evolution of eukaryotes after the Marinoan glaciation. Highly diverse Ediacaran acanthomorphs have been reported from fine-grained siliciclastic rocks in Australia, East European Platform, and Siberia (e.g., Golubkova et al., 2010; Grey, 2005; Vorob'eva et al., 2009). The Ediacaran Complex Acanthomorphic Palynoflora (ECAP) in Australia has been correlated with the acanthomorph assemblage zone in Member III of the Doushantuo Formation in the Yangtze Gorges area of South China (e.g., Liu et al., 2013), thus is stratigraphically higher than the fossil assemblage from Member II of the Doushantuo Formation reported in this paper. In the East European Platform, the Vychegda Formation yielding Ediacaran acanthomorphs has been correlated with the "Nepa Horizon" in Siberia (Golubkova et al., 2010), which might be correlated with the lower part of Zhuya Group that yields the Zhuya (Shuram) negative carbon isotopic excursion (Chumakov et al., 2007; Moczydłowska and Nagovitsin, 2012; Pokrovskii et al., 2006). Consequently, the Vychegda acanthomorphs are also younger than those from Member II, which is much older than the Shuram excursion. Ediacaran acanthomorphs from the "Ura Horizon" in eastern Siberia is thought to be lower than the "Nepa Horizon" and higher than the lower Member II acritarchs in South China (Moczydłowska and Nagovitsin, 2012). A recent study of the Oppokun Formation in Siberia reported the co-occurrence of Doushantuo-Pertatataka type acanthomorphs and early Cambrian shelly fossils, suggesting certain Ediacaran acanthomorphs may have a longer stratigraphic range than previously thought (Grazhdankin et al., 2020). In the Lesser Himalaya area of northern India, where the Ediacaran succession can be readily correlated with that in South China (Jiang et al., 2003b), acanthomorphs have been reported from the Infra Krol Formation and the overlying Krol A Formation (Joshi and Tiwari, 2016; Shukla and Tiwari, 2014; Tiwari and Knoll, 1994; Tiwari and Pant, 2004). The lowest acanthomorph record in Lesser Himalaya is in lower Infra Krol Formation (Tiwari and Pant, 2004), well below a carbon isotopic excursion that has been correlated with EN2 in South China (Kaufman et al., 2006), thus may be coeval with Member II acanthomorphs in the Yangtze Gorges area in South China. Acanthomorph horizons in the Lake Mjøsa area of southern Norway (Vidal, 1990) and Svalbard islands (Knoll, 1992) are sparse, and their stratigraphic correlation with the Ediacaran System in South China is uncertain. Acritarchs from the the Khuvsgul terrane of northern Mongolia was constrained to a latest Ediacaran age, much younger than the Doushantuo acanthomorphs (Anderson et al., 2017, 2019). Taken together, most Ediacaran acanthomorphs outside South China likely postdate Member II acanthomorphs from the Yangtze Gorges area, with the possible exception of those from the Infra Krol and Krol A formations in the Lesser Himalaya area. Current available data from South China and northern India seem to suggest that post-glacial radiation of Ediacaran acanthomorphs may have taken place shortly after the termination of the Cryogenian Marinoan global glaciation. However, given that lower Ediacaran strata around the world are poorly constrained by radiometric dates (Xiao and Narbonne, 2020) and most are not suitable for the preservation of organic-walled microfossils, the global picture of post-glacial diversification of Ediacaran acanthomorphs remains murky.

6. Conclusions

Abundant and diverse acanthomorphic acritarchs (24 genera and 69 species) have been found from Member II of the Doushantuo Formation at the Jiulongwan, Jinguadun, and Wuzhishan sections in the Yangtze Gorges area. More than half (59.4%) of the recovered species occur at only one section, indicating significant spatial variation in acanthomorph composition among sections in the Yangtze Gorges area. Despite the spatial variation, correlative acanthomorph FAD sequence in Member II is recognized in the Yangtze Gorges area: the FADs of *Appendisphaera grandis* and *Tianzhushania spinosa* are the lowest among all Member II species, whereas the FADs of *A. heliaca*, *Cavaspina acuminata*, and *Ericiasphaera fibrilla*, which are also present in lower Member II, are consistently higher than those of *T. spinosa*. Stratigraphic variations in relative abundance of acanthomorphs are also comparable among the three studied sections, especially between Jiulongwan and Jinguadun. For example, combined relative abundance of *Tianzhushania* and *Yinitianzhushania* decreases in upper Member II, where the relative abundance of certain small acanthomorphs (e.g., *A. heliaca*, species of *Dicrospinasphaera*) increases. Consistent acanthomorph occurrence and abundance data at multiple sections lend confidence to the biostratigraphic significance of those regionally traceable acanthomorph taxa.

Seven genera and ten species of eukaryotic microfossils (including acanthomorphic acritarchs and multicellular algae) occur at the lowest chert nodule horizon ~2.8 m above the cap dolostone at the Jiulongwan section, indicating the appearance of eukaryotic organisms shortly after the Marinoan glaciation. Diversification of the acanthomorphs occurred rapidly, with more than half of the Member II species appearing within the lower 20 m of Member II at multiple sections, which represents about 10 Myrs according to astrostratigraphic tuning. A possible second wave of diversification is recorded in the upper Member II, as evidenced by the appearance of new acanthomorph taxa and an increase in acanthomorph evenness in this interval. The integration of biostratigraphic data from South China and elsewhere forms a foundation to sharpen our view of post-glacial evolution of Ediacaran eukaryotes.

7. Systematic paleontology

Systematic description is given in alphabetic order for acanthomorphic acritarch taxa that are newly erected or emended in this study. Descriptive terms follow those in Xiao et al. (2014b). All illustrated

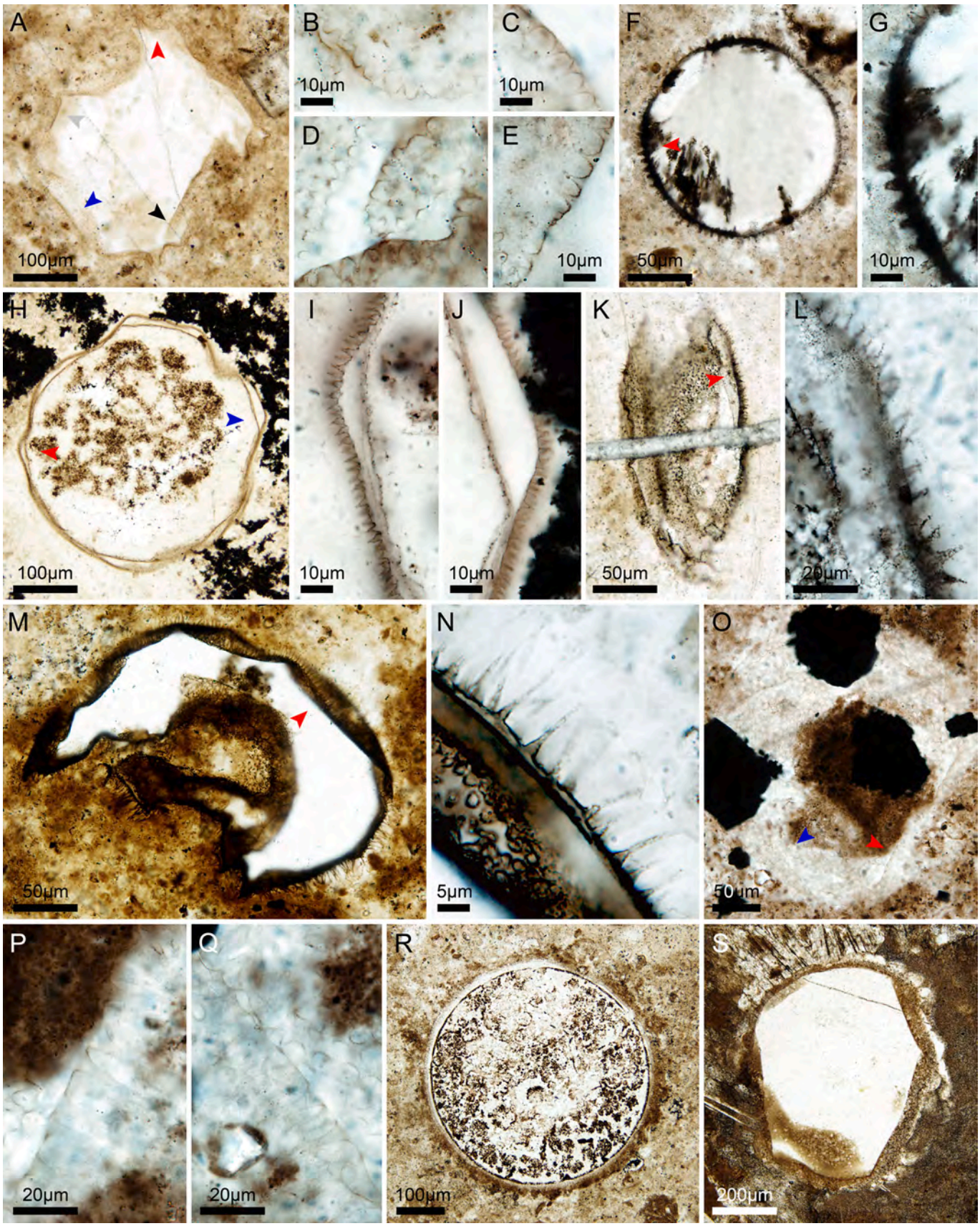

(caption on next page)

Fig. 15. Acanthomorphic acritarchs from Member II in the Yangtze Gorges area. (**A**–**E**, **H**–**J**) *Knollisphaeridium coniformum* Liu and Moczydłowska, 2019. (**A**–**E**) PB23351, thin section # 14JLW-34a-13, J35/3 (ef). (**B**–**E**) Magnified views of (**A**) (red, blue, black, and gray arrowhead, respectively). Scale bars in (**B**, **C**, **E**) also applies to (**D**). (**H**–**J**) PB23353, thin section # 15HFL-2a-2, M33/4 (ef). (**I** and **J**) Magnified views of (**H**) (red and blue arrowhead, respectively). (**F** and **G**) *K. denticulatum* Liu et al., 2014b, PB23352, thin section # 15HFL-9a-1, H41/1 (ef). (**G**) Magnified view of (**F**) (red arrowhead). (**K**–**N**) *K. maximum* (Yin, 1987) Willman and Moczydłowska, 2008. (**K** and **L**) PB23354, thin section # 14JLW-34a-6, U38/2 (ef). (**L**) Magnified view of (**K**) (red arrowhead). (**M** and **N**) PB23355, thin section # 16ZC32-15, H33/4 (ef). (**N**) Magnified view of (**M**) (red arrowhead). (**O**–**Q**) *K. longilatum* Liu et al., 2014b, PB23356, thin section # 14JLW-103a-14, O43/3 (ef). (**P** and **Q**) Magnified views of (**O**) (red and blue arrowhead, respectively). (**R** and **S**) *Megasphaera ornata* Xiao and Knoll, 2000 emend. Xiao et al., 2014b. (**R**) PB23357, thin section # 15HFL-12a-9, L35/2 (ef). (**S**) PB23358, thin section # 16ZC29-6, K41 (ef). (For interpretation of the references to colour in this figure legend, the reader is referred to the web version of this article.)

acanthomorphic acritarch specimens are housed at the Fossil Repository of Nanjing Institute of Geology and Palaeontology, Chinese Academy of Sciences, each with a museum catalog number prefixed with PB.

Annularidens gen. nov.

Type species. *Annularidens inconditus* gen. et sp. nov.

Diagnosis. Small vesicle with a thick wall. Processes arise from the outer surface of the thick wall, have a wide and deflated base with a concave profile, and taper gradually to a rounded, blunt or truncated termination. Process basally joined. Processes circular in transverse cross section.

Etymology. Derived from Latin *anularis*, ring-like, and *dens*, tooth; with reference to the terminal blunt or truncated processes surrounding the vesicle, forming a gearwheel-like outline in a cross-sectional view.

Remarks. This genus is recognized for its small vesicle size and tooth-like processes. This genus is somewhat similar to *Distosphaera* Zhang et al., 1998 emend. However, compared with *Distosphaera*, its vesicle is relatively larger (about 100 μm in vesicle diameter), its processes are wider and can be terminally truncated, and it lacks thin cylindrical processes between the inner and the outer walls of the vesicle.

Annularidens inconditus gen. et sp. nov.
(Fig. 10C–E, H, I)

Holotype. Specimen PB23307 (Fig. 10C–E) is designated as the holotype.

Diagnosis. A species of *Annularidens* gen. nov. with numerous processes that vary in basal width and terminal shape.

Etymology. Derived from Latin *inconditus*, irregular, with reference to the processes that differ in morphology on a single specimen.

Material. Two well-preserved specimens from Member II of the Doushantuo Formation, Wuzhishan section.

Description. Vesicle spheroidal and small, enveloped by a wall of even thickness. Processes arise from the outer surface of vesicle wall and taper gradually to rounded, blunt or truncated terminations, with deflated basal expansions. Processes are basally broad, deflated, and joined, with a hemispherical space between neighboring process tips, thus resulting in a scalloped outline of the vesicle in cross-sectional view. Processes are variable in basal and terminal width, but nearly uniform in length.

Dimension. Holotype: vesicle diameter, ~85 μm; membrane thickness, ~6 μm; processes length, 4.1–8.2 μm ($\bar{x}$ = 6.4 μm, n = 24, s.d. = 1.0 μm); process terminal truncation width, 2.4–31.3 μm ($\bar{x}$ = 10.2 μm, n = 18, s.d. = 7.5 μm; rounded or blunt tips are not included); space between process terminations, 6.8–12.2 μm ($\bar{x}$ = 9.6 μm, n = 24, s.d. = 1.5 μm). The other specimen (Fig. 10H, I): vesicle diameter, ~91 μm; membrane thickness, ~7 μm; processes length, 5.7–11.2 μm ($\bar{x}$ = 8.3 μm, n = 7, s.d. = 1.9 μm); process terminal truncation width, 3.0–16.0 μm ($\bar{x}$ = 6.0 μm, n = 7, s.d. = 4.2 μm); space between process terminations, 7.8–15.0 μm ($\bar{x}$ = 12.3 μm, n = 7, s.d. = 2.2 μm).

Remarks. The scalloped outline in cross-sectional view of *Annularidens inconditus* gen. et sp. nov. implies that, in three dimensions, this taxon might represent a vesicle with a thick vesicle wall ornamented with craters on the outer surface, in a way similar to the ornamented vesicle of *Megasphaera patella* Xiao et al., 2014b (see figs. 2 and 23 in Xiao et al., 2014b). However, it is clear that the scalloped outline of *A. inconditus* is not a manifest of vesicle ornaments; rather, it is defined by processes, which are circular in transverse cross section (see red arrowheads in Fig. 10F, G of *Annularidens* sp.). In addition, *M. patella* is much larger than *A. inconditus* in vesicle size.

Annularidens sp.
(Fig. 10F, G, J)

Material. One well-preserved specimen from Member II of the Doushantuo Formation, Wuzhishan section.

Description. Vesicle spheroidal and small, enveloped by a wall of even thickness. Evenly distributed, homomorphic processes arise directly from the outer surface of the wall, basally deflated and joined, and taper to rounded tips. There is no separation between the interior of the processes and the thick vesicle wall. Processes are circular in transverse cross section (red arrowheads in Fig. 10F, G).

Dimension. Vesicle diameter, ~80 μm; membrane thickness, ~4 μm; processes length, 4.0–5.2 μm ($\bar{x}$ = 4.5 μm, n = 13, s.d. = 0.3 μm); space between process terminations, 8.3–12.6 μm ($\bar{x}$ = 9.8 μm, n = 12, s.d. = 1.1 μm).

Remarks. This specimen is similar to *Annularidens inconditus* gen. et sp. nov. in vesicle size, thick vesicle wall, and tapering processes. However, it is different in its uniform processes with rounded or blunt, but not truncated terminations. This specimen also resembles *Distosphaera speciosa* Zhang et al., 1998 emend. except for its lack of thin, cylindrical processes within the outer wall. Since there is only one specimen in our collection, it is tentatively placed in an open nomenclature as *Annularidens* sp.

Appendisphaera Moczydłowska et al., 1993 emend. Moczydłowska, 2005

Type species. *Appendisphaera grandis* Moczydłowska et al., 1993 emend. Moczydłowska, 2005.

Appendisphaera heliaca (Liu and Moczydłowska, 2019) n. comb.
(Fig. 11A–F)

Synonyms.

2015 *Appendisphaera*? *hemisphaerica* Liu et al., 2014b; Ouyang et al., p. 215, pl. I, figs. 3, 5).

2019 *Knollisphaeridium heliacum* Liu and Moczydłowska, p. 118, fig. 63A–F.

Basionym. *Knollisphaeridium heliacum* Liu and Moczydłowska, 2019.

Material. Thirty-nine specimens from Member II of the Doushantuo Formation at the Jiulongwan and Jinguadun sections.

Description. Vesicle small and spheroidal, bearing densely distributed, hollow, uniform processes. Processes are very thin, cylindrical for most parts, but taper from slightly broadened bases to pointed tips. In some specimens, the processes are filled with dark material.

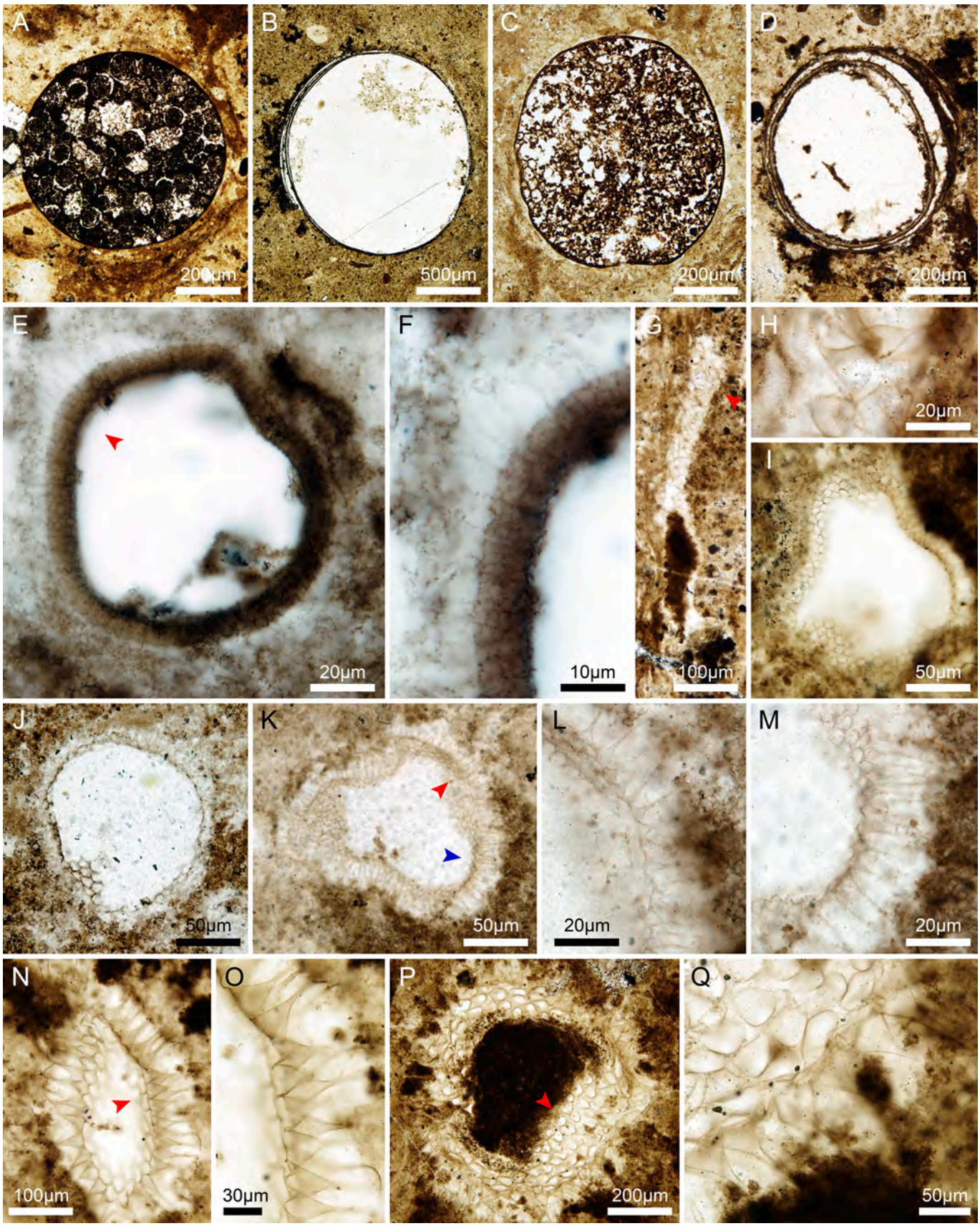

(caption on next page)

Fig. 16. Acanthomorphic acritarchs from Member II in the Yangtze Gorges area. (**A**–**D**) *Megasphaera inornata* Chen and Liu, 1986 emend. Xiao et al., 2014b. (**A**) PB23359, thin section # 15HFL-3ad-1, 42.6 × 136.4 (st). (**B**) PB23360, thin section # 15HFL-19a-1, N40/2 (ef). (**C**) PB23361, thin section # 16ZC28-8, O46 (ef). (**D**) PB23362, thin section # 14JLW-99a-12, Q37/4. (**E** and **F**) *Membranosphaera formosa* Liu and Moczydłowska, 2019, PB23363, thin section # 15HFL-2a-7, J37/3 (ef). (**F**) Magnified view of (**E**) (red arrowhead). (**G**–**J**) *Mengeosphaera chadianensis* (Chen and Liu, 1986) Xiao et al., 2014b. (**G** and **H**) PB23364, thin section # 05MZX-6-5, O35/4 (ef). (**H**) Magnified view of (**G**) (red arrowhead). (**I**) PB23365, thin section # 15HFL-17-5, M40/4 (ef). (**J**) PB23366, thin section # 16ZC33-16, V37/3 (ef). (**K**–**M**) *Mengeosphaera gracilis* Liu et al., 2014b, PB23367, thin section # 15HFL-7b-4, H43/3 (ef). (**L** and **M**) Magnified views of (**K**) (red and blue arrowhead, respectively). (**N**–**Q**) *Mengeosphaera grandispina* Liu et al., 2014b. (**N** and **O**) PB23368, thin section # 15HFL-8-8, L39/1 (ef). (**O**) Magnified view of (**N**) (red arrowhead). (**P** and **Q**) PB23369, thin section # 15HFL-17–3, N41/2 (ef). (**Q**) Magnified view of (**P**) (red arrowhead). (For interpretation of the references to colour in this figure legend, the reader is referred to the web version of this article.)

Dimension. Vesicle diameter, 45–71 μm ($\bar{x}$ = 59 μm, n = 37, s.d. = 6 μm); process length, 2.9–9.7 μm ($\bar{x}$ = 5.8 μm, n = 33, s.d. = 1.3 μm) or 5.7%–21.1% of the vesicle diameter ($\bar{x}$ = 10.0%, n = 33, s.d. = 2.6%); process basal width, 0.4–1.2 μm ($\bar{x}$ = 0.7 μm, n = 31, s.d. = 0.2 μm); space between processes, 1.0–2.8 μm ($\bar{x}$ = 1.5 μm, n = 15, s.d. = 0.5 μm).

Remarks. This species is transferred to the genus *Appendisphaera* Moczydłowska et al., 1993 emend. Moczydłowska, 2005 because its densely distributed, thin, hollow processes are characteristic of *Appendisphaera*. It was described as a species of *Knollisphaeridium* Willman and Moczydłowska, 2008 emend. Liu and Moczydłowska, 2019. However, the genus *Knollisphaeridium* was diagnosed by a medium-sized to large vesicle with short conical processes. The thin, relatively long (~10% of vesicle diameter), and slightly tapering processes of the current species better fit the diagnosis of the genus *Appendisphaera*. The vesicle size and relative process length (as a percentage of vesicle diameter) of *A. heliaca* are comparable to *A. minima* Nagovitsin and Faizullin in Nagovitsin et al., 2004 and *A. minutiforma* Grey, 2005, which have been synonymized by Liu and Moczydłowska (2019) with *A. tenuis* Moczydłowska et al., 1993 emend. Moczydłowska, 2005 and *A. tabifica* Moczydłowska et al., 1993 emend. Liu and Moczydłowska, 2019 respectively. However, *A. heliaca* is characterized by a constant vesicle size that is significantly smaller than that of *A. tenuis* and *A. tabifica*, and a process length to vesicle diameter ratio that is generally smaller than that of *A. tabifica* but larger than that of *A. tenuis*. Taking into consideration its distinctive morphology and abundance of specimens in our collection, *A. heliaca* is accepted as a distinct species.

Specimens identified as *Appendisphaera*? *hemisphaerica* Liu et al., 2014b by Ouyang et al. (2015, pl. I, Figs. 3, 5) are here reassigned to *A. heliaca* after re-examination of the specimens. Their vesicle size, process length, and process density are identical to those of *A. heliaca*, and their slightly domical basal expansions of processes may be a taphonomic artifact.

Bispinosphaera Liu et al., 2014b emend.

Type species. *Bispinosphaera peregrina* Liu et al., 2014b.

Emended diagnosis. Large and spheroidal vesicle with two types of processes (bimorphic), including (1) larger, hollow, and conical processes; and (2) densely distributed, shorter, solid, and hair-like processes.

Remarks. The original diagnosis of *Bispinosphaera* Liu et al., 2014b included interior tabulae or cross-walls in the large hollow processes. This feature is removed from the diagnosis to accommodate *B. vacua* sp. nov. Based on the emended diagnosis, *Bispinosphaera* can be differentiated from *Sinosphaera* Zhang et al., 1998 emend. Xiao et al., 2014b, which also has bimorphic processes but both types of processes are hollow. *Verrucosphaera* Liu and Moczydłowska, 2019 has both hollow and solid processes, but its solid processes are located on top of the hollow ones.

Bispinosphaera vacua sp. nov.
(Fig. 12C–E)

Holotype. Specimen PB23324 (Fig. 12C–E) is designated as the holotype.

Diagnosis. Vesicle large and spheroidal, bearing both hollow and solid processes. Hollow processes are large, conical, without internal structures, and communicate freely with vesicle cavity. Solid processes are hair-like, short, and largely equal in length. Both hollow and solid processes are evenly distributed and basally separate.

Etymology. Derived from Latin *vacuus*, blank, empty; with reference to the lack of internal structures in the large hollow processes.

Material. One well-preserved specimen from Member II of Doushantuo Formation, Wuzhishan section.

Description. Same as diagnosis.

Dimension. Vesicle and process size cannot be measured precisely because the specimen is tangentially cut in the thin section. Vesicle diameter is estimated to be 200–500 μm. Large hollow processes ≥45 μm in length, ≥28 μm in basal width, and ~13 μm in spacing. Short solid processes at least 3 μm in length, ≤0.5 μm in diameter, and ~1.5 μm in spacing.

Remarks. Although there is only one specimen, it is exceptionally well preserved and displays key morphological characters that distinguish it from *B. peregrina* Liu et al., 2014b, whose large conical processes are more sparsely distributed and decorated with internal tabulae or cross-walls.

Crassimembrana gen. nov.

Type species. *Crassimembrana multitunica* gen. et sp. nov.

Diagnosis. Vesicle large, enveloped by a thick multi-laminate wall. Fine laminations of the vesicle wall can be smoothly flattened, wrinkled, or bent to different degrees. The vesicle bears no process or any other ornamentation.

Etymology. Derived from Latin *crassus*, thick, and *membrana*, membrane; with reference to the multi-laminate wall enveloping the vesicle.

Remarks. Acritarchs with such large and thick-walled vesicles are rare in the Ediacaran Period and they are only known from chert nodules (e.g., *Granitunica mcfaddeniae* Liu et al., 2014b). This is partly because such thick vesicle walls are best seen in thin sections of permineralized specimens. If observed as acid-extracted individuals, similarly thick-walled specimens would appear as large and smooth-walled microfossils and would resemble and perhaps be misidentified as *Megasphaera* Chen and Liu, 1986 emend. Xiao et al., 2014b.

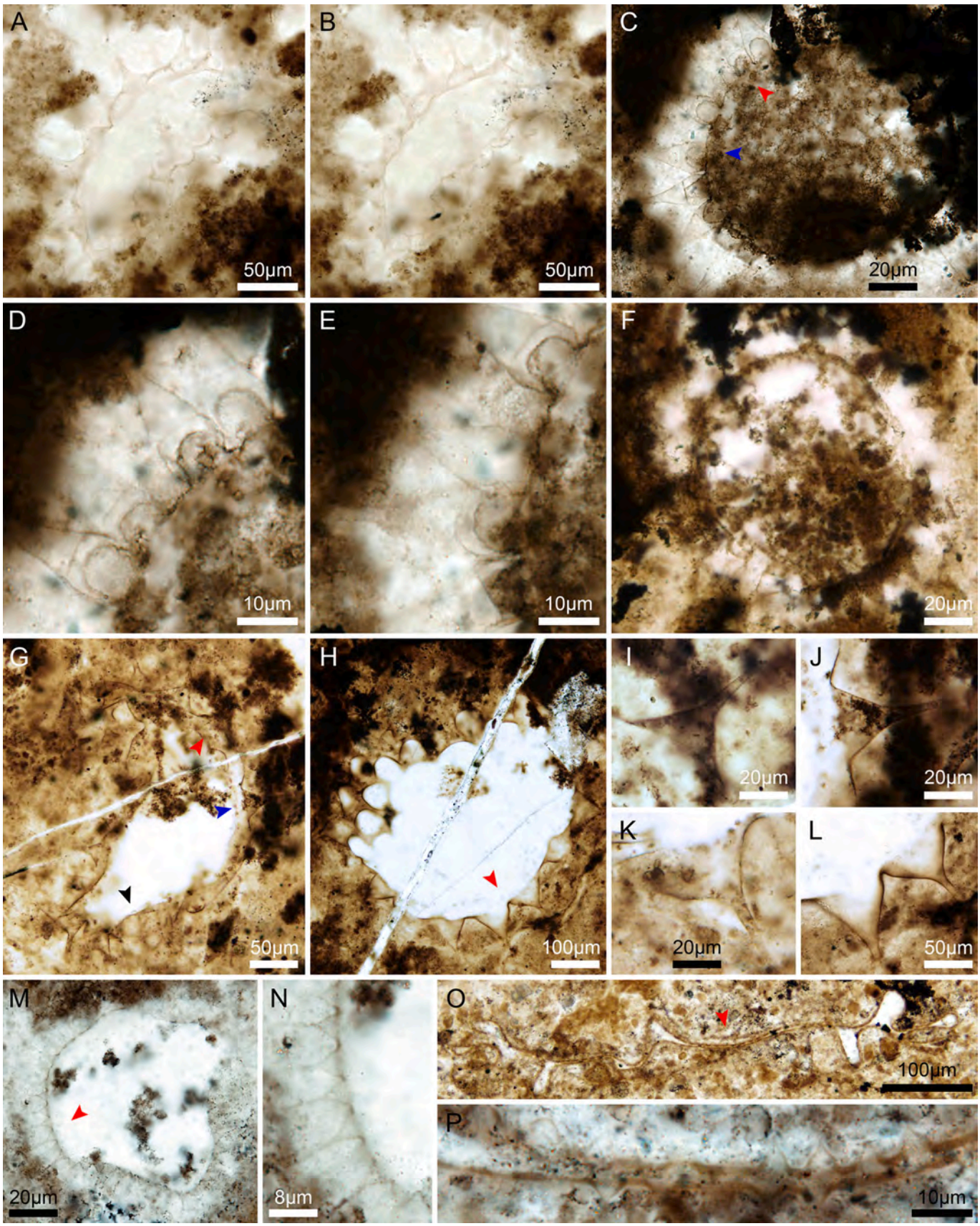

(caption on next page)

Fig. 17. Acanthomorphic acritarchs from Member II in the Yangtze Gorges area. (**A** and **B**) *Mengeosphaera latibasis* Liu et al., 2014b emend. Liu and Moczydłowska, 2019, PB23370, thin section # 15HFL-12-3, Q37/1 (ef), at different focal levels. (**C**–**F**) *M. matryoshkaformis* sp. nov. (**C**–**E**) Holotype, PB23371, thin section # 15HFL-2b-15, K41/1 (ef). (**D** and **E**) Magnified views of (**C**) (red and blue arrowhead, respectively). (**F**) PB23372, thin section # 15HFL-2-5, N34 (ef). (**G**, **I**–**K**) *Mengeosphaera* sp. 1, PB23373, thin section # 15HFL-8-8, H40/3 (ef). (**I**–**K**) Magnified views of (**G**) (red, blue, and black arrowheads, respectively). (**H** and **L**) *Mengeosphaera* sp. 2, PB23374, thin section # 15HFL-8-8, K41/4 (ef). (**L**) Magnified view of (**H**) (red arrowhead). (**M** and **N**) *M. minima* Liu et al., 2014b, PB23375, thin section # 15HFL-2ad-4, 31.4 × 119.4 (st). (**N**) Magnified view of (**M**) (red arrowhead). (**O** and **P**) *M. lunula* Liu and Moczydłowska, 2019, PB23376, thin section # 14JLW-47–2-10, V29/1 (ef). (**P**) Magnified view of (**O**) (red arrowhead). (For interpretation of the references to colour in this figure legend, the reader is referred to the web version of this article.)

Crassimembrana crispans gen. et sp. nov.
(Fig. 13B–F)

Holotype. Specimen PB23330 (Fig. 13B–D) is designated as the holotype.

Diagnosis. A species of *Crassimembrana* gen. nov. with a multilaminate vesicle wall consisting of thin, wavy, wrinkled, and somewhat irregular layers, that appear to anastomose so that in cross-sectional view they superficially resemble the dissepiments of cystiphyllid corals.

Etymology. Derived from Latin *crispans*, curly; with reference to wrinkled laminae that comprise the vesicle wall.

Material. One well-preserved and three fairly well-preserved specimens from Member II of Doushantuo Formation, Wuzhishan section.

Description. Vesicle large and deformed to different degrees, originally spherical. Vesicle wall of even thickness, and consists of numerous irregularly wrinkled thin layers or laminae. The outer layers are more strongly wrinkled than the inner ones, and they anastomose to form a spongy texture (Fig. 13C, D), resembling the dissepiments of cystiphyllid corals (e.g., Berkowski and Zapalski, 2018). The inner layers are more regularly and more densely arranged.

Dimension. Holotype: vesicle diameter, ~525 μm; vesicle wall thickness, ~36 μm. Other specimens: vesicle diameter, 555–705 μm (n = 2); vesicle wall thickness, 33.5–69.7 μm (measured on one specimen illustrated in Fig. 13F).

Remarks. This species is erected for its distinctive vesicle wall consisting of wrinkled multi-laminae. These wrinkled layers are very well preserved with sharp boundaries (Fig. 13C, D). Petrographic observation under cross polarized light showed that the spongy texture within the vesicle wall has no relation with crystal boundaries of micro-quartz minerals, suggesting that the wrinkled layers are primary structures rather than taphonomic artifacts related to recrystallization (e.g., Brasier et al., 2005).

Crassimembrana cf. *C. crispans*
(Fig. 13G–I)

Material. One well- and one fairly well-preserved specimens from Member II of Doushantuo Formation, Jinguadun section.

Description. Vesicle large and spherical, enveloped by a thick wall consisting of fine layers that are bent gently and in contact with each other.

Dimension. Vesicle diameter, 210–256 μm; vesicle wall thickness, 24.2–25.7 μm.

Remarks. The two specimens illustrated in Fig. 13G–I are similar to *Crassimembrana crispans* gen. et sp. nov in having a thick vesicle wall consisting of wavy layers. However, their vesicles are smaller, and their vesicle walls are thinner and consist of more gently bent laminae. Thus, they are tentatively placed in an open nomenclature as *Crassimembrana* cf. *C. crispans*.

Crassimembrana multitunica gen. et sp. nov.
(Fig. 13J–O)

Synonym.
2017 possible *Tianzhushania spinosa*, Hawkins et al., fig. 7A, B.
partim 2019 *Laminasphaera capillata* Liu and Moczydłowska, p. 124, fig. 67A–H.

Holotype. Specimen PB23336 (Fig. 13L, M) is designated as the holotype.

Diagnosis. A species of *Crassimembrana* gen. nov. with a thick vesicle wall consisting of regularly spaced and finely-laminated layers.

Etymology. Derived from Latin *multi*, many, and *tunica*, coat; with reference to the multilayered vesicle wall.

Material. Nine well- to fairly well-preserved specimens from Member II of Doushantuo Formation, Wuzhishan section.

Description. Vesicle large and originally spherical but deformed to different degrees. The vesicle is enveloped by a thick and finely laminated wall. The laminae are flat or slightly wavy, mostly parallel to each other, and evenly spaced. Neighboring laminae are occasionally bent and make contact. In one specimen, the innermost laminae are folded to form a pointed cusp (red arrowhead in Fig. 13K), but this may be a taphonomic artifact because other laminae in this specimen are not folded in a similar fashion.

Dimension. Vesicle diameter estimated to be ≥1 mm. Holotype, vesicle wall thickness, ~58.0 μm; lamina spacing, ~3.5 μm. Other specimens, vesicle wall thickness, 22.2–104.0 μm ($\bar{x}$ = 53.4 μm, n = 7, s.d. = 23.5 μm); lamina spacing, 2.0–4.2 μm ($\bar{x}$ = 2.9 μm, n = 8, s.d. = 0.8 μm).

Remarks. *Crassimembrana multitunica* gen. et sp. nov. is recognized for its distinctively large vesicle and finely-laminated vesicle wall. *Megasphaera* also has a large vesicle, but its vesicle wall is not multilayered, and some *Megasphaera* species have sculptures of various shapes on the vesicle. *Tianzhushania* Yin and Li, 1978 emend. Yin et al., 2008 and *Yinitianzhushania* Xiao et al., 2014b both have a multilaminate layer surrounding the vesicle wall, but they also have hollow processes that penetrate the multilaminate layer (Fig. 21A–M, 23O, P). Hawkins et al. (2017) illustrated a specimen identified as possible *Tianzhushania spinosa* (their fig. 7A, B). This specimen is characterized by a thick multilaminate vesicle and lacks discernable processes. It is likely a poorly preserved specimen of *Crassimembrana multitunica*.

Two specimens identified as *Laminasphaera capillata* Liu and Moczydłowska, 2019 are here reassigned to *Crassimembrana multitunica* gen. et sp. nov. The holotype of *L. capillata* has a much thinner, double-layered vesicle wall with numerous processes. The two specimens in question (fig. 67A–H of Liu and Moczydłowska, 2019), however, bear no processes even though the multi-layered vesicle wall is exceptionally well-preserved with a thickness of ~20 μm. Thus, we consider the lack of processes in these specimens as a biological feature rather than a taphonomic artifact, and they are reclassified as *C. multitunica*.

Distosphaera Zhang et al., 1998 emend.

Type species. *Distosphaera speciosa* Zhang et al., 1998 emend. Liu and Moczydłowska, 2019.

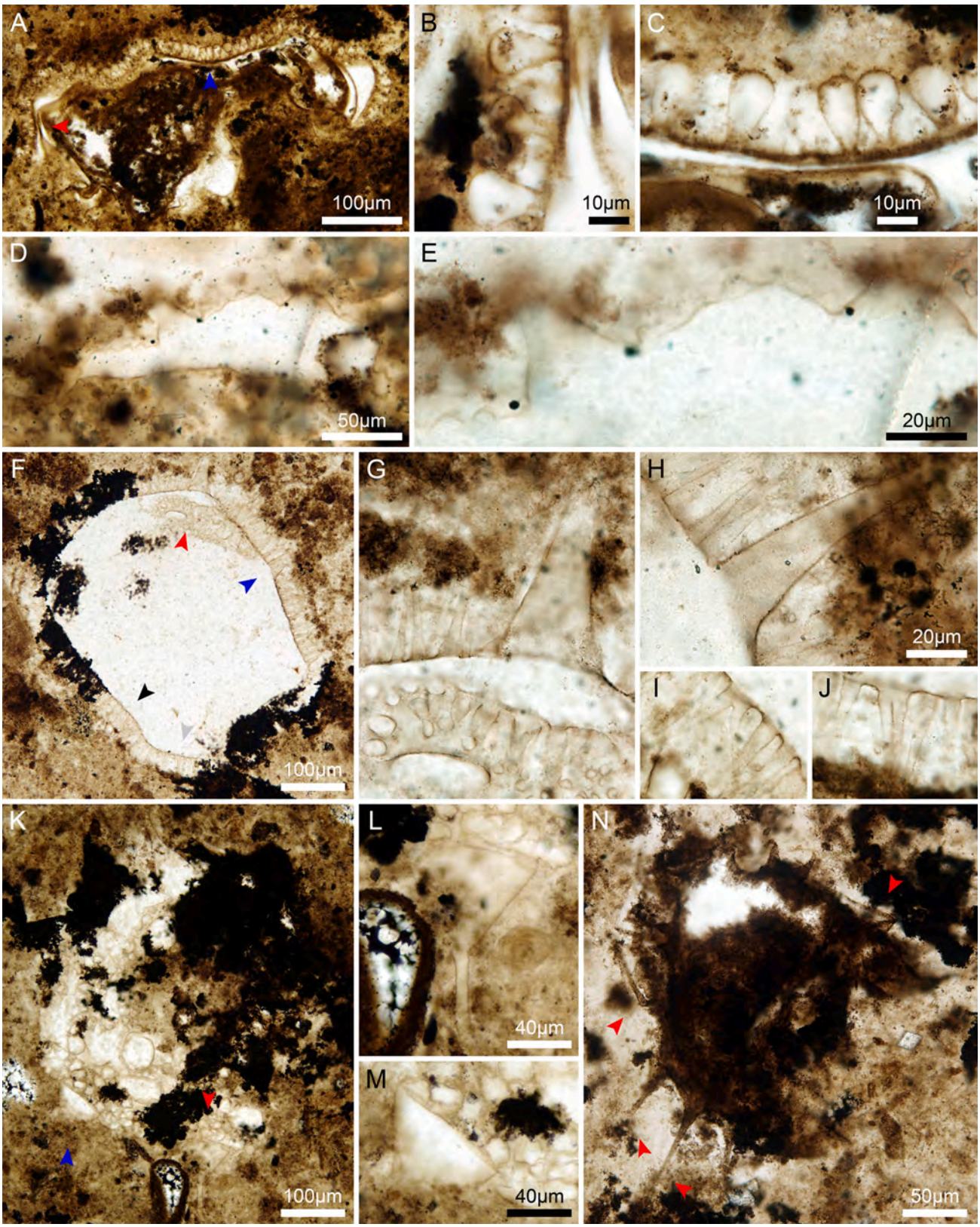

Fig. 18. Acanthomorphic acritarchs from Member II in the Yangtze Gorges area. (**A**–**C**) *Papillomembrana compta* Spjeldnaes, 1963 emend. Vidal, 1990, PB23377, thin section # 15HFL-2ad-3, 34.9 × 146.1 (st). (**B** and **C**) Magnified views of (**A**) (red and blue arrowhead, respectively). (**D** and **E**) *Sinosphaera speciosa* (Zhou et al., 2001) Xiao et al., 2014b, PB23378, thin section # 05WH-9b, C30/1 (ef). (**E**) Magnified view of (**D**) (upper central). (**F**–**J**) *S. asteriformis* Liu et al., 2014b, PB23379, thin section # 15HFL-2b-15, J36/3 (ef). (**G**–**J**) Magnified views of (**F**) (red, blue, black, and gray arrowhead, respectively). Scale bar in (**H**) also applies to (**G**, **I**, **J**). (**K**–**M**) *Sinosphaera* sp., PB23380, thin section # 15HFL-2ad-8, 18.7 × 135.4 (st). (**L** and **M**) Magnified views of (**K**) (red and blue arrowhead, respectively). (**N**) *Tanarium* cf. *T. conoideum*, PB23381, thin section # 15HFL-2b-10, L39/2 (ef). (For interpretation of the references to colour in this figure legend, the reader is referred to the web version of this article.)

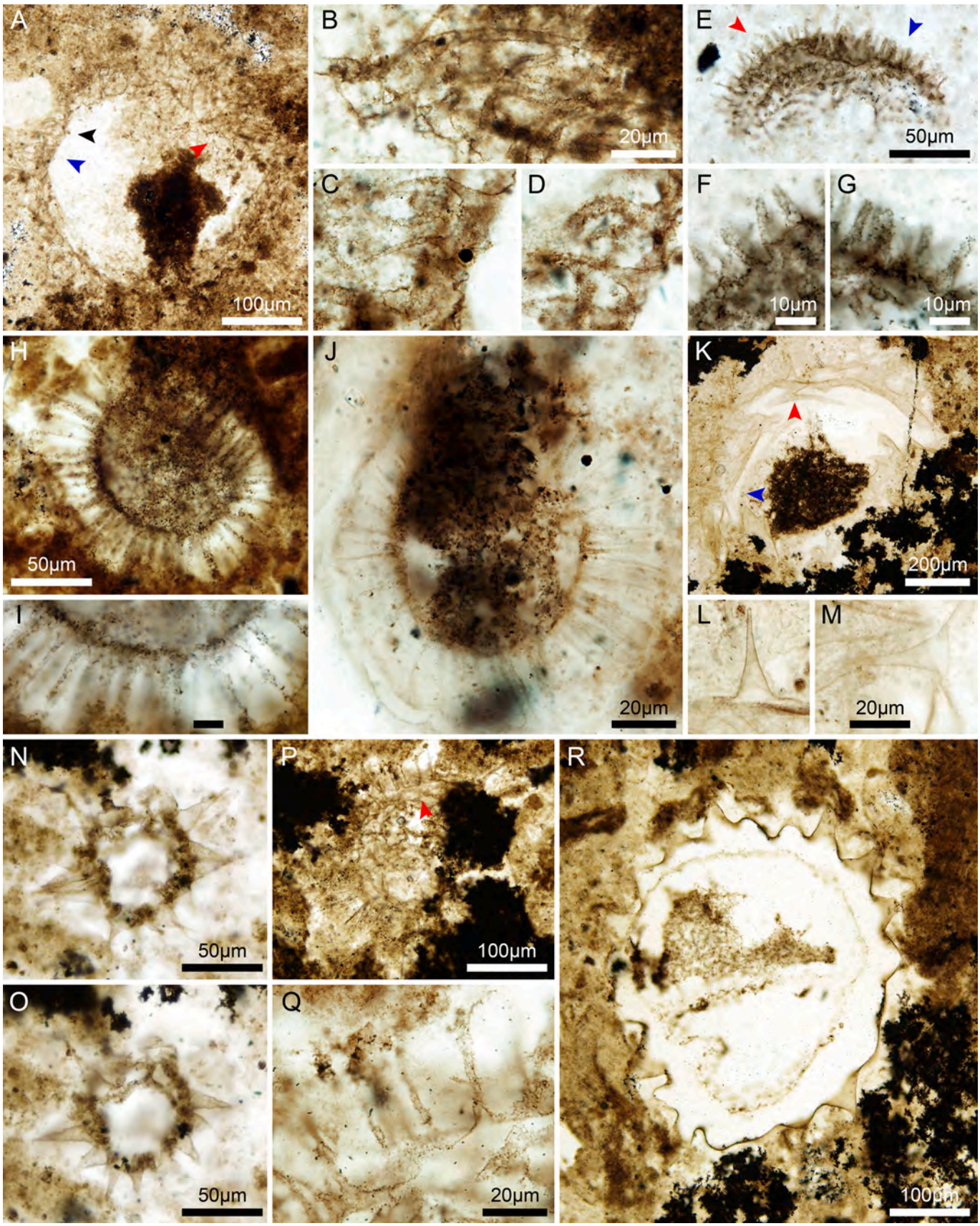

(caption on next page)

Fig. 19. Acanthomorphic acritarchs from Member II in the Yangtze Gorges area. (**A**–**D**) *Tanarium capitatum* Liu and Moczydłowska, 2019, PB23382, thin section # 15HFL-2b-19, K40 (ef). (**B**–**D**) Magnified views of (**A**) (red, blue, and black arrowheads, respectively). Scale bar in (**B**) also applies to (**C** and **D**). (**E**–**G**) *T. digitiforme* (Nagovitsin and Faizulin in Nagovitsin et al., 2004) Sergeev et al. (2011) PB23383, thin section # 15HFL-12a-7, J41/4 (ef). (**F** and **G**) Magnified views of (**E**) (red and blue arrowhead, respectively). (**H**–**J**) *T. gracilentum* (Yin in Yin and Liu, 1988) n. comb. emend. (**H** and **I**) PB23384, thin section # 14JLW-47-2-d-3, 14.3 × 124 (st). (**I**) Magnified view of (**H**) (lower middle). (**J**) PB23385, thin section # 14JLW-115-179, E37/4 (ef). Scale bar in (**I**) represents 10 μm. (**K**–**M**) *T. pilosiusculum* Vorob'eva et al., 2009, PB23386, thin section # 15HFL-2-4, J36 (ef). (**L** and **M**) Magnified views of (**K**) (red and blue arrowhead, respectively). (**N** and **O**) *T. obesum* Liu et al., 2014b, PB23387, thin section # 15HFL-2a-2, N35/3 (ef), at different focal levels. (**P** and **Q**) *Tanarium pluriprotensum* Grey, 2005, PB23388, thin section # 15HFL-2-5, M41/1 (ef). (**Q**) Magnified view of (**P**) (red arrowhead). (**R**) *Tanarium tuberosum* Moczydłowska et al., 1993, PB23389, thin section # 15HFL-8-2, J34 (ef). (For interpretation of the references to colour in this figure legend, the reader is referred to the web version of this article.)

Emended diagnosis. Vesicle small, spheroidal, with thin, hollow, cylindrical processes evenly distributed around the vesicle. The cylindrical processes are equal in length and support an outer layer at their distal ends. Hollow processes arise from this outer layer and are open to the inter-space between the outer layer and the vesicle.
Remarks. This emendation is based on the emendation by Liu and Moczydłowska (2019), in which the inner cylindrical processes are re-described as hollow. The new emendation adopted here removes the tapering, conical morphology of outer processes as a diagnostic feature of *Distosphaera*, so that *Distosphaera jinguadunensis* sp. nov. with cylindrical outer processes described below can also be accepted as a species of this genus.

Distosphaera jinguadunensis sp. nov.
(Fig. 14H, I)

Holotype. Specimen PB23345 (Fig. 14H) is designated as the holotype.
Diagnosis. A species of *Distosphaera* Zhang et al., 1998 emend. in which the outer processes are cylindrical with rounded or blunt terminations.
Etymology. With reference to the type locality (Jinguadun section) of this species.
Material. Four fairly well-preserved and four poorly-preserved specimens from Member II of Doushantuo Formation at the Jiulongwan and Jinguadun sections.
Description. Vesicle small, bearing two vesicle walls, each ornamented with cylindrical processes. The inner processes are very thin, equal in length, and arise directly from the inner wall. The inner processes support a continuous thin outer wall. The outer processes are robust, cylindrical, terminally rounded or blunt, arise from the outer wall, and communicate freely with the inter-space between the inner and the outer walls. Both the inner and outer processes are evenly distributed. Typically there is only one inner process between two neighboring outer processes.
Dimension. Holotype: vesicle diameter, ~48 μm; outer process length, ~5.8 μm; outer process diameter, ~5.7 μm; outer process spacing, ~3.3 μm; inner process length, ~2.0 μm; inner process diameter, ~0.4 μm. Other specimens: vesicle diameter, 42–58 μm ($\bar{x}$ = 48 μm, n = 7, s.d. = 5 μm); outer process length, 2.1–5.5 μm ($\bar{x}$ = 4.0 μm, n = 7, s.d. = 1.1 μm) and 4.5%–12.3% of the vesicle diameter ($\bar{x}$ = 8.4%, n = 7, s.d. = 2.4%); outer process diameter, 2.6–6.3 μm ($\bar{x}$ = 3.8 μm, n = 7, s.d. = 1.2 μm); ratio between basal width and height of the outer processes, 0.8–1.2 ($\bar{x}$ = 1.0, n = 7, s.d. = 0.1); outer process spacing, 2.0–5.6 μm ($\bar{x}$ = 3.8 μm, n = 4, s.d. = 1.3 μm); inner process length, 1.7–3.0 μm ($\bar{x}$ = 2.3 μm, n = 7, s.d. = 0.4 μm); inner process diameter, ≤ 0.5 μm.
Remarks. *Distosphaera jinguadunensis* sp. nov. differs from the type species, *D. speciosa* Zhang et al., 1998 emend. Liu and Moczydłowska, 2019 in its more densely-distributed, cylindrical outer processes. In thin sections, the outer processes of *D. jinguadunensis* are rectangular, whereas those of *D. speciosa* are triangular. *D. jinguadunensis* also resembles *Eotylotopalla quadrata* Liu and Moczydłowska, 2019 in thin section. When the inner processes are not preserved, *D. jinguadunensis* would be easily misidentified as *E. quadrata*. In this occasion, *D. jinguadunensis* can still be distinguished from *E. quadrata* by its double vesicle walls.

Mengeosphaera Xiao et al., 2014b

Type species. *Mengeosphaera chadianensis* (Chen and Liu, 1986) Xiao et al., 2014b

Mengeosphaera matryoshkaformis sp. nov.
(Fig. 17C–F)
Synonym.
partim 2014b *Mengeosphaera* sp., Xiao et al., p. 43, fig. 28.1–28.6.

Holotype. Specimen PB23371 (Fig. 17C–E) is designated as the holotype.
Diagnosis. Vesicle small to medium-sized, spheroidal, bearing densely distributed, hollow, and biform processes. The basal part of the process is cylindrical to bulbous, basally inflated, and constricted at the connection with the vesicle wall. The terminal part of the process is conical, tapering gradually to a pointed tip. The basal part of the process contains one or two nested domal structures, and thus resemble a Russian matryoshka.
Etymology. Derived from the Russian doll matryoshka and Latin *-formis*, with reference to the nested dome-in-dome structure in the basal expansion of the biform processes.
Material. One well- and three fairly well-preserved specimens from Member II of Doushantuo Formation, Wuzhishan section.
Description. Same as diagnosis. In most specimens only the outermost of the nested domal structures is discernable in the basal part of the processes.
Dimension. Holotype: vesicle diameter, ~100 μm; process full length, 28.2–30.1 μm (n = 3); height of basal part, 4.1–6.5 μm ($\bar{x}$ = 5.1 μm, n = 7, s.d. = 0.9 μm) and 17.0%–23.1% (n = 3) of the whole process; width of basal part at the connection with the vesicle, 7.4–12.8 μm ($\bar{x}$ = 9.6 μm, n = 7, s.d. = 1.8 μm); maximum width of the basal part, 10.3–13.4 μm ($\bar{x}$ = 11.6 μm, n = 7, s.d. = 1.0 μm); difference between the maximum and minimum width of the basal part, 0.6–4.0 μm ($\bar{x}$ = 2.0 μm, n = 7, s.d. = 1.1 μm). Other specimens: vesicle diameter, 86–102 μm (n = 3); full length of processes could not be measured due to poor preservation; height of basal part of processes, 5.7–10.7 μm (n = 3); width of basal part at the connection with the vesicle, 9.7–12.6 μm (n = 3); maximum width of basal expansion, 12.4 μm (measured on one specimen illustrated in Fig. 17F).
Remarks. This species can be distinguished by its nested processes. Yuan and Hofmann (1998) and Xiao et al. (2014b) both reported unnamed species ("*Meghystrichosphaeridium*" sp. and *Mengeosphaera* sp., respectively) with an opaque inner core nested within the basal part of biform processes, some of which (fig. 28.1–28.6 in Xiao et al.,

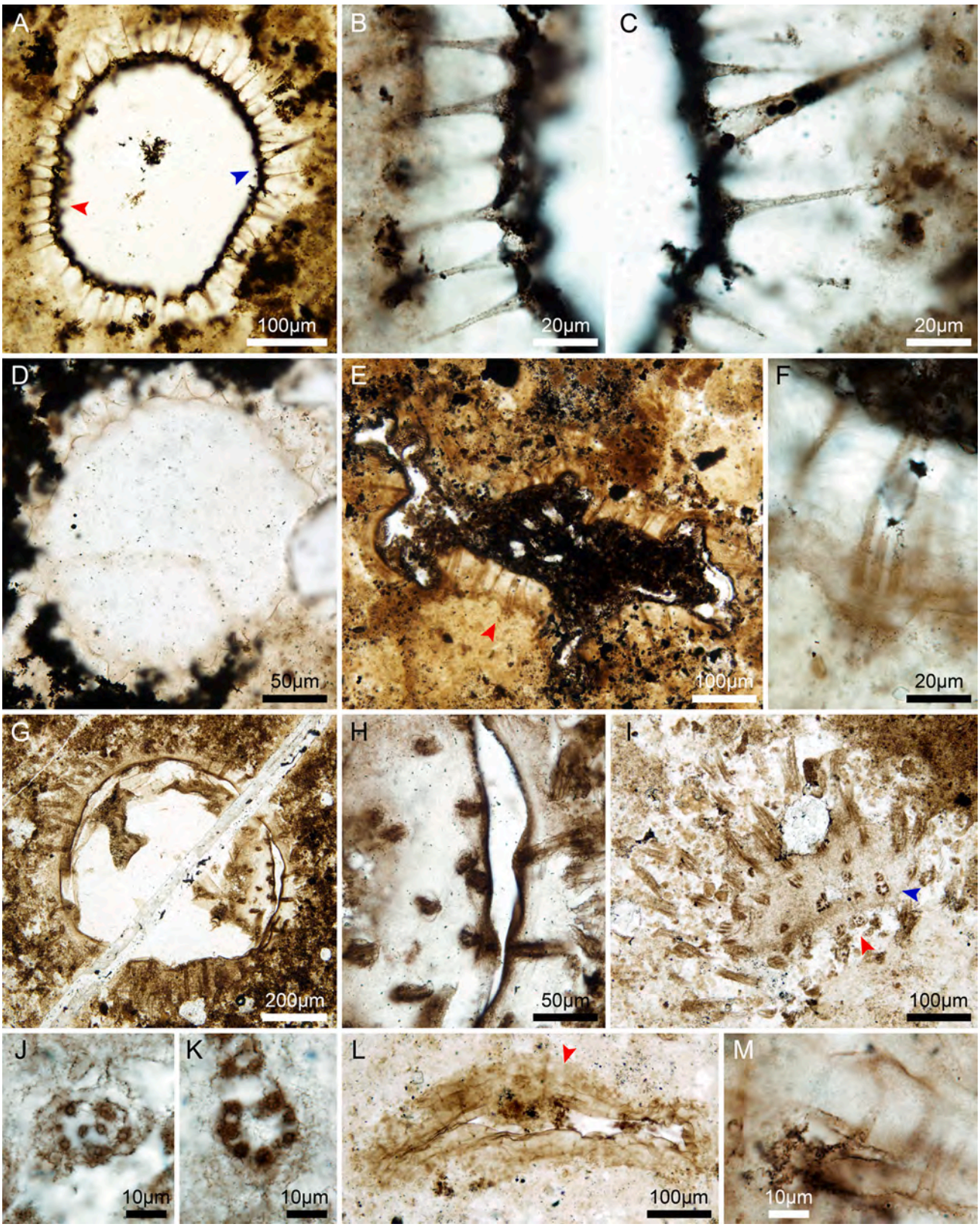

Fig. 20. Acanthomorphic acritarchs from Member II in the Yangtze Gorges area. (**A**–**C**) *Tanarium varium* Liu et al., 2014b, PB23390, thin section # 15HFL-2-4, L31/2 (ef). (**B** and **C**) Magnified views of (**A**) (red and blue arrowhead, respectively). (**D**) *Tanarium triangulare* (Liu et al., 2014b) Liu and Moczydłowska, 2019, PB23391, thin section # 15HFL-2b-16, R36/2 (ef). (**E**–**K**) *Tianzhushania polysiphonia* Yin in Yin and Liu, 1988. (**E** and **F**) PB23392, thin section # 14JLW-115-157, N40/4 (ef). (**F**) Magnified view of (**E**) (red arrowhead). (**G** and **H**) PB23393, thin section # 14JLW-49a-4, L40/3 (ef). (**H**) Magnified view of (**G**) (middle right). (**I**–**K**) PB23394, thin section # 14JLW-49a-4, M33 (ef). (**J** and **K**) Magnified views of (**I**) (red and blue arrowhead, respectively). (**L** and **M**) *Tianzhushania rara* Xiao et al., 2014b, PB23395, thin section # 14JLW-115–32, P48/3 (ef). (**M**) Magnified view of (**L**) (red arrowhead). (For interpretation of the references to colour in this figure legend, the reader is referred to the web version of this article.)

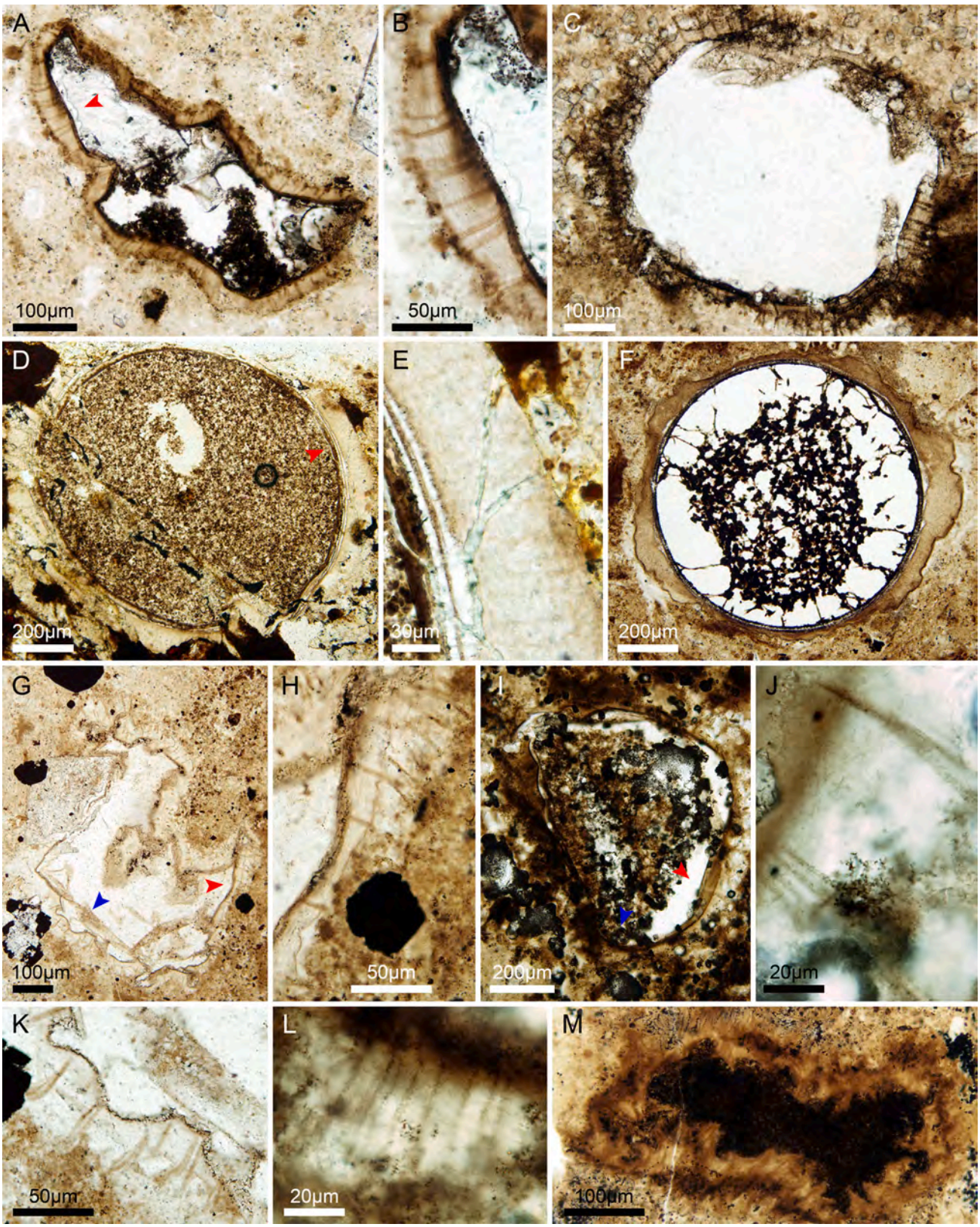

Fig. 21. Acanthomorphic acritarchs from Member II in the Yangtze Gorges area. (**A**–**L**) *Tianzhushania spinosa* Yin and Li, 1978 emend. Yin in Yin and Liu, 1988. (**A** and **B**) PB23396, thin section # 14JLW-115-20, K31 (ef). (**B**) Magnified view of (**A**) (red arrowhead). (**C**) PB23397, thin section # 16ZC28-17, K42/1 (ef). (**D** and **E**) PB23398, thin section # 14JLW-99-12, S33/1 (ef). (**E**) Magnified view of (**D**) (red arrowhead). (**F**) PB23399, thin section # 16ZC31-7, K34 (ef). (**G**, **H**, **K**) PB23400, thin section # 14JLW-75-19, L49/2 (ef). (**H** and **K**) Magnified views of (**G**) (red and blue arrowhead, respectively). (**I**, **J**, **L**) PB23401, thin section # 05MZX-3a-2, 24.7 × 136.9 (st). (**J** and **L**) Magnified views of (**I**) (red and blue arrowhead, respectively). (**M**) *Tianzhushania* sp. indet., PB23402, thin section 14JLW-115–163, G40/1 (ef). (For interpretation of the references to colour in this figure legend, the reader is referred to the web version of this article.)

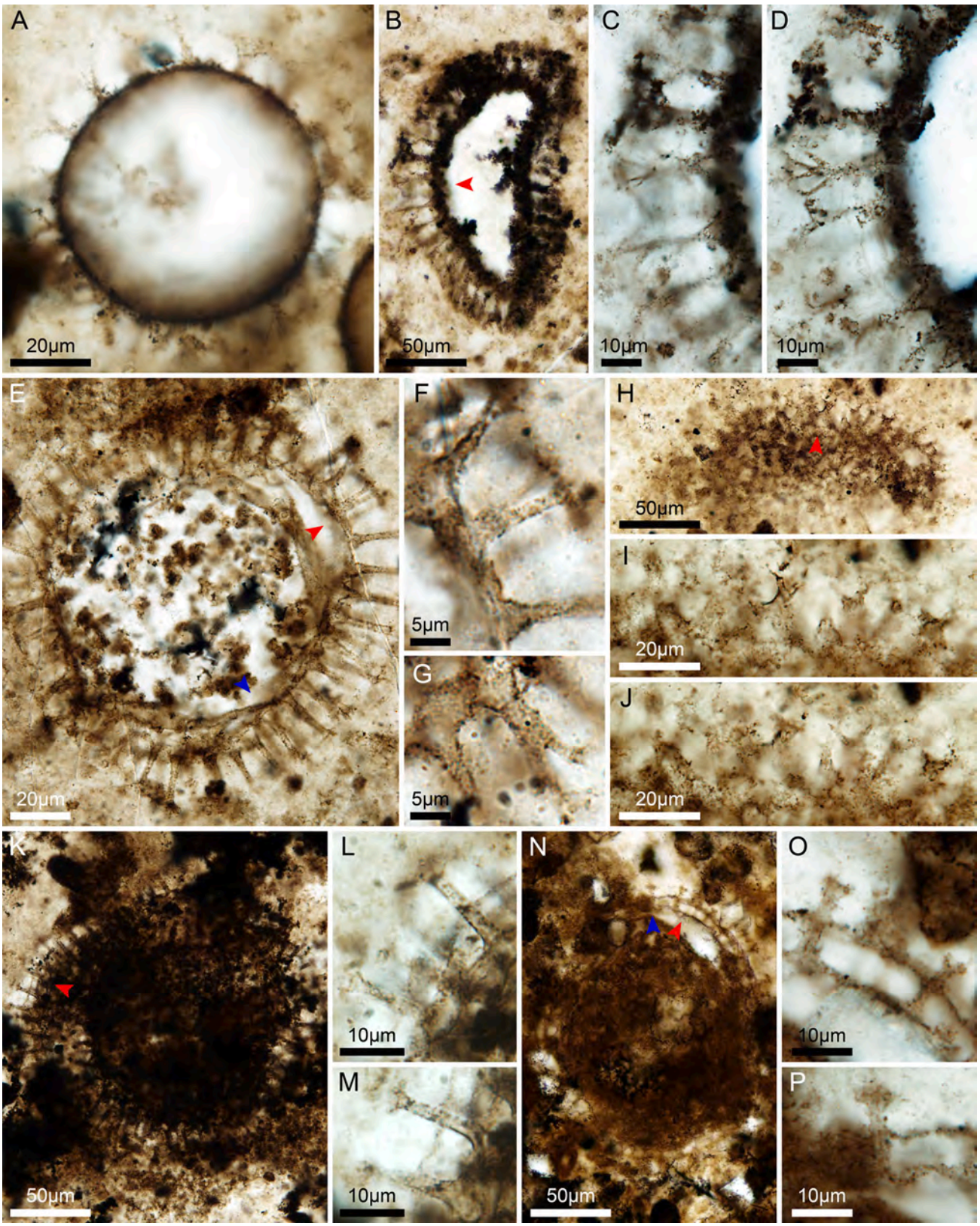

Fig. 22. Acanthomorphic acritarchs from Member II in the Yangtze Gorges area. (**A**) *Variomargosphaeridium gracile* Xiao et al., 2014b, PB23403, thin section # 15HFL-12-1, K34/4 (ef). (**B**–**G**) *V. litoschum* Zang in Zang and Walter, 1992. (**B**–**D**) PB23404, thin section # 15HFL-3a-1, O44/2 (ef). (**C** and **D**) Magnified views of (**B**) (red arrowhead), at different focal levels. (**E**–**G**) PB23405, thin section # 15HFL-2b-3, N36/2 (ef). (**F** and **G**) Magnified views of (**E**) (red and blue arrowhead, respectively). (**H**–**J**) *V. varietatum* Liu and Moczydłowska, 2019, PB23406, thin section # 15HFL-8-7, O31/4 (ef). (**I** and **J**) Magnified views of (**H**) (red arrowhead), at different focal levels. (**K**–**P**) *Variomargosphaeridium* sp. (**K**–**M**) PB23407, thin section # 15HFL-2b-10, M40 (ef). (**L** and **M**) Magnified views of (K) (upper and lower than the red arrowhead). (**N**–**P**) PB23408, thin section # 15HFL-2a-10, M34/2 (ef). (**O** and **P**) Magnified views of (**N**) (red and blue arrowhead, respectively). (For interpretation of the references to colour in this figure legend, the reader is referred to the web version of this article.)

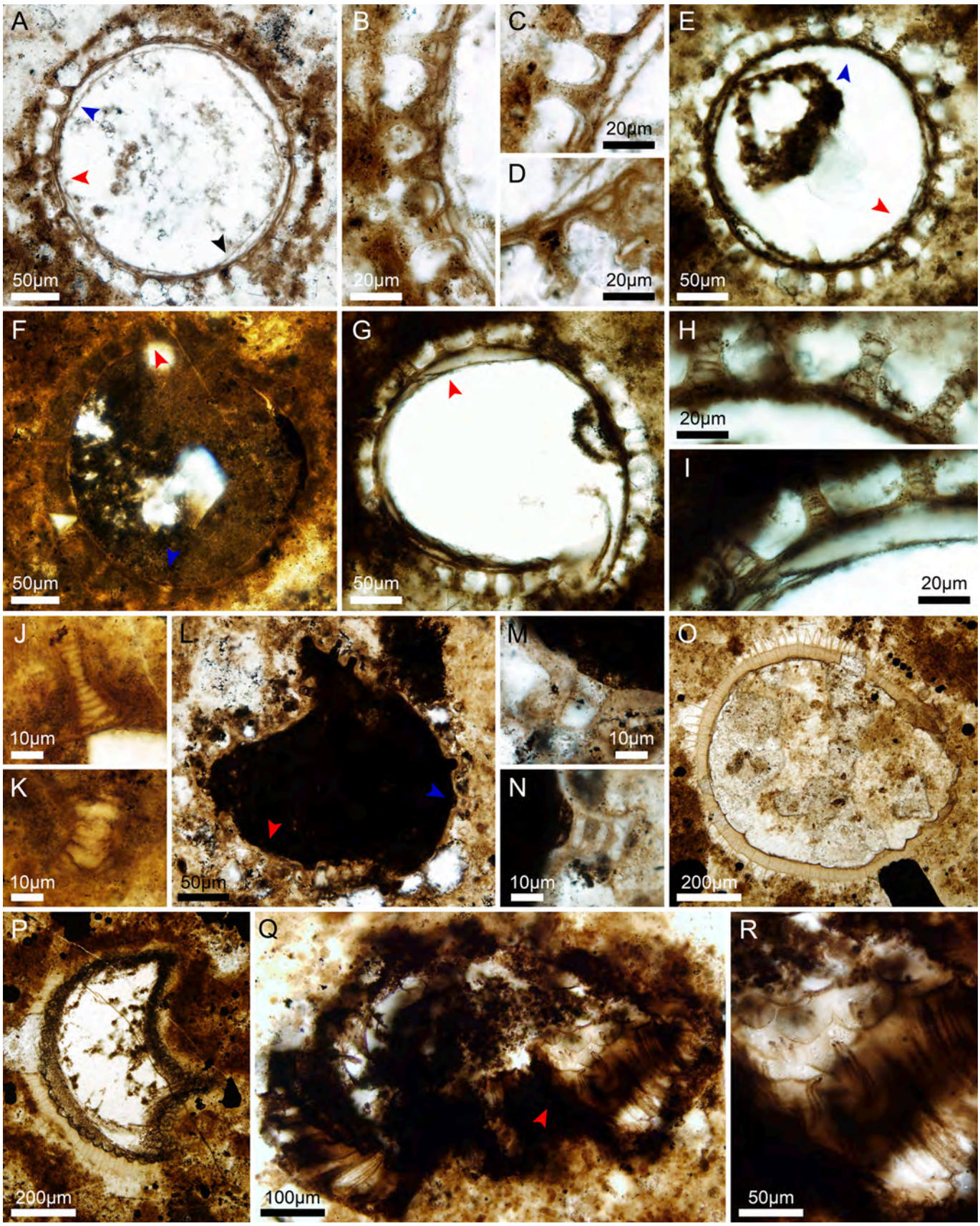

(caption on next page)

Fig. 23. Acanthomorphic acritarchs from Member II in the Yangtze Gorges area. (**A**–**N**) *Weissiella brevis* Xiao et al., 2014b emend. (**A**–**D**) PB23409, thin section # 05MZX-3-1, P30/2 (ef). (**B**–**D**) Magnified views of (**A**) (red, blue, and black arrowheads, respectively). (**E** and **H**) PB23410, thin section # 05MZX-3a-2, 29.9 × 133.7 (st). (**H**) Magnified view of (**E**) (blue arrowhead; the red arrowhead denotes magnification shown in Fig. 6C, D). (**F**, **J**, **K**) PB23411, thin section # 05MZX-3a-19, W38/2 (ef). (**J** and **K**) Magnified views of (**F**) (red and blue arrowhead, respectively). (**G** and **I**) PB23412, thin section # 05MZX-3a-2, 28 × 148.3 (st). (**I**) Magnified view of (**G**) (red arrowhead). (**L**–**N**) PB23413, thin section # 16ZC28-16, H40/4 (ef). (**M** and **N**) Magnified views of (**L**) (red and blue arrowhead, respectively). (**O**–**R**) *Yinitianzhushania tuberifera* (Yin et al., 2001) Xiao et al., 2014b. (**O** and **P**) Thin section # 14JLW-75-9. (**O**) PB23414, K44 (ef). (**P**) PB23415, Q36 (ef). (**Q** and **R**) PB23416, thin section # 14JLW-49–7, P35/3 (ef). (**R**) Magnified view of (**Q**) (red arrowhead). (For interpretation of the references to colour in this figure legend, the reader is referred to the web version of this article.)

2014b) resemble the embedded domes within the processes of *Mengeosphaera matryoshkaformis* sp. nov. However, the inner cores of some of these specimens are thin and conical (fig. 11A, B in Yuan and Hofmann (1998); fig. 28.7–28.10 in Xiao et al., 2014b), different from the nested domical structures of *Mengeosphaera matryoshkaformis*, but somewhat similar with those of *Mastosphaera changyangensis* Yin, 1999 (pl. 3, Figs. 6, 7). Therefore, specimens illustrated in fig. 28.7–28.10 (Xiao et al., 2014b) and fig. 11A, B (Yuan and Hofmann, 1998) are not assigned to *Mengeosphaera matryoshkaformis*, and may synonymize with *Mastosphaera changyangensis* pending further investigations.

Mengeosphaera sp. 1
(Fig. 17G, I–K)

Material. One fairly well-preserved specimen from Member II of Doushantuo Formation, Wuzhishan section.
Description. Vesicle large, originally spheroidal, bearing sparsely distributed biform processes with a conical basal part and a relatively long, cylindrical distal end.
Dimension. Vesicle diameter, ~267 μm; full length of processes could not be measured; basal expansion width of processes, up to 42.1 μm; basal expansion height of processes, up to 25.7 μm; diameter of cylindrical terminal part, 2.7–5.8 μm (n = 3).
Remarks. This specimen has much fewer processes and could not be assigned to any previously published *Mengeosphaera* species. With only one specimen, it could not be determined whether this sparse distribution of processes is a stable character, thus this specimen is placed in an open nomenclature.

Mengeosphaera sp. 2
(Fig. 17H, L)

Material. One fairly well-preserved specimen from Member II of Doushantuo Formation, Wuzhishan section.
Description. Vesicle large and spheroidal, bearing densely distributed biform processes with a strongly inflated basal expansion and a relatively long, cylindrical distal end.
Dimension. Vesicle diameter, ~439 μm; full length of processes could not be measured; basal expansion width of processes, 59.0–95.7 μm ($\bar{x}$ = 78.1 μm, n = 6, s.d. = 11.5 μm); basal expansion height of processes, 41.8–61.9 μm ($\bar{x}$ = 51.9 μm, n = 6, s.d. = 7.5 μm); diameter of cylindrical terminal part, 7.0–8.4 μm ($\bar{x}$ = 7.9 μm, n = 4, s.d. = 0.5 μm).
Remarks. This specimen has processes with a wide basal expansion and a cylindrical distal end, the combination of which has not been reported before, and its vesicle and process sizes are much greater than those of other *Mengeosphaera* species. It is provisionally placed in open nomenclature, possibly representing new species of *Mengeosphaera* Xiao et al., 2014b.

Sinosphaera Zhang et al., 1998 emend. Xiao et al., 2014b

Type species. *Sinosphaera rupina* Zhang et al., 1998 emend. Liu et al., 2014b.

Sinosphaera sp.
(Fig. 18K–M)

Material. One fairly well-preserved specimen from Member II of Doushantuo Formation, Wuzhishan section.
Description. Large vesicle with two groups of hollow processes of different sizes. The small processes are numerous, but their three-dimensional morphology is uncertain because none of them is cut longitudinally. The large processes are much fewer and biform in shape, with inflated conical bases and cylindrical terminations.
Dimension. Vesicle diameter is estimated to be 200–500 μm; basal width of small processes, 16.6–29.6 μm ($\bar{x}$ = 21.3 μm, n = 10, s.d. = 3.6 μm); basal expansion of large processes, 59.8–80.8 μm ($\bar{x}$ = 66.1 μm, n = 5, s.d. = 7.8 μm) in width and 68.3–83.8 μm (n = 2) in height; tubular termination of large processes, 7.7–12.1 μm (n = 2) in diameter.
Remarks. This specimen is assigned to the genus *Sinosphaera* Zhang et al., 1998 emend. Xiao et al., 2014b for its distinct bimorphic processes. According to the emendation by Xiao et al. (2014b), the large processes of *Sinosphaera* are conical or cylindrical, but the large processes of this specimen are biform, with a conical base and a cylindrical distal end. Thus, if this specimen is accepted as *Sinosphaera* it should represent a new species and the diagnosis of *Sinosphaera* needs to be emended. However, as the three-dimensional shape of the small processes in this specimen is unclear, we refrain from establishing a new species at present. Thus, this specimen is tentatively placed in an open nomenclature as *Sinosphaera* sp.

Tanarium Kolosova, 1991 emend. Moczydłowska et al., 1993

Type species. *Tanarium conoideum* Kolosova, 1991 emend. Moczydłowska et al., 1993.

Tanarium cf. *T. conoideum*
(Fig. 18N)

Material. One fairly well-preserved specimen from Member II of Doushantuo Formation, Wuzhishan section.
Description. Vesicle medium-sized, originally spheroidal, bearing evenly distributed, basally separated processes. The processes are long and conical, basally deflated and taper toward a very thin, nearly cylindrical distal end (red arrowheads in Fig. 18N). Many processes are broken in the middle.
Dimension. Vesicle diameter, ~193 μm; process length, 71.3–90.5 μm (n = 2) or 36.9%–46.9% of vesicle diameter; process basal width, ~20.2 μm; process space, ~19.7 μm.
Remarks. The vesicle size, process shape, and process density are similar to those of *Tanarium conoideum* Kolosova, 1991 emend. Moczydłowska et al., 1993. However, this specimen has much longer processes and their cylindrical terminations are different from the pointed termination of *T. conoideum* processes. Few *Tanarium* species

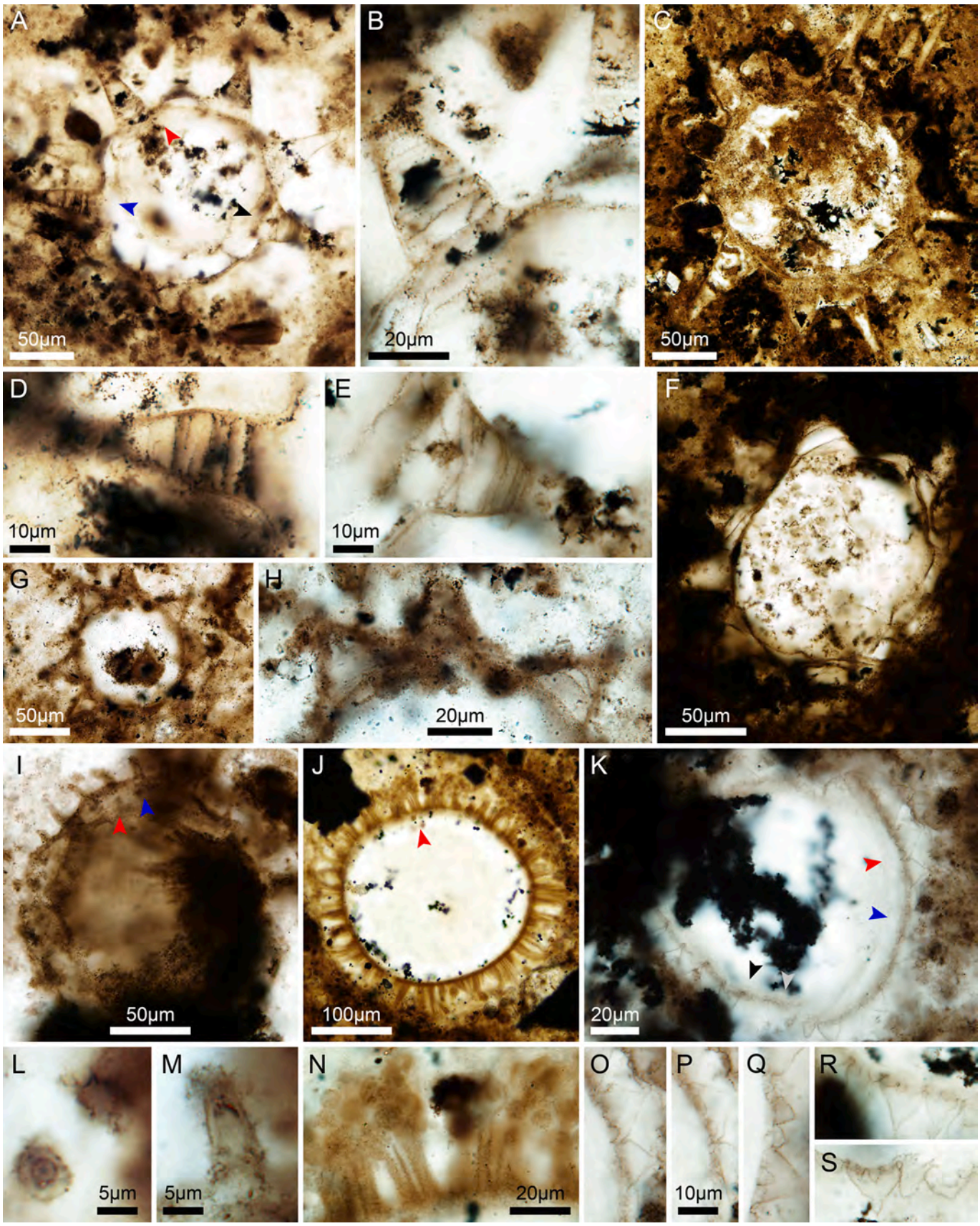

(caption on next page)

Fig. 24. Acanthomorphic acritarchs from Member II in the Yangtze Gorges area. (**A**–**H**) *Weissiella* cf. *W. grandistella*. (**A**, **B**, **D**, **E**) PB23417, thin section # 15HFL-2a-2, J36/2 (ef). (**B**, **D**, **E**) Magnified views of (**A**) (red, blue, and black arrowheads, respectively). (**C**) PB23418, thin section # 15HFL-2-1, J44/4 (ef). (**F**) PB23419, thin section # 15HFL-2-4, P39/1 (ef). (**G** and **H**) PB23420, thin section # 16ZC31-20, G38/1 (ef). (**H**) Magnified view of (**G**) (upper middle). (**I**–**S**) Indeterminate acanthomorphs. (**I**, **L**, **M**) Acanthomorphic acritarch with short, cylindrical, double-layered processes, PB23421, thin section # 05WH-25b, M37/4 (ef). (**L** and **M**) Magnified views of (**I**) (red and blue arrowhead, respectively). (**J** and **N**) Acanthomorphic acritarch with clustered, terminally inflated cylindrical processes, PB23422, thin section # 14JLW-110-12, G37 (ef). (**N**) Magnified view of (**J**) (red arrowhead). (**K**, **O**–**S**) Acanthomorphic acritarch surrounded by basally constricted, biform processes with complex internal structures, PB23423, thin section # 15HFL-2a-2, L37/1 (ef). (**O** and **P**) Magnified views of (**K**) (red arrowhead), at different focal levels. (**Q**–**S**) Magnified views of (**K**) (blue, black, and gray arrowheads, respectively). (For interpretation of the references to colour in this figure legend, the reader is referred to the web version of this article.)

have processes reaching 40% of vesicle diameter as does the specimen illustrated in Fig. 18N, exceptions being *T. gracilentum* (Yin in Yin and Liu, 1988) n. comb. emend. (processes generally exceeding 20% and reaching 46% of vesicle diameter, see emendation and dimensions below), *T. megaconicum* Grey, 2005 (processes at least 60% of vesicle diameter), and *T. paucispinosum* Grey, 2005 (processes ~40% of vesicle diameter). However, *T. gracilentum* is smaller and has more densely distributed processes, whereas the latter two species have much more sparsely distributed processes. Thus, the current specimen is tentatively placed in an open nomenclature as *Tanarium* cf. *T. conoideum*.

Tanarium gracilentum (Yin in Yin and Liu, 1988) n. comb. emend.
(Fig. 19H–J)

Synonyms.

1985 *Baltisphaeridium* spiny microfossil, Awramik et al., 1985, fig. 3b.

1988 *Baltisphaeridium gracilentum* Yin in Yin and Liu, p. 174, pl. 8, figs. 1–3.

1990 *Baltisphaeridium gracilentum* Yin, 1990 in (Yin and Liu, 1988), Yin, pl. I, fig. 8.

nom. invalid. 1998 *Meghystrichosphaeridium gracilentum* (Yin in Yin and Liu, 1988) Zhang et al., p. 36, fig. 9.13, 9.14.

nom. invalid. 2002 *Meghystrichosphaeridium gracilentum* (Yin in Yin and Liu, 1988) Zhang et al., 1998, Zhou et al., 2002 p. 183, pl. II, figs. 3, 4.

non 1999 *Solisphaeridium gracilentum* (Yin, 1988) Yin, p. 12, pl. 3, fig. 1.

nom. non rite public. 2011b *Tanarium gracilentum*, Yin et al., fig. 3H, 3I.

nom. invalid. 2019 *Tanarium gracilentum*, Ouyang et al., fig. 12E–H.

Basionym. *Baltisphaeridium gracilentum* Yin in Yin and Liu (1988).

Holotype. As the original designation, the specimen illustrated in plate 8, fig. 3 in Yin and Liu, 1988, thin section Ycy-292.

Original diagnosis (translated from Yin and Liu, 1988). Vesicle compressed horizontally to an oval or irregular shape, bearing densely distributed, blade-like processes. The processes are thin, have granular surfaces as does the vesicle, and most of them do not communicate with vesicle interior. Vesicle diameter 45–70 μm (average 50 μm), processes basal width 1.5–2.5 μm, processes length 12–20 μm.

Emended diagnosis. Vesicle small, spheroidal, bearing evenly distributed hollow processes that communicate freely with the vesicle interior. Processes conical and thin, nearly cylindrical in the distal end, and somewhat basally expanded. Length of processes generally exceeds one fifth of vesicle diameter, and some may reach half of the vesicle diameter. Processes basally separated but densely distributed.

Material. One well-preserved and one fairly well-preserved specimen from Member II of Doushantuo Formation, Jiulongwan section.

Description. Same as emended diagnosis.

Dimension. The first specimen (Fig. 19H, I): vesicle diameter, ~95 μm; process length, 32.2–39.0 μm ($\bar{x}$ = 35.1 μm, n = 6, s.d. = 2.1 μm), or 33.9%–41.1% of vesicle diameter; process basal width, 3.4–6.0 μm ($\bar{x}$ = 4.9 μm, n = 6, s.d. = 0.8 μm); height of deflated basal expansion, 4.3–6.7 μm ($\bar{x}$ = 5.2 μm, n = 5, s.d. = 0.8 μm). The second specimen (Fig. 19J): vesicle diameter, ~59 μm; process length, 19.0–27.2 μm ($\bar{x}$ = 23.3 μm, n = 6, s.d. = 2.9 μm), or 32.2%–46.1% of vesicle diameter; process basal width, 1.4–2.0 μm ($\bar{x}$ = 1.7 μm, n = 5, s.d. = 0.2 μm).

Remarks. This species was first described as a species of *Baltisphaeridium* (Eisenack, 1958) Eisenack, 1969 by Yin and Liu (1988). Zhang et al. (1998) transferred it to *Meghystrichosphaeridium* Zhang et al., 1998 non Chen and Liu, 1986, which has been considered as invalid (Grey, 2005; Xiao et al., 2014b). As a consequence, the taxonomic placement of this species became a problem. Yin et al. (2007) and Yin et al. (2011b) used the name *Tanarium gracilentum*, but without any description, formalization of the combination, or reference to the previous names. Specimens described here are morphologically identical to those previously described as *Baltisphaeridium gracilentum*, "*Meghystrichosphaeridium gracilentum*", and "*Tanarium gracilentum*", although the specimen in Fig. 19J is relatively smaller. Based on the long and conical processes, *Baltisphaeridium gracilentum* is here formally transferred to *Tanarium* Kolosova, 1991 emend. Moczydłowska et al., 1993, and a complete systematic description is given.

As Grey (2005) has already pointed out, *Tanarium pycnacanthum* Grey, 2005 is morphologically similar with *T. gracilentum* (Yin in Yin and Liu, 1988) n. comb. emend. The processes of *T. pycnacanthum* may be thinner than those of *T. gracilentum*, but this can be a taphonomic artifact, given that *T. pycnacanthum* was erected based on organic-walled fossils preserved as carbonaceous compressions and extracted using HF maceration. Nevertheless, as there are no firm reasons to synonymize these two species (in which case *T. gracilentum* would take priority), here we follow Grey (2005) in accepting them as separate species.

Variomargosphaeridium Zang in Zang and Walter, 1992 emend. Xiao et al., 2014b

Type species. *Variomargosphaeridium litoschum* Zang in Zang and Walter,1992.

Variomargosphaeridium sp.
(Fig. 22K–P)

Table 2
Occurrence and abundance data of eukaryotic microfossils at the Jiulongwan section. The table shows the number of specimens recovered in this study. Blank: absent. *: present but not counted. Stratigraphic heights were measured from the top of the cap dolostone (the base of Member II).

sample	stratigraphic height (m)	*Alicesphaeridium medusoidum*	*Appendisphaera grandis*	*Appendisphaera heliaca* n. comb.	*Appendisphaera tenuis*	*Briareus boreadis*	*Cavaspina acuminata*	*Cymatiosphaeroides kullingii*	*Dicrospinasphaera improcera*	*Dicrospinasphaera zhangii*	*Distosphaera jinguadunensis* n. sp.	*Distosphaera speciosa*	*Eotylotopalla dactylos*	*Eotylotopalla delicata*	*Ericiasphaera fibrilla*	*Knollisphaeridium coniformum*	*Knollisphaeridium longilatum*	*Knollisphaeridium maximum*	*Megasphaera inornata*	*Megasphaera ornata*	*Mengeosphaera chadianensis*	*Mengeosphaera lumula*	*Mengeosphaera minima*	*Mengeosphaera* sp. indet.	*Sinosphaera speciosa*	*Tanarium digitiforme*	*Tanarium gracilentum* n. comb. emend.	*Tanarium* sp. indet.	*Tianzhushania polysiphonia*	*Tianzhushania rara*	*Tianzhushania spinosa*	*Tianzhushania* sp. indet.	*Variomargosphaeridium litoschum*	*Weissiella brevis* emend.	*Yinitianzhushania tuberifera*	Indeterminate acanthomorphs	Multicellular algae
14JLW-115	2.8		1						1										1								1		1	1	12	9				2	*
14JLW-29	3.6																																				*
14JLW-31	3.8																														1					1	*
14JLW-33	4				1																										1					*
14JLW-34	4.1															1		1	1												1	1					*
14JLW-37	4.9		1							1																											*
05WH-5/ 14JLW-47	8								1		1								1			1	1				1		8		3	16			12		
14JLW-48	8.1																					1										3					
05WH-6/ 14JLW-49	8.2				1			1				1						1	1			3							6		1	18			13		*
14JLW-57-1	10.2																												1			1					
14JLW-57-2	10.3										1											3							2		1	5			10	1	
05WH-8/ 14JLW-58	10.4		1								3											3							5		1	8		1	11		
14JLW-112	12.2																		5												2	5			2		*
05WH-9/ 14JLW-69	18																								1						12	4				1	
14JLW-113	18.7			2		1													1													1			1		
05WH-10/ 14JLW-114	18.8																		1					1							5	7		3	1		*
05WH-11~13/ 14JLW-74	29.3																			2											21	6			6		*
14JLW-75	31.1																			2									2		44	7		15	9		*

(*continued on next page*)

Table 2 (*continued*)

sample	stratigraphic height (m)	*Alicesphaeridium medusoidum*	*Appendisphaera grandis*	*Appendisphaera heliaca* n. comb.	*Appendisphaera tenuis*	*Briareus borealis*	*Cavaspina acuminata*	*Cymatiosphaeroides kullingii*	*Dicrospinasphaera improcera*	*Dicrospinasphaera zhangii*	*Distosphaera jinguadunensis* n. sp.	*Distosphaera speciosa*	*Eotylotopalla dactylos*	*Eotylotopalla delicata*	*Ericiasphaera fibrilla*	*Knollisphaeridium coniformum*	*Knollisphaeridium longilatum*	*Knollisphaeridium maximum*	*Megasphaera inornata*	*Megasphaera ornata*	*Mengeosphaera chadianensis*	*Mengeosphaera lunula*	*Mengeosphaera minima*	*Mengeosphaera* sp. indet.	*Sinosphaera speciosa*	*Tanarium digitiforme*	*Tanarium gracilentum* n. comb. emend.	*Tanarium* sp. indet.	*Tianzhushania polysiphonia*	*Tianzhushania rara*	*Tianzhushania spinosa*	*Tianzhushania* sp. indet.	*Variomargosphaeridium litoschum*	*Weissiella brevis* emend.	*Yinitianzhushania tuberifera*	Indeterminate acanthomorphs	Multicellular algae
05WH-15/ 14JLW-76	31.5																													13	3		4	4	4	*
14JLW-77	32																			1								2		8	11			5		
05WH-17/ 14JLW-78	32.2		1																1											8	5			1	1	*
14JLW-79	32.3																											1		6				1		
05WH-21/ 14JLW-80	32.8								1													1						2		22	12		1	6	2	*
14JLW-87	48.4								2	1																					1					*
14JLW-89	48.5								3										3												2					*
14JLW-90	48.6	1							4																						3					*
14JLW-91	48.8								2									1																		*
14JLW-92	49			1	1				5						1																					
14JLW-93	49.1								3																						1				1	*
05WH-23/ 14JLW-99	57.2			10	1		1		4	3									5		4			9						2	8				1	*
05WH-24/ 14JLW-103	57.5			2						1		1	1	1			1		2		1								1	3					*
14JLW-101	57.7	1		2	1			1				1	1		1				1												1				1	*
14JLW-102	57.9			1											1																1					*
05WH-25/ 14JLW-104	59.1			2						1							1	2			1						1			1		1	4		7	*
05WH-26/ 14JLW-107	69.5								1	1																					1					*
14JLW-108	69.8				1														2												1					*
14JLW-109	70												1						4	1				1		1				4	1			1		*
14JLW-110	70.3																	1	1					1							2			1	1	*

Table 1
Occurrence and abundance data of acanthomorphic acritarchs from the Member II of Doushantuo Formation at Jiulongwan, Jinguadun, and Wuzhishan sections. The table shows the number of specimens recovered in this study. Blank: absent.

	Jiulongwan	Jinguadun	Wuzhishan
Alicesphaeridium medusoidum	2		
Annularidentatus inconditus n. sp.			2
Annularidentatus sp.			1
Appendisphaera clava		1	3
Appendisphaera grandis	4	1	10
Appendisphaera heliaca n. comb.	20	19	
Appendisphaera longispina			1
Appendisphaera magnifica		1	
Appendisphaera setosa		1	2
Appendisphaera tabifica		4	13
Appendisphaera tenuis	6	1	
Bacatisphaera baokangensis			2
Briareus borealis	1		
Briareus vasformis		1	
Bispinosphaera vacua n. sp.			1
Cavaspina acuminata	1	1	3
Crassimembrana crispans n. sp.			4
Crassimembrana cf. *C. crispans*		2	
Crassimembrana multitunica n. sp.			9
Cymatiosphaeroides kullingii	2	2	
Cymatiosphaeroides yinii			3
Dicrospinasphaera improcera	27	2	2
Dicrospinasphaera zhangii	8	5	
Distosphaera jinguadunensis n. sp.	5	3	
Distosphaera speciosa	3	6	1
Eotylotopalla dactylos	3	1	5
Eotylotopalla delicata	1		
Eotylotopalla strobilata			1
Ericiasphaera fibrilla	3	6	4
Knollisphaeridium coniformum	1		2
Knollisphaeridium denticulatum			3
Knollisphaeridium longilatum	2		
Knollisphaeridium maximum	6	5	1
Megasphaera inornata	30	57	135
Megasphaera ornata	6	6	1
Membranosphaera formosa			1
Mengeosphaera chadianensis	6	4	1
Mengeosphaera gracilis			1
Mengeosphaera grandispina			3
Mengeosphaera latibasis			2
Mengeosphaera lunula	12		
Mengeosphaera matryoshkaformis n. sp.			4
Mengeosphaera minima	1		1
Mengeosphaera sp. 1			1
Mengeosphaera sp. 2			1
Mengeosphaera sp. indet.	12	16	13
Papillomembrana compta			6
Sinosphaera asteriformis			4
Sinosphaera speciosa	1		
Sinosphaera sp.			1
Tanarium capitatum			1
Tanarium cf. *T. conoideum*			1
Tanarium digitiforme	1		2
Tanarium gracilentum n. comb. emend.	2		
Tanarium obesum			2
Tanarium pilosiusculum			3
Tanarium pluriprotensum			2
Tanarium triangulare			2
Tanarium tuberosum			2
Tanarium varium			1
Tanarium sp. indet.	1		1
Tianzhushania polysiphonia	30	9	
Tianzhushania rara	1		
Tianzhushania spinosa	170	161	4
Tianzhushania sp. indet.	147	78	5
Variomargosphaeridium gracile			5
Variomargosphaeridium litoschum	1		5
Variomargosphaeridium varietatum		1	2
Variomargosphaeridium sp.			2
Weissiella brevis emend.	28	106	1
Weissiella cf. *W. grandistella*		1	18
Yinitianzhushania tuberifera	84	18	
Indeterminate acanthomorphs	23	14	56
ALL	651	533	363

Material. Two fairly well-preserved specimens from Member II of Doushantuo Formation, Wuzhishan section.

Description. Vesicle medium-sized, spheroidal, consisting of concentric double walls. Processes arise from inner wall and penetrate outer wall. Processes are evenly arranged on inner wall, cylindrical in shape between vesicle walls, and terminally branch into very short branchlets. In poorly-preserved parts, these branchlets appear as terminal flaring structures.

Dimension. The first specimen (Fig. 22K–M): vesicle diameter, ~155 μm; process length, 12.3–14.9 μm ($\bar{x}$ = 13.6 μm, n = 6, s.d. = 0.8 μm); process diameter, 2.0–2.6 μm ($\bar{x}$ = 2.2 μm, n = 11, s.d. = 0.2 μm); space between processes, ~5 μm (n = 1); distance between outer and inner vesicle walls, ~6 μm. The second specimen (Fig. 22N–P): vesicle diameter, ~123 μm; process length, 11.7–15.8 μm ($\bar{x}$ = 13.3 μm, n = 4, s.d. = 1.6 μm); process diameter, 4.4–5.6 μm ($\bar{x}$ = 5.0 μm, n = 4, s.d. = 0.4 μm); space between processes, 7.6–14.2 μm (n = 3); distance between outer and inner vesicle walls, ~6 μm.

Remarks. The specimens are similar to *Variomargosphaeridium floridum* (Liu et al., 2014b) in their cylindrical and terminally branching processes, but differ in their double vesical walls. The double vesicle walls are not a taphonomic artifact; the outer wall cannot be a result of deformed process tips or the accumulation of organic matter at process terminations. Although these two specimens may represent a new species of *Variomargosphaeridium* Zang in Zang and Walter,1992 emend. Xiao et al., 2014b, their terminal branchlets are not well-preserved. Thus, they are currently placed in an open nomenclature.

Weissiella Vorob'eva et al., 2009

Type species. *Weissiella grandistella* Vorob'eva et al., 2009.

Remarks. Two groups of *Weissiella* specimens have been recognized from our fossil collection, which are identified as *W. brevis* Xiao et al., 2014b emend. and *Weissiella* cf. *W. grandistella*, respectively. As described below, specimens identified as *Weissiella* cf. *W. grandistella* are essentially identical to *W. grandistella* Vorob'eva et al., 2009 in process size and morphology, but differ in their smaller vesicle size (and as a result, their proportionally longer and larger processes). The two groups of *Weissiella* specimens are statistically different in vesicle size (Fig. 28A; two-tailed Student's *t*-test, $p < 0.001$), do not overlap in proportional length of processes or proportional basal width of processes (Fig. 28B), and their processes are different in morphology (see species description for details). Compared with *Weissiella* cf. *W. grandistella*, the processes of *W. brevis* are statistically shorter and thinner (one-tailed Student's *t*-test, both $p < 0.001$). Liu and Moczydłowska (2019) argued that the shorter processes of *W. brevis* may be resulted from broken processes and indeed this interpretation may account for some bluntly terminated processes of *W. grandistella* (e.g., Fig. 10.1f in Vorob'eva et al., 2009), but the thinner processes of *W. brevis* cannot be explained by process breakage (Fig. 28). Thus, the proposal by Liu and Moczydłowska (2019) to synonymize *W. brevis* Xiao et al., 2014b with *W. grandistella* Vorob'eva et al., 2009 is not followed in this study.

There are rare transitional forms between *W. brevis* Xiao et al., 2014b emend. and *Weissiella* cf. *W. grandistella*. For example, one specimen identified by Liu and Moczydłowska (2019, fig. 92F, G) has proportionally small but conical processes with well-preserved pointed tips. Transitional forms are also found in other

Table 4
Occurrence and abundance data of eukaryotic microfossils at the Wuzhishan section. The table shows the number of specimens recovered in this study. Blank: absent. *: present but not counted. Stratigraphic depths were measured down-section from the Member II-III boundary, with 15HFL-1 being the lowest and 15HFL-21 being the highest sample.

Sample	15HFL-1	15HFL-2	15HFL-3	15HFL-4	15HFL-5	15HFL-6	15HFL-7	15HFL-8	15HFL-9	15HFL-10	15HFL-11	15HFL-12	15HFL-13	15HFL-14	15HFL-16	15HFL-17	15HFL-18	15HFL-19	15HFL-20	15HFL-21
stratigraphic depth (m)	–50	–49.4	–48.8	–45.5	–43.3	–35.5	–28	–27.4	–26.8	–26	–23.5	–22	–20.5	–20	–16	–11.5	–10.5	–7.5	–2.5	–1.5
Annularidens inconditus n. sp.												1		1						
Annularidens sp.															1					
Appendisphaera clava																				3
Appendisphaera grandis		8	1									1								
Appendisphaera longispina								1												
Appendisphaera setosa												2								
Appendisphaera tabifica		8	1	1												1				2
Bacatisphaera baokangensis		1													1					
Bispinosphaera vacua n. sp.								1												
Cavaspina acuminata			1									1								1
Crassimembrana crispans n. sp.	1		1	1								1								
Crassimembrana multitunica n. sp.							2	2	2	1						1	1			
Cymatiosphaeroides yinii			1							1		1								
Dicrospinasphaera improcera								1	1											
Distosphaera speciosa												1								
Eotylotopalla dactylos							1	1											3	
Eotylotopalla strobilata	1																			
Ericiasphaera fibrilla							1			1						1	1			
Knollisphaeridium coniformum		1						1												
Knollisphaeridium denticulatum									2	1										
Knollisphaeridium maximum							1													
Megasphaera inornata		6	4			1	1		9		40	7	5	2	3		2	55		
Megasphaera ornata												1								
Membranosphaera formosa		1																		
Mengeosphaera chadianensis																1				
Mengeosphaera gracilis							1													
Mengeosphaera grandispina								2								1				
Mengeosphaera latibasis					1							1								
Mengeosphaera matryoshkaformis n. sp.		4																		
Mengeosphaera minima		1																		
Mengeosphaera sp. 1								1												
Mengeosphaera sp. 2								1												
Mengeosphaera sp. indet.		2						6				1				1	3			
Papillomembrana compta		5	1																	
Sinosphaera asteriformis		3		1																
Sinosphaera sp.		1																		
Tanarium capitatum		1																		
Tanarium digitiforme		1										1								
Tanarium cf. *T. conoideum*		1																		
Tanarium obesum		1	1																	
Tanarium pilosiusculum		2										1								
Tanarium pluriprotensum		2																		
Tanarium triangulare		1										1								
Tanarium tuberosum		1						1												
Tanarium varium		1																		
Tanarium sp. indet.																1				
Tianzhushania spinosa		1					1				1							1		
Tianzhushania sp. indet.			1					1	1	2										
Variomargosphaeridium gracile										1		4								

(*continued on next page*)

Table 4 (*continued*)

Sample	15HFL-1	15HFL-2	15HFL-3	15HFL-4	15HFL-5	15HFL-6	15HFL-7	15HFL-8	15HFL-9	15HFL-10	15HFL-11	15HFL-12	15HFL-13	15HFL-14	15HFL-16	15HFL-17	15HFL-18	15HFL-19	15HFL-20	15HFL-21
Variomargosphaeridium litoschum		2	1			2														
Variomargosphaeridium variétatum								1		1									3	3
Variomargosphaeridium sp.		2																		
Weissiella brevis emend.		1										2	1			6	2			
Weissiella cf. *W. grandistella*		14	1					4	3			5								
Indeterminate acanthomorphs	1	17	4	1		1	6													
Multicellular algae	*	*	*	*	*		*	*	*	*		*	*	*	*	*	*			

acanthomorph taxa, such as *Tianzhushania*. *T. polysiphonia* is diagnosed by its clustered processes (Fig. 20E–K), but there are *T. spinosa* specimens with both clustered and isolated processes (Fig. 21G–L). In these cases, end-members are chosen as different species as long as the end-members are dominant morphotypes and transitional forms are rare. Based on our biometric data (Fig. 28), *W. brevis* and *Weissiella* cf. *W. grandistella* are here considered as two end-members with statistically distinct process size and shape, and they are treated as two separate species.

Weissiella brevis Xiao et al., 2014b emend.
(Fig. 6C, D, 23A–N)
Synonyms.
2014b *Weissiella brevis* Xiao et al., p. 61, fig. 38.1–38.12.
2014 *Weissiella* cf. *grandistella*, Shukla and Tiwari, p. 219, fig. 8A–E.
2015 *Weissiella* cf. *brevis*, Ouyang et al., p. 221, pl. III, Figs. 7–13.
2015 Weissiella sp. Ouyang et al., p. 221, pl. IV, Figs. 8–13.
2019 *Weissiella grandistella* Vorob'eva et al., 2009 emend. Liu and Moczydłowska, Shang et al., p. 28, Fig. 19A–H.
partim 2019 *Weissiella grandistella* Vorob'eva et al., 2009 emend. Liu and Moczydłowska, p. 163, fig. 91A–E.

Emended diagnosis. Vesicle large to medium-sized, with relatively small conical or cylindrical processes. Process length generally ≤20% of vesicle diameter, and process basal width generally ≤15% of vesicle diameter. Some processes have both basal and terminal expansions, forming a constricted waist and resemble a dumbbell. Processes densely distributed but basally separated.
Material. One hundred and thirty-five well- to fairly well-preserved specimens from Member II of Doushantuo Formation at the Jiulongwan, Jinguadun and Wuzhishan sections.
Description. Same as emended diagnosis. In some specimens, an organic membrane drapes between processes (Fig. 23B–D, I). This drape may be a taphonomic artifact.
Dimensions. Vesicle diameter, 88–280 μm ($\bar{x}$ = 217 μm, n = 130, s.d. = 34 μm, see Fig. 28A for histogram); process length, 13.6–38.4 μm ($\bar{x}$ = 24.0 μm, n = 113, s.d. = 5.0 μm) and 6.0%–18.8% of vesicle diameter ($\bar{x}$ = 11.3%, n = 112, s.d. = 2.6%; Fig. 28B); process basal width, 7.3–25.7 μm ($\bar{x}$ = 14.1 μm, n = 129, s.d. = 3.5 μm) and 3.1%–12.6% of vesicle diameter ($\bar{x}$ = 6.6%, n = 127, s.d. = 1.8%; Fig. 28B).
Remarks. The diagnosis for *Weissiella brevis* Xiao et al., 2014b is emended to accommodate new specimens with similar morphology but their processes are slightly expanded terminally (Fig. 23B–D, H, J, K, N). It is possible that some apparently cylindrical processes, particularly those with truncated terminations (e.g., Fig. 23M), may represent distally broken processes.

One specimen identified as *W.* cf. *grandistella* by Shukla and Tiwari (2014) from the Krol A Formation in Lesser Himalaya is here reassigned to *W. brevis* Xiao et al., 2014b emend. This specimen has a large vesicle (~250 μm in diameter) and proportionally small processes (length 19–32 μm, basal width 12–18 μm). Although the processes of this specimen were described as conical, most of them are better described as cylindrical (fig. 8C, D in Shukla and Tiwari, 2014). Therefore, this specimen better fits the diagnosis of *W. brevis*. Similarly, several specimens described as *W. grandistella* by Liu and Moczydłowska (2019, fig. 91A–E) and Shang et al. (2019, fig. 19A–H) have relatively small processes and they are more appropriately assigned to *W. brevis*.

Weissiella cf. *W. grandistella*
(Fig. 24A–H)
Synonyms.
2013 *Weissiella grandistella*, Liu et al., 2013, fig. 13E.
2014a *Weissiella grandistella*, Liu et al., fig. 9E.
2014b *Weissiella grandistella* Vorob'eva et al., 2009, Liu et al., p. 128,

Table 3
Occurrence and abundance data of eukaryotic microfossils at the Jinguadun section. The table shows the number of specimens recovered in this study. Blank: absent. *: present but not counted. Stratigraphic heights were measured from the top of cap dolostone (base of Member II). Stars denote presence at the given horizon.

Sample	05MZX-1/ 16ZC25	05MZX-2/ 16ZC26	05MZX-3/ 16ZC28	16ZC29	16ZC30	05MZX-4/ 16ZC31	05MZX-5/ 16ZC32	05MZX-6	05MZX-7	05MZX-8/ 16ZC33	05MZX-9
stratigraphic height (m)	9.5	14.5	20	39.5	41	61	62.5	63.1	63.25	63.5	65
Appendisphaera clava										1	
Appendisphaera grandis		1									
Appendisphaera heliaca n. comb.						6	2			11	
Appendisphaera magnifica							1				
Appendisphaera setosa										1	
Appendisphaera tabifica		1	2			1					
Appendisphaera tenuis							1				
Briareus vasformis			1								
Cavaspina acuminata							1				
Crassimembrana cf. *C. crispans*		1	1								
Cymatiosphaeroides kullingii			1				1				
Dicrospinasphaera improcera		1				1					
Dicrospinasphaera zhangii						1	2		1	1	
Distosphaera jinguadunensis n. sp.		1	2								
Distosphaera speciosa							1			1	4
Eotylotopalla dactylos	1										
Ericiasphaera fibrilla		2	1	1		1				1	
Knollisphaeridium maximum		1					2			1	1
Megasphaera inornata	1	1	3	9	1	18	12			11	1
Megasphaera ornata		1	2	3							
Mengeosphaera chadianensis								3		1	
Mengeosphaera sp. indet.		1	3			3				8	1
Tianzhushania polysiphonia		4	4			1					
Tianzhushania spinosa	9	53	90		6		1				2
Tianzhushania sp. indet.		37	28	2	6	3		1		1	
Variomargosphaeridium varietatum											1
Weissiella brevis emend.		5	101								
Weissiella cf. *W. grandistella*						1					
Yinitianzhushania tuberifera		2	14	2							
Indeterminate acanthomorphs		1	7			3		1		2	
Multicellular algae		*	*	*		*	*	*	*	*	*

figs. 94.1–94.7, 95.

non 2014 *Weissiella* cf. *grandistella*, Shukla and Tiwari, p. 219, fig. 8A–E.

partim 2019 *Weissiella grandistella* Vorob'eva et al., 2009 emend. Liu and Moczydłowska, p. 163, figs. 91F, G, 92A–G.

Material. Nineteen well- to fairly well-preserved specimens from Member II of Doushantuo Formation at the Jinguadun and Wuzhishan sections.

Description. Vesicle medium-sized, spheroidal, bearing evenly distributed, homomorphic, hollow, and conical processes, that taper from a wide base to a pointed or blunt tip. Processes contain numerous fine cross-walls in their interior cavity. Full length of processes can hardly be observed because they are cut obliquely in the thin section.

Dimensions. Vesicle diameter, 95–194 μm ($\bar{x}$ = 147 μm, n = 18, s.d. = 25 μm, see Fig. 28A for histogram); process length, 26.8–113.2 μm ($\bar{x}$ = 80.5 μm, n = 13, s.d. = 21.4 μm) and 28.4%–76.8% of vesicle diameter ($\bar{x}$ = 53.9%, n = 13, s.d. = 13.4%; Fig. 28B); process basal width, 13.3–53.8 μm ($\bar{x}$ = 32.2 μm, n = 18, s.d. = 9.0 μm) and 12.2%–31.4% of the vesicle diameter ($\bar{x}$ = 22.1%, n = 18, s.d. = 5.8%; Fig. 28B); space between process bases, 6.4–30.7 μm ($\bar{x}$ = 16.8 μm, n = 9, s.d. = 9.5 μm).

Remarks. These specimens are similar to *W. grandistella* in process shape, length, and cross-walls. Their processes are proportionally longer than those of *W. grandistella* (Fig. 28B), but in principal this could be related to the fact that, in thin section observations, vesicle diameter is more biased toward underestimation than process length. On the other hand, none of the 19 specimens in our collection are even close to the dimensions of *W. grandistella* specimens from the type area in the East European Platform (vesicle diameter 450–500 μm, process length 80–110 μm, process basal width 70–140 μm, Vorob'eva et al., 2009). Thus, we tentatively place our specimens in an open nomenclature as *Weissiella* cf. *W. grandistella*. The same can be said of *W. grandistella* specimens illustrated in Liu et al. (2013), Liu et al. (2014a), Liu et al. (2014b), as well as several *W. grandistella* specimens in Liu and Moczydłowska (2019).

Indeterminate acanthomorphs

Ninety-three acanthomorphic specimens in our collection are not taxonomically identified to any published genera or species, because of poor preservation, limited specimens, or unstable morphologies. Some

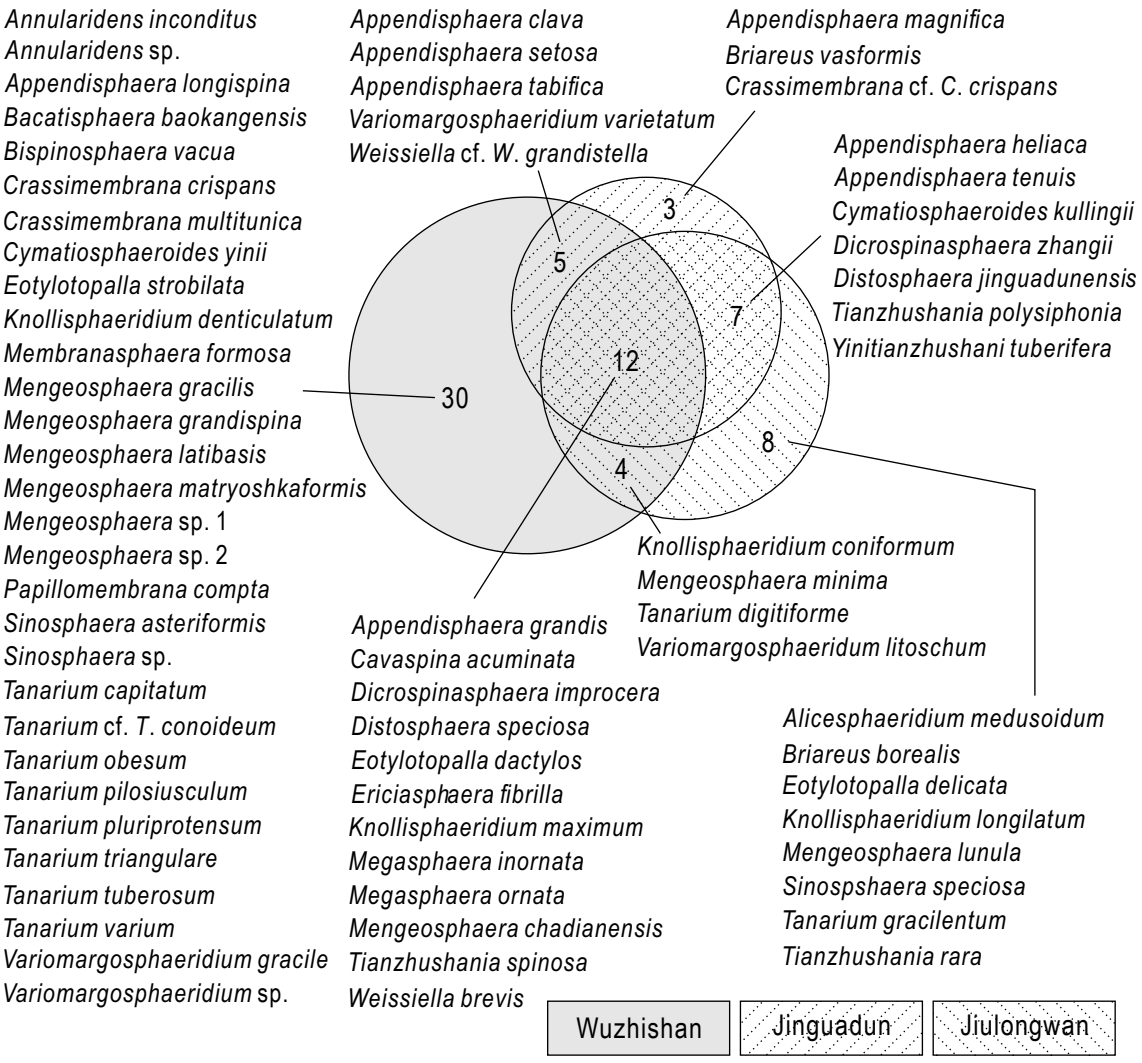

Fig. 25. Venn diagram showing the distribution of acanthomorphic acritarch species in the three sections in this study.

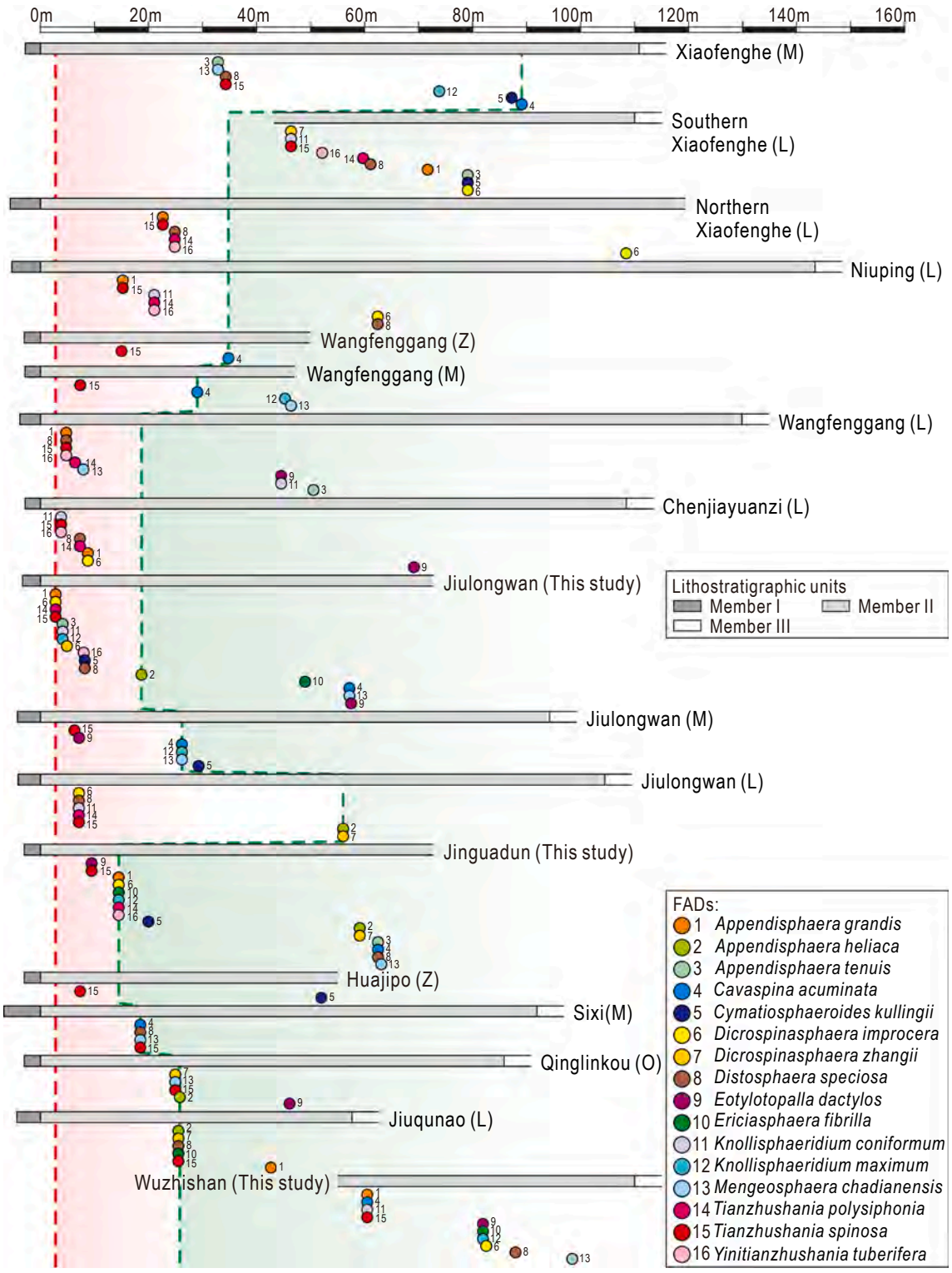

Fig. 26. First appearance data (FADs) of some regionally traceable acanthomorph taxa in Member II from the Yangtze Gorges area. Data sources: L, Liu and Moczydłowska (2019); M, McFadden et al. (2009); Z, Zhou et al. (2007). Red line represents the presumed regional FADs of *Appendisphaera grandis*, *Dicrospinasphaera improcera*, *Knollisphaeridium coniformum*, *Tianzhushania polysiphonia*, *T. spinosa*, and *Yinitianzhushania tuberifera*; green line represents the presumed regional FADs of *Appendisphaera heliaca*, *Cavaspina acuminata*, and *Ericiasphaera fibrilla*. (For interpretation of the references to colour in this figure legend, the reader is referred to the web version of this article.)

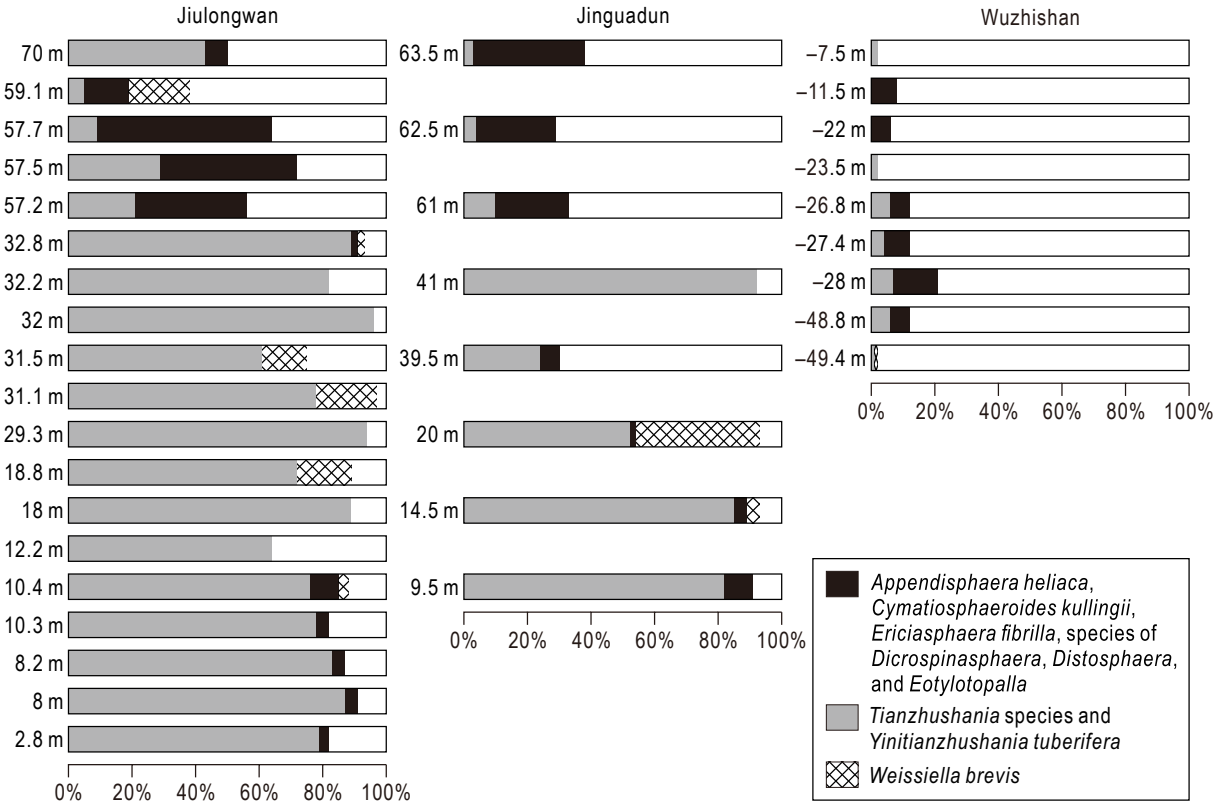

Fig. 27. Relative abundance (percentages) of three acanthomorph groups at each horizon in Member II at the three studied sections. Only fossiliferous horizons that yielded more than ten acanthomorphic acritarch specimens are shown. The three acanthomorph groups are small spiny acritarch group (black box) including *Appendisphaera heliaca*, *Cymatiosphaeroides kullingii*, *Ericiasphaera fibrilla*, and all species of *Dicrospinasphaera*, *Distosphaera*, and *Eotylotopalla*; *Tianzhushania* form group (gray box) including all species of *Tianzhushania* and *Yinitianzhushania*; and *Weissiella brevis* (cross-hatched box).

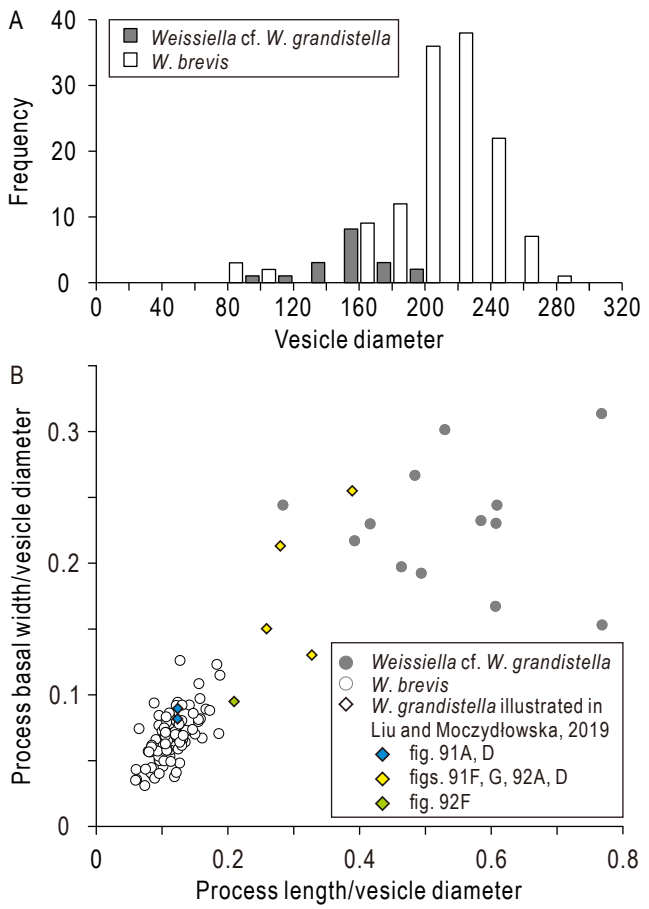

Fig. 28. Comparison of the dimensions between *Weissiella brevis* Xiao et al., 2014b emend. and *Weissiella* cf. *W. grandistella*. (**A**) Histogram of vesicle diameter. (**B**) Cross plot between proportional length of process (as a fraction of vesicle diameter) and proportional basal width (as a fraction of vesicle diameter) of *Weissiella brevis* Xiao et al., 2014b emend. and *Weissiella* cf. *W. grandistella*. Illustrated specimens assigned to *W. grandistella* in Liu and Moczydłowska (2019) are also plotted in (B).

well-preserved examples are illustrated in Fig. 24I–S, but detailed systematic description is not given here. Pending more and better-preserved specimens in the future, some of these species might represent new genus or species.

Declaration of Competing Interest

The authors declare that they have no known competing financial interests or personal relationships that could have appeared to influence the work reported in this paper.

Acknowledgements

This study was supported by the National Key R & D Program of China (2017YFC0603101), National Natural Science Foundation of China (41672027, 41902006, 41921002), and the Strategic Priority Research Program (B) of Chinese Academy of Sciences (XDB18000000, XDB26000000). S.X. acknowledges support from the U.S. National Science Foundation (EAR-2021207). We thank three anonymous reviewers for constructive reviews.

References

An, Z., Jiang, G., Tong, J., Tian, L., Ye, Q., Song, H., Song, H., 2015. Stratigraphic position of the Ediacaran Miaohe biota and its constrains on the age of the upper Doushantuo $\delta^{13}C$ anomaly in the Yangtze Gorges area, South China. Precambr. Res. 271, 243–253.

An, Z., Tong, J., Ye, Q., Tian, L., Song, H., Zhao, X., 2014. Neoproterozoic Stratigraphic Sequence and Sedimentary Evolution at Qinglinkou Section, East Yangtze Area. Earth Sciences—Journal of China University of. Geosciences 39, 795–806.

Anderson, R.P., Macdonald, F.A., Jones, D.S., McMahon, S., Briggs, D.E.G., 2017. Doushantuo-type microfossils from latest Ediacaran phosphorites of northern Mongolia. Geology 45, 1079–1082.

Anderson, R.P., McMahon, S., Macdonald, F.A., Jones, D.S., Briggs, D.E.G., 2019. Palaeobiology of latest Ediacaran phosphorites from the upper Khesen Formation, Khuvsgul Group, northern Mongolia. J. Syst. Paleontol. 17, 501–532.

Awramik, S.M., McMenamin, D.S., Yin, C., Zhao, Z., Ding, Q., Zhang, S., 1985. Prokaryotic and eukaryotic microfossils from a Proterozoic/Phanerozoic transition in China. Nature 315, 655–658.

Berkowski, B., Zapalski, M.K., 2018. Large dwellers of the Silurian *Halysites* biostrome: rhizosessile life strategies of cystiphyllid rugose corals from the Llandovery of Gotland. Lethaia 51, 581–595.

Bobrovskiy, I., Hope, J.M., Golubkova, E., Brocks, J.J., 2020. Food sources for the Ediacara biota communities. Nat. Commun. 11, 1261.

Bosak, T., Lahr, D.J.G., Pruss, S.B., Macdonald, F.A., Dalton, L., Matys, E., 2011. Agglutinated tests in post-Sturtian cap carbonates of Namibia and Mongolia. Earth Planet. Sci. Lett. 308, 29–40.

Brasier, M.D., Green, O.R., Lindsay, J.F., McLoughlin, N., Steele, A., Stoakes, C., 2005. Critical testing of Earth's oldest putative fossil assemblage from the ~3.5Ga Apex chert, Chinaman Creek, Western Australia. Precamb. Res. 140, 55–102.

Brocks, J.J., Jarrett, A.J.M., Sirantoine, E., Hallmann, C., Hoshino, Y., Liyanage, T., 2017. The rise of algae in Cryogenian oceans and the emergence of animals. Nature 548, 578–581.

Chen, M., Liu, K., 1986. The geological significance of newly discovered microfossils from the upper Sinian (Doushantuo age) phosphorites. Sci. Geol. Sin. 46–53.

Chen, Z., Zhou, C., Xiao, S., Wang, W., Guan, C., Hua, H., Yuan, X., 2014. New Ediacara fossils preserved in marine limestone and their ecological implications. Sci. Rep. 4, 4180.

Chumakov, N.M., Pokrovskii, B.G., Melezhik, V.A., 2007. Geological history of the Late Precambrian Patom Supergroup (Central Siberia). Dokl. Earth Sci. 413, 343–346.

Cohen, P.A., Vizcaíno, M., Anderson, R.P., 2020. Oldest fossil ciliates from the Cryogenian glacial interlude reinterpreted as possible red algal spores. Palaeontology. https://doi.org/10.1111/pala.12497.

Cole, D.B., Mills, D.B., Erwin, D.H., Sperling, E.A., Porter, S.M., Reinhard, C.T., Planavsky, N.J., 2020. On the co-evolution of surface oxygen levels and animals. Geobiology 18, 260–281.

Condon, D., Zhu, M., Bowring, S., Wang, W., Yang, A., Jin, Y., 2005. U-Pb Ages from the Neoproterozoic Doushantuo Formation, China. Science 308, 95–98.

Dalton, L.A., Bosak, T., Macdonald, F.A., Lahr, D.J.G., Pruss, S.B., 2013. Preservational and morphological variability of assemblages of agglutinated eukaryotes in Cryogenian cap carbonates of Northern Namibia. Palaios 28, 67–79.

Dong, L., Xiao, S., Shen, B., Zhou, C., Li, G., Yao, J., 2009. Basal Cambrian Microfossils from the Yangtze Gorges Area (South China) and the Aksu Area (Tarim Block, Northwestern China). J. Paleontol. 83, 30–44.

Eisenack, A., 1958. Mikroplankton aus dem norddeutschen Apt, nebst einigen Bemerkungen über fossile Dinoflagellaten. Neues Jb. Geol. Paläontol. Abh. 106, 383–422.

Eisenack, A., 1969. Zur Systematik einiger paläozoischer Hystrichosphären (Acritarcha) des baltischen Gebietes. Neues Jb. Geol. Paläontol. Abh. 133, 245–266.

Faizullin, M.S., 1998. New data on microfossils Bailalia of the Patom Upland. Geol Geofiz 39, 328–337.

Golubkova, E.Y., Raevskaya, E.G., Kuznetsov, A.B., 2010. Lower Vendian microfossil assemblages of East Siberia: Significance for solving regional stratigraphic problems. Stratigr. Geol. Correl. 18, 353–375.

Grazhdankin, D., Nagovitsin, K., Golubkova, E., Karlova, G., Kochnev, B., Rogov, V., Marusin, V., 2020. Doushantuo-Pertatataka–type acanthomorphs and Ediacaran ecosystem stability. Geology 48, 708–712.

Grey, K., 2005. Ediacaran palynology of Australia. Association of Australasian Palaeontologists 1–439.

Hawkins, A.D., Xiao, S., Jiang, G., Wang, X., Shi, X., 2017. New biostratigraphic and chemostratigraphic data from the Ediacaran Doushantuo Formation in intra-shelf and upper slope facies of the Yangtze platform: Implications for biozonation of acanthomorphic acritarchs in South China. Precambr. Res. 300, 28–39.

Hermann, T.N., 1974. Nakhodki massovykh skoplenij trikhornov v rifee. In: Timofeev, B. V. (Ed.), Mikrofitofossilii Proterozoia i Rannego Paleozoia SSSR. Nauka, Leningrad, pp. 6–10.

Hoffman, P.F., 2016. Cryoconite pans on Snowball Earth: supraglacial oases for Cryogenian eukaryotes? Geobiology 14, 531–542.

Jiang, G., Kaufman, A.J., Christie-Blick, N., Zhang, S., Wu, H., 2007. Carbon isotope variability across the Ediacaran Yangtze platform in South China: Implications for a large surface-to-deep ocean $\delta^{13}C$ gradient. Earth Planet. Sci. Lett. 261, 303–320.

Jiang, G., Kennedy, M.J., Christie-Blick, N., 2003a. Stable isotopic evidence for methane seeps in Neoproterozoic postglacial cap carbonates. Nature 426, 822–826.

Jiang, G., Kennedy, M.J., Christie-Blick, N., Wu, H., Zhang, S., 2006. Stratigraphy, Sedimentary Structures, and Textures of the Late Neoproterozoic Doushantuo Cap Carbonate in South China. J. Sediment. Res. 76, 978–995.

Jiang, G., Shi, X., Zhang, S., Wang, Y., Xiao, S., 2011. Stratigraphy and paleogeography of the Ediacaran Doushantuo Formation (ca. 635–551 Ma) in South China. Gondwana Res. 19, 831–849.

Jiang, G., Sohl, L.E., Christie-Blick, N., 2003b. Neoproterozoic stratigraphic comparison of the Lesser Himalaya (India) and Yangtze block (south China): Paleogeographic implications. Geology 31, 917–920.
Joshi, H., Tiwari, M., 2016. *Tianzhushania spinosa* and other large acanthomorphic acritarchs of Ediacaran Period from the Infrakrol Formation, Lesser Himalaya, India. Precambr. Res. 286, 325–336.
Kaufman, A.J., Jiang, G., Christie-Blick, N., Banerjee, D.M., Rai, V., 2006. Stable isotope record of the terminal Neoproterozoic Krol platform in the Lesser Himalayas of northern India. Precambr. Res. 147, 156–185.
Knoll, A.H., 1982. Microfossils from the Late Precambrian Draken Conglomerate, Ny Friesland, Svalbard. J. Paleontol. 56, 755–790.
Knoll, A.H., 1984. Microbiotas of the late Precambrian Hunnberg Formation, Nordaustlandet, Svalbard. J. Paleontol. 58, 131–162.
Knoll, A.H., 1992. Vendian microfossils in metasedimentary cherts of the Scotia group, Prins Karls Forland, Svalbard. Palaeontology 35, 751–774.
Kolosova, S.P., 1991. Pozdnedokembriyskie shipovatie mikrofossilii vostoka sibirkoy platformi. Algologiya 1, 53–59.
Lang, X., Shen, B., Peng, Y., Huang, K., Lv, J., Ma, H., 2016. Ocean oxidation during the deposition of basal Ediacaran Doushantuo cap carbonates in the Yangtze Platform, South China. Precambr. Res. 281, 253–268.
Lang, X., Shen, B., Peng, Y., Xiao, S., Zhou, C., Bao, H., Kaufman, A.J., Huang, K., Crockford, P.W., Liu, Y., Tang, W., Ma, H., 2018. Transient marine euxinia at the end of the terminal Cryogenian glaciation. Nat. Commun. 9, 3019.
Liu, P., Chen, S., Zhu, M., Li, M., Yin, C., Shang, X., 2014a. High-resolution biostratigraphic and chemostratigraphic data from the Chenjiayuanzi section of the Doushantuo Formation in the Yangtze Gorges area, South China: Implication for subdivision and global correlation of the Ediacaran System. Precambr. Res. 249, 199–214.
Liu, P., Moczydłowska, M., 2019. Ediacaran microfossils from the Doushantuo Formation chert nodules in the Yangtze Gorges area, South China, and new biozones. Fossils Strata 65, 1–172.
Liu, P., Xiao, S., Yin, C., Chen, S., Zhou, C., Li, M., 2014b. Ediacaran acanthomorphic acritarchs and other microfossils from chert nodules of the upper Doushantuo Formation in the Yangtze Gorges Area, South China. J. Paleontol. Memior 88, 1–139.
Liu, P., Yin, C., Chen, S., Tang, F., Gao, L., 2013. The biostratigraphic succession of acanthomorphic acritarchs of the Ediacaran Doushantuo Formation in the Yangtze Gorges area, South China and its biostratigraphic correlation with Australia. Precambr. Res. 225, 29–43.
Liu, P., Yin, C., Gao, L., Tang, F., Chen, S., 2009. New material of microfossils from the Ediacaran Doushantuo Formation in the Zhangcunping area, Yichang, Hubei Province and its zircon SHRIMP U-Pb age. Chin. Sci. Bull. 54, 1058–1064.
Luo, H., Jiang, Z., Wu, X., Song, X., Ouyang, L., 1982. The Sinian-Cambrian boundary in eastern Yunnan. Yunnan People's Publishing House, Kunming, China, p. 302.
McFadden, K.A., Huang, J., Chu, X., Jiang, G., Kaufman, A.J., Zhou, C., Yuan, X., Xiao, S., 2008. Pulsed oxidation and biological evolution in the Ediacaran Doushantuo Formation. Proc. Natl. Acad. Sci. 105, 3197–3202.
McFadden, K.A., Xiao, S., Zhou, C., Kowalewski, M., 2009. Quantitative evaluation of the biostratigraphic distribution of acanthomorphic acritarchs in the Ediacaran Doushantuo Formation in the Yangtze Gorges area, South China. Precambr. Res. 173, 170–190.
Moczydłowska, M., 2005. Taxonomic review of some Ediacaran acritarchs from the Siberian Platform. Precambr. Res. 136, 283–307.
Moczydłowska, M., Nagovitsin, K.E., 2012. Ediacaran radiation of organic-walled microbiota recorded in the Ura Formation, Patom Uplift, East Siberia. Precambr. Res. 198–199, 1–24.
Moczydłowska, M., Vidal, G., Rudavskaya, V.A., 1993. Neoproterozoic (Vendian) phytoplankton from the Siberian platform, Yakutia. Palaeontology 36, 495–521.
Moore, K.R., Bosak, T., Macdonald, F.A., Lahr, D.J.G., Newman, S., Settens, C., Pruss, S. B., 2017. Biologically agglutinated eukaryotic microfossil from Cryogenian cap carbonates. Geobiology 15, 499–515.
Muscente, A.D., Hawkins, A.D., Xiao, S., 2015. Fossil preservation through phosphatization and silicification in the Ediacaran Doushantuo Formation (South China): a comparative synthesis. Palaeogeogr. Palaeoclimatol. Palaeoecol. 434, 46–62.
Nagovitsin, K.E., Faizullin, M.S., Yakshin, M.S., 2004. New forms of Baikalian acanthomorphytes from the Ura Formation of the Patom Uplift, East Siberia. Geol. Geofisika 45, 7–19.
Nagy, R.M., Porter, S.M., Dehler, C.M., Shen, Y., 2009. Biotic turnover driven by eutrophication before the Sturtian low-latitude glaciation. Nat. Geosci. 2, 415–418.
Narbonne, G.M., Xiao, S., Shields, G.A., Gehling, J.G., 2012. Chapter 18 - The Ediacaran Period. In: Gradstein, F.M., Ogg, J.G., Schmitz, M.D., Ogg, G.M. (Eds.), The Geologic Time Scale. Elsevier, Boston, pp. 413–435.
Ouyang, Q., Zhou, C., Guan, C., Wang, W., 2015. New microfossils from the Ediacaran Doushantuo Formation in the Yangtze Gorges area, South China, and their biostratigraphic implications. Acta Palaeontologica Sinica 54, 207–229.
Ouyang, Q., Zhou, C., Xiao, S., Chen, Z., Shao, Y., 2019. Acanthomorphic acritarchs from the Ediacaran Doushantuo Formation at Zhangcunping in South China, with implications for the evolution of early Ediacaran eukaryotes. Precambr. Res. 320, 171–192.
Pokrovskii, B.G., Melezhik, V.A., Bujakaite, M.I., 2006. Carbon, oxygen, strontium, and sulfur isotopic compositions in late Precambrian rocks of the Patom Complex, central Siberia: Communication 1. results, isotope stratigraphy, and dating problems. Lithol. Min. Resour. 41, 450–474.
Riedman, L.A., Porter, S.M., Halverson, G.P., Hurtgen, M.T., Junium, C.K., 2014. Organic-walled microfossil assemblages from glacial and interglacial Neoproterozoic units of Australia and Svalbard. Geology 42, 1011–1014.
Riedman, L.A., Sadler, P.M., 2018. Global species richness record and biostratigraphic potential of early to middle Neoproterozoic eukaryote fossils. Precambr. Res. 319, 6–18.
Schenfil, V.Y., 1980. Obruchevelly v rifejskikh otlozheniyakh Yenisej skogo kryazha. J Doklady Akademii Nauk SSSR 254, 993–994.
Schopf, J.W., 1968. Microflora of the Bitter Springs Formation, Late Precambrian, Central Australia. J. Paleontol. 42, 651–688.
Sergeev, V.N., Knoll, A.H., Vorob'eva, N.G., 2011. Ediacaran Microfossils from the Ura Formation, Baikal-Patom Uplift, Siberia: Taxonomy and Biostratigraphic Significance. J. Paleontol. 85, 987–1011.
Shang, X., Liu, P., Moczydłowska, M., 2019. Acritarchs from the Doushantuo Formation at Liujing section in Songlin area of Guizhou Province, South China: Implications for early–middle Ediacaran biostratigraphy. Precambr. Res. 334, 105453.
Shukla, R., Tiwari, M., 2014. Ediacaran acanthomorphic acritarchs from the Outer Krol Belt, Lesser Himalaya, India: Their significance for global correlation. Palaeoworld 23, 209–224.
Spjeldnaes, N., 1963. A New Fossil (*Papillomembrana* sp.) from the Upper Precambrian of Norway. Nature 200, 63–64.
Sui, Y., Huang, C., Zhang, R., Wang, Z., Ogg, J., Kemp, D.B., 2018. Astronomical time scale for the lower Doushantuo Formation of early Ediacaran, South China. Sci. Bull. 63, 1485–1494.
Timofeev, B.V., Hermann, T.N., Mikhailova, N.S., 1976. Mikrofitogosilli dokembriya, kembriya i ordovika. Nauka, Moskow, pp. 1–107.
Tiwari, M., Knoll, A.H., 1994. Large acanthomorphic acritarchs from the Infrakrol Formation of the Lesser Himalaya and their stratigraphic significance. J. Himalayan Geol. 5, 193–201.
Tiwari, M., Pant, C.C., 2004. Neoproterozoic silicified microfossils in Infra Krol Formation, Lesser Himalaya, India. Himalaya Geol. 25, 1–21.
Vidal, G., 1990. Giant acanthomorph acritarchs from the upper Proterozoic in southern Norway. Palaeontology 33, 287–298.
Vorob'eva, N.G., Sergeev, V.N., Knoll, A.H., 2009. Neoproterozoic microfossils from the northeastern margin of the East European Platform. J. Paleontol. 83, 161–196.
Wang, W., Guan, C., Zhou, C., Peng, Y., Pratt, L.M., Chen, X., Chen, L., Chen, Z., Yuan, X., Xiao, S., 2017. Integrated carbon, sulfur, and nitrogen isotope chemostratigraphy of the Ediacaran Lantian Formation in South China: Spatial gradient, ocean redox oscillation, and fossil distribution. Geobiology 15, 552–571.
Wang, X., Erdtmann, B.D., Chen, X., Mao, X., 1998. Integrated Sequence-, Bio- and Chemostratigraphy of the Terminal Proterozoic to Lowermost Cambrian "Black Rock Series" from Central South China. Episodes 21, 178–189.
Wang, X., Jiang, G., Shi, X., Xiao, S., 2016. Paired carbonate and organic carbon isotope variations of the Ediacaran Doushantuo Formation from an upper slope section at Siduping, South China. Precambr. Res. 273, 53–66.
Willman, S., Moczydłowska, M., 2008. Ediacaran acritarch biota from the Giles 1 drillhole, Officer Basin, Australia, and its potential for biostratigraphic correlation. Precambr. Res. 162, 498–530.
Xiao, S., 2004. New multicellular algal fossils and acritarchs in Doushantuo chert nodules (Newproterozoic; Yangtze Gorges, South China). J. Paleontol. 78, 393–401.
Xiao, S., Chen, Z., Pang, K., Zhou, C., Yuan, X., 2020. The Shibantan Lagerstätte: Insights into the Proterozoic-Phanerozoic transition. J. Geol. Soc. https://doi.org/10.1144/jgs2020-135.
Xiao, S., Knoll, A.H., 1999. Fossil preservation in the Neoproterozoic Doushantuo phosphorite Lagerstätte, South China. Lethaia 32, 219–238.
Xiao, S., Knoll, A.H., 2000. Phosphatized animal embryos from the Neoproterozoic Doushantuo formation at Weng'an, Guizhou, South China. J. Paleontol. 74, 767–788.
Xiao, S., Muscente, A.D., Chen, L., Zhou, C., Schiffbauer, J.D., Wood, A.D., Polys, N.F., Yuan, X., 2014a. The Weng'an biota and the Ediacaran radiation of multicellular eukaryotes. Natl. Sci. Rev. 1, 498–520.
Xiao, S., Narbonne, G.M., 2020. The Ediacaran Period. In: Gradstein, F.M., Ogg, J.G., Schmitz, M.D., Ogg, G.M. (Eds.), Geological Time Scale 2020. Elsevier, Oxford.
Xiao, S., Narbonne, G.M., Zhou, C., Laflamme, M., Grazhdankin, D.V., Moczydlowska-Vidal, M., Cui, H., 2016. Towards an Ediacaran Time Scale: Problems, Protocols, and Prospects. Episodes 39, 540–555.
Xiao, S., Schiffbauer, J.D., McFadden, K.A., Hunter, J., 2010. Petrographic and SIMS pyrite sulfur isotope analyses of Ediacaran chert nodules: Implications for microbial processes in pyrite rim formation, silicification, and exceptional fossil preservation. Earth Planet. Sci. Lett. 297, 481–495.
Xiao, S., Tang, Q., 2018. After the boring billion and before the freezing millions: evolutionary patterns and innovations in the Tonian Period. Emerg. Top. Life Sci. 2, 161–171.
Xiao, S., Yuan, X., Steiner, M., Knoll, A.H., 2002. Macroscopic carbonaceous compressions in a terminal Proterozoic shale: A systematic reassesment of the Miaohe Biota, South China. J. Paleontol. 76, 347–376.
Xiao, S., Zhou, C., Liu, P., Wang, D., Yuan, X., 2014b. Phosphatized acanthomorphic acritarchs and related microfossils from the Ediacaran Doushantuo Formation at Weng'an (South China) and their implications for biostratigraphic correlation. J. Paleontol. 88, 1–67.
Ye, Q., Tong, J., An, Z., Hu, J., Tian, L., Guan, K., Xiao, S., 2017. A systematic description of new macrofossil material from the upper Ediacaran Miaohe Member in South China. J. Syst. Paleontol. 17, 183–238.
Ye, Q., Tong, J., Xiao, S., Zhu, S., An, Z., Tian, L., Hu, J., 2015. The survival of benthic macroscopic phototrophs on a Neoproterozoic snowball Earth. Geology 43, 507–510.
Yin, C., 1990. Spinose acritarchs from the Toushantou Formation in the Yangtze Gorges and its geological significance. Acta Micropalaeontol. Sin. 7, 265–270.
Yin, C., 1999. Microfossils from the Upper Sinian (Late Neoproterozoic) Doushantuo Formation in Changyang, Western Hubei, China. Continental Dyn. 4, 1–18.

Yin, C., Gao, L., Xing, Y., 2001. Discovery of *Tianzhushania* in Doushantuo Phosphorites in Weng'an, Guizhou Province. Acta Palaeontol. Sin. 40, 497–504.
Yin, C., Liu, G., 1988. Micropaleofloras. In: Zhao, Z., Xing, Y., Ding, Q., Liu, G., Zhao, Y., Zhang, S., Meng, X., Yin, C., Ning, B., Han, P. (Eds.), The Sinian System of Hubei. China University of Geosciences Press, Wuhan, pp. 170–180.
Yin, C., Liu, P., Awramik, S.M., Chen, S., Tang, F., Gao, L., Wang, Z., Riedman, L.A., 2011a. Acanthomorph Biostratigraphic Succession of the Ediacaran Doushantuo Formation in the East Yangtze Gorges, South China. Acta Geol. Sin. – Engl. Ed. 85, 283–295.
Yin, L., 1987. Microbiotas of latest Precambrian sequences in China, in: Nanjing Institute of Geology and Palaeontology Academia Sinica (Ed.), Stratigraphy and Palaeontology of Systemic Boundaries in China: Precambrian–Cambrian Boundary (1). Nanjing University Press, Nanjing, pp. 415–494.
Yin, L., Li, Z., 1978. Pre-cambrian microfloras of southwest China, with preference to their stratigraphical significance. Mem. Nanjing Inst. Geol. Palaeontol. Acad. Sin. 10, 41–108.
Yin, L., Wang, D., Yuan, X., Zhou, C., 2011b. Diverse small spinose acritarchs from the Ediacaran Doushantuo Formation, South China. Palaeoworld 20, 279–289.
Yin, L., Zhou, C., Yuan, X., 2008. New data on *Tianzhushania*—An Ediacaran diapause egg cyst from Yichang, Hubei. Acta Palaeontol. Sin. 47, 129–140.
Yin, L., Zhu, M., Knoll, A.H., Yuan, X., Zhang, J., Hu, J., 2007. Doushantuo embryos preserved inside diapause egg cysts. Nature 446, 661–663.
Yuan, X., Chen, Z., Xiao, S., Zhou, C., Hua, H., 2011. An early Ediacaran assemblage of macroscopic and morphologically differentiated eukaryotes. Nature 470, 390–393.
Yuan, X., Hofmann, H.J., 1998. New microfossils from the Neoproterozoic (Sinian) Doushantuo Formation, Wengan, Guizhou Province, southwestern China. Alcheringa: Aust. J. Palaeontol. 22, 189–222.
Zang, W., Walter, M.R., 1992. Late Proterozoic and Cambrian microfossils and biostratigraphy, Amadeus basin, central Australia. Mem. Assoc. Aust. Paleontol. 12, 1–132.
Zhang, Y., 1989. Multicellular thallophytes with differentiated tissues from Late Proterozoic phosphate rocks of South China. Lethaia 22, 113–132.
Zhang, Y., Yin, L., Xiao, S., Knoll, A.H., 1998. Permineralized Fossils from the Terminal Proterozoic Doushantuo Formation, South China. J. Paleontol. Mem. Supplement to 72, 1–52.
Zhang, Y., Yuan, X., 1992. New data on multicellular thallophytes and fragments of cellular tissues from Late Proterozoic phosphate rocks, South China. Lethaia 25, 1–18.
Zhang, Z., 1984. On the occurrence of *Obruchevella* from the Toushantou Formation (late Sinian) of western Hubei and its significance. Acta Palaeontol. Sin. 23, 447–451.
Zhang, Z., 1986. New material of filamentous fossil cyanophytes from the Doushantuo Formation (Late Sinian) in the eastern Yangtze Gorge. Sci. Geol. Sin. 30–37.
Zhou, C., Brasier, M.D., Xue, Y., 2001. Three-dimensional phosphatic preservation of giant acritarchs from the terminal Proterozoic Doushantuo Formation in Guizhou and Hubei Provinces, South China. Palaeontology 44, 1157–1178.
Zhou, C., Chen, Z., Xue, Y., 2002. New microfossils form the Late Neoproterozoic Doushantuo Formation at Chaoyang phosphorite deposit in Jiangxi Province, South China. Acta Palaeontol. Sin. 41, 178–192.
Zhou, C., Li, X., Xiao, S., Lan, Z., Ouyang, Q., Guan, C., Chen, Z., 2017a. A new SIMS zircon U-Pb date from the Ediacaran Doushantuo Formation: age constraint on the Weng'an biota. Geol. Mag. 154, 1193–1201.
Zhou, C., Xiao, S., 2007. Ediacaran $\delta^{13}C$ chemostratigraphy of South China. Chem. Geol. 237, 89–108.
Zhou, C., Xiao, S., Wang, W., Guan, C., Ouyang, Q., Chen, Z., 2017b. The stratigraphic complexity of the middle Ediacaran carbon isotopic record in the Yangtze Gorges area, South China, and its implications for the age and chemostratigraphic significance of the Shuram excursion. Precambr. Res. 288, 23–38.
Zhou, C., Xie, G., McFadden, K.A., Xiao, S., Yuan, X., 2007. The diversification and extinction of Doushantuo-Pertatataka acritarchs in South China: causes and biostratigraphic significance. Geol. J. 42, 229–262.
Zhou, C., Yuan, X., Xiao, S., Chen, Z., Hua, H., 2019. Ediacaran integrative stratigraphy and timescale of China. Science China Earth Sciences 62, 7–24.
Zhu, M., Lu, M., Zhang, J., Zhao, F., Li, G., Yang, A., Zhao, X., Zhao, M., 2013. Carbon isotope chemostratigraphy and sedimentary facies evolution of the Ediacaran Doushantuo Formation in western Hubei, South China. Precambr. Res. 225, 7–28.